Design and Analysis of a Hybrid Composite/ Metal Structural System For Underwater Lifting Bodies

Project Report for the

Modular Advanced Composite Hull form (MACH) Technology Project

Prepared by:

Larry Thompson, PhD. P.E., Applied Thermal Sceinces

Josh Walls, Applied Thermal Sceinces, and

Vincent Caccese, PhD. P.E , University of Maine, Principal Investigator

Prepared for:

Office of Naval Research

800 N Quincy St.

Arlington VA. 22217-5660

Grant No. N00014-01-1-0916

Dr. Roshdy G.S. Barsoum,

Program Manager

University of Maine

Department of Mechanical Engineering

Orono, ME 04469-5711

Applied Thermal Sciences

P.O. Box C, 1861 Main Street

Sanford, ME 04073

June 2005

Report No. UM-MACH-RPT-01-08

Acknowledgements

The authors gratefully acknowledge funding for this project through the Office of Naval Research under grant number N00014-01-1-0916. Dr. Roshdy G.S. Barsoum of ONR is the cognizant program officer. His support and encouragement is greatly appreciated. The author would also like to thank Milt Crichfield, Loc Nguyen and Gene Camponeschi of NSWC Carderock (NSWCCD) for their assistance and advice. Furthermore, the support of the other partners involved in this effort, particularly, Steven Loui, Todd Pelzer and Eric Schiff of Pacific Marine, Navatek Division and the project team at the University of Maine including Randy Bragg, Keith Berube and Jean-Paul Kabche. The guidance and support of other personnel at Applied Thermal Sciences is also acknowledged including Kendrick Light and SteveWebber.

TABLE OF CONTENTS

THE UNIVERSITY OF
MAINE

Vincent Caccese
Associate Professor

Department of Mechanical Engineering
5711 Boardman Hall
Orono, ME 04469-5711

phone: (207) 581-2131
fax: (207) 581-2379
email: vince_caccese@umit.maine.edu

August 1, 2005

Roshdy G. S. Barsoum
Office of Naval Research
Ballston Centre Tower One
800 North Quincy Street
Arlington, VA 22217-5660

Dear Dr. Barsoum:

Enclosed please find two copies of the report entitled "Design and Analysis of a Hybrid Composite/Metal Structural System for Underwater Lifting Bodies" including the required SF298. This report is submitted under the Modular Advanced Composite Hullform Technology (MACH) project, Grant No. N000014-01-1-0916. If you have questions or comments please do not hesitate to contact me.

Regards,

Vincent Caccese, Ph.D
Associate Professor of Mechanical Engineering

pc
DTIC
NRL
ONR Boston

Page

Page

LIST OF TABLES

Page

LIST OF FIGURES

Page

Page

Page

1. Introduction

The body of this work is a partial fulfillment for sub-contract UM-S412 between Applied Thermal Sciences, Inc. of Sanford, Maine and the University of Maine, Orono, Maine in support of a grant from the Office on Naval Research (ONR) (Grant # N00014-01-1-0916), Dr. Roshdy Barsoum, ONR Program Officer.

This report summarizes the analysis and design of a hybrid underwater lifting body structure. It is part of an ongoing effort to investigate the response of hybrid composite/metal construction techniques and hybrid connection connections in U.S. Navy vessels. This effort includes structural analysis of a lifting body structure designed by Navatek, Ltd of Honolulu HI that was constructed of aluminum for the SES 200. Analysis of this structural system as an e-glass/vinylester – aluminum hybrid was undertaken. Additionally, a hydrostatic test system was developed used for a proof-of-concept study for a hybrid structural system, based upon the lifting body design.

The work was performed under the Modular Advanced Composite Hull-form (MACH) project where the focus was to develop and test hybrid metal/composite structural system and connections for naval ship applications. The primary motivation for this project is to provide alternatives to conventional hull construction techniques and conventional hull forms by using modular hybrid construction methods. The major effort of the MACH project is to develop a hybrid structural system that is comprised of polymer matrix composite structural panels connected to metallic supporting structure. In addition to enabling advanced hull shapes, the hybrid concept used in MACH is also expected to decrease system weight, which in turn should lead to faster and more efficient vessels. Also, due to the modularity of the system, access to the hull interior would be greatly improved. Various connection methods are being examined for the project, including adhesive bonding, embedded metallic inserts, and bolted connections. Use of bolted connections is desirable in cases where removable panels are required. Design of removable panels enables easier access for maintenance and exchanging of equipment for mission specific tasks.

During the past few years, Navatek has built experimental ships that incorporate lifting bodies, in order to provide enhanced sea-keeping through reduction in motions, higher lift-to-drag ratios, and greater compatibility with multiple hull types. One example of such ships is the Sea Flyer, shown in Figure 1.1. The Sea Flyer is a modified Surface Effect Ship, the SES 200, that uses an underwater lifting body as shown in Figure 1.2. The research team at the University of Maine has studied the metal framework and composite panel hybrid system for use in this type of lifting body. This study has been lead by the University of Maine and performed in conjunction with a team of governmental, industry and academic partners including Applied Thermal Sciences, Inc. (ATS) of Sanford, Navatek, Ltd. of Honolulu, Hawaii, Maine, and the Naval Surface Warfare Center at Carderock, Maryland (NSWCCD).

Figure 1.1 - SEA FLYER (photo courtesy of ONR via www.military.com)

Figure 1.2 – Underwater Lifting Body (photo courtesy of Navatek via www.military.com)

The development of hybrid structures requires extensive research prior to their application. A robust and reliable hybrid structure relies upon an adequate connection between composites and metals. A critical issue in the design of these structures is the joining of composite sections to metallic sub-structures. It is imperative to understand the inherently non-linear behavior of these joints, the interactions between the constituents, and the structural response in severe environments.

Connections present a problem with regard to stress concentration in hybrid structures. For instance, in a bolted connection composites tend to creep over time, due to the viscoelastic nature of the matrix material. This creep leads to stress relaxation and potential loss of preload in bolted connections. This along with the dynamic loading of the structure may compromise watertight integrity. Methods of designing robust connections and testing watertight integrity of the structural system are highly desirable. This work addresses the design of a system level test tank used to study watertight integrity of hybrid structures.

1.1 Objectives

The objective of this effort is to quantify the stress relaxation of transversely compressed composites in bolted aluminum/e-glass vinylester hybrid structural systems. The intent is to perform a case study of the design and development of a hybrid structural system implemented on an existing lifting body design. The study is intended to investigate the following:

1) Analysis of the panelized lifting body design.
2) Analysis of a representative SES 200 ship section
3) Analysis of baseline aluminum structure
4) Optimal preliminary detailing of composite panels
5) Design and implementation of tank test system to study watertight integrity of hybrid structure.

1.2 Scope of the Report

Chapter 2 through Chapter 8 details the development of a hybrid (composite skin with a metallic endoskeleton) lifting body utilizing the Modular Advanced Composite Hull-form (MACH) concepts. Which include panel studies and frame spacing studies aimed to reduce the overall structural weight of the lifting body. Additionally, initial work for developing effective connection models using piecewise nonlinear springs to incorporate the effects of connections in a large global finite element model were considered.

Chapter 9 and Chapter 10 present preliminary finite element models and techniques for developing detailed models of bolted connections, which include the long-term viscoelastic effects (creep) material property.

Chapter 11 through Chapter 14 details the design and implementation of a full-scale hydrostatic panel testing apparatus at the Advance Structures Lab at the University of Maine. By using a four-panel configuration connected with simulated bulkhead beams, a realistic loading scenario can be achieved for evaluating the structural performance and watertight integrity of the MACH hybrid joint concepts and paneling concept under true hydrostatic loading.

Additional efforts not specifically covered in this report include oversight during fabrication and installation of the MACH panel test apparatus, test specimen preparation and installation as well as efforts supporting the structural testing.

2. Panelized Lifting Body

2.1 Model Purpose

The primary purpose of the lifting body FE model is to evaluate the performance of a composite paneling scheme compared to the baseline aluminum design for below waterline marine hulls. Due to the complex loading scenarios present in a marine lifting body structure, a global model of the lifting body is necessary to capture the effects of the various structure loads imparted on the panels.

2.2 FE Model Development

The lifting body model is based on the existing aluminum H-body, designed for the SES 200, by Nigel Gee and Associates LTD. A scale of 1:1 is used for the model with the base unit of measure in inches. The overall dimensions of the model are shown in Figure 2.1a – b, with the global origin located on the leading edge of the port strut at the intersection point of the strut and ship hull. The model is built entirely with 8-noded, linear layered structural shell elements to incorporate composite panels.

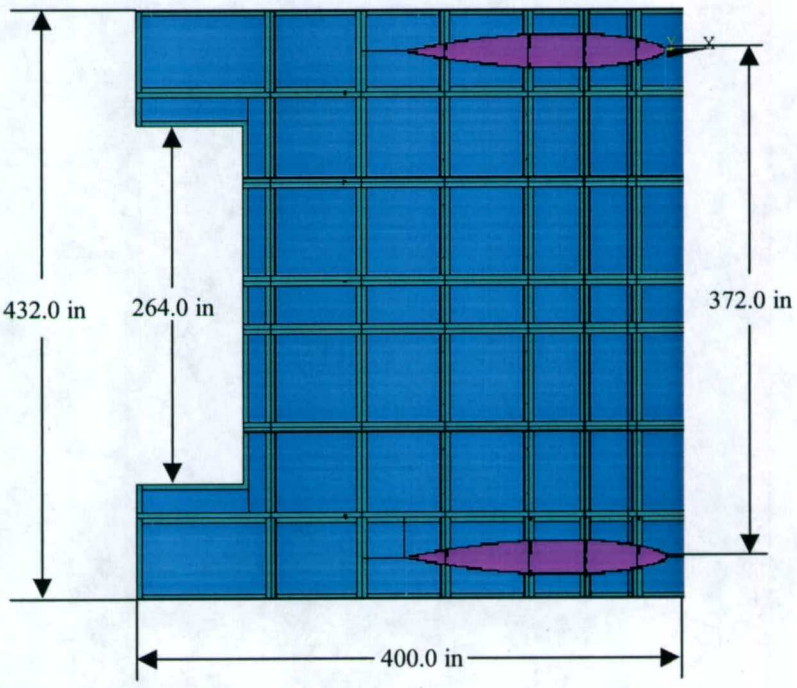

Figure 2.1a – Lifting Body Dimensions, Top View

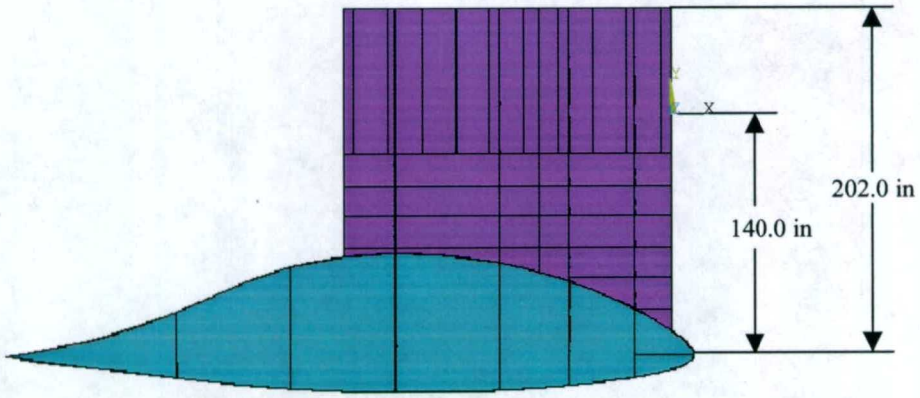

Figure 2.1b – Lifting Body Dimensions, Starboard Side

The sub-frame structural geometry of the lifting body is represented in the model with adequate detail to capture the global structural properties, while minimizing certain small details in an effort to maintain a realistic model size. To illustrate the level of detail maintained throughout the model Figure 2.2 shows a typical longitudinal bulkhead. Eight-inch flanges have been added to the perimeter of all bulkheads to accommodate the composite panel connections. The plate thickness for the longitudinal bulkheads is 1/2-in., while the plate thickness for the transverse bulkheads is 5/8-in. All riders have a width of three inches with thickness corresponding to the bulkhead plate thickness. Figure 2.3a-b illustrates the lifting body sub-frame geometry and bulkhead spacing. The strut bulkheads are a continuation of the transverse bulkheads and maintain the 5/8-in thickness, while the strut diaphragms are 3/8-in thick. The strut diaphragm cutouts, and strut panel J-stiffeners are omitted to reduce model size and aid mesh generation.

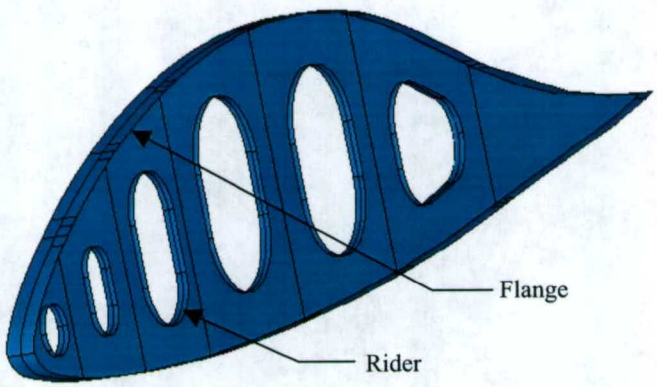

Figure 2.2 – Typical Longitudinal Bulkhead

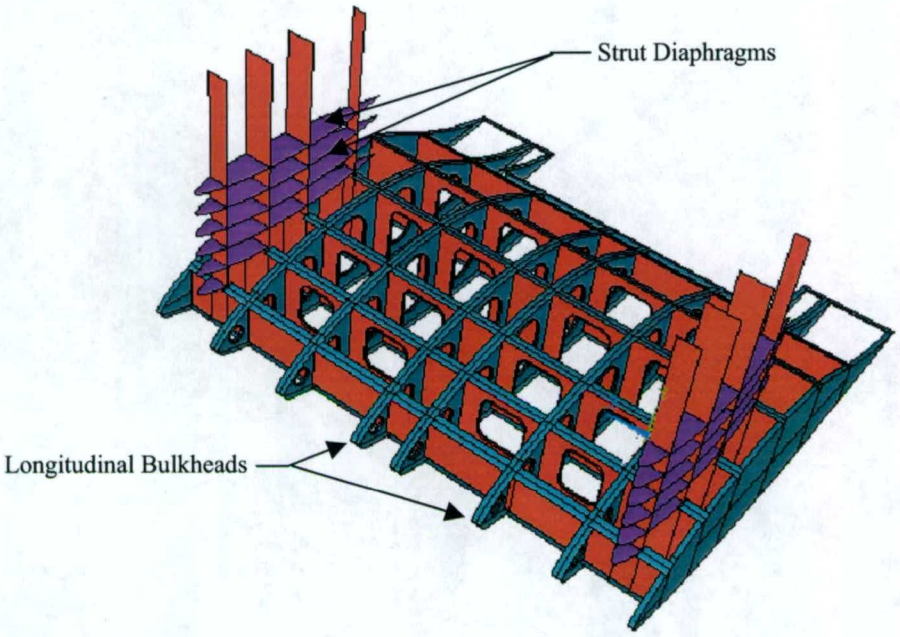

Figure 2.3a – Lifting Body Sub-frame

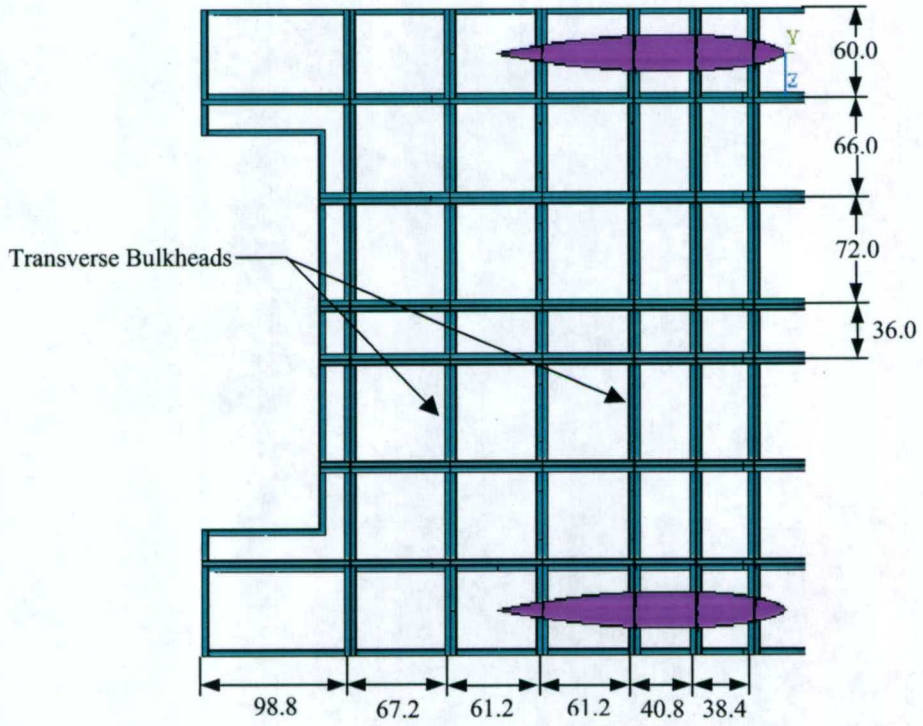

Figure 2.3b – Lifting Body Bulkhead Spacing (inches)

Currently, the connection between the composite panels and aluminum alloy sub frame are modeled only by partitioning the top and bottom surface of the lifting body at the boundary of the panels and aluminum flanges. This method may not realistically capture the mechanics of the composite-metal joint however, non-linear connection models are currently being investigated in an effort to better model the composite-metal joints. These models have been successfully generated on a local scale, as described in Section 8.

2.3 Material Systems

Aluminum, 6061-T6, is used for the entire sub-frame, including all transverse bulkheads, longitudinal bulkheads, strut diaphragms, and strut panels. The first panel scheme used for developing the lifting body model incorporates a two-inch, closed cell foam core with e-glass/vinyl ester skins. The e-glass/vinylester skins are composed of three layers of 600g, 0/90 cloth, which corresponds two six individual layers for each laminate in the FE model and results in a face sheet approximately 0.1-in thick. Additional composite panel schemes, such as hat-stiffened and single skin are also investigated, which are discussed in Section 7, and will be further analyzed in the global model. The material properties input into the current FE model are summarized in Table 2.1.

Table 2.1 – Material Properties

Material System	Properties								
	Ex ksi	Ey ksi	Ez ksi	G_{xy} ksi	G_{yz} ksi	G_{xz} ksi	nu_{xy}	nu_{yz}	nux_z
aluminum	10,000	10,000	10,000	3,760	3,760	3,760	0.33	0.33	0.33
eglass/vinylesyter	5,500	1,370	490	860	180	180	0.28	0.35	0.35
closed cell foam, Divinycell HD250	31.9	31.9	40.6	16.0	16.0	16.0	0.32	0.32	0.32

3. SES 200 Ship Section

3.1 Model Purpose

The purpose of the SES 200 ship section model is to provide realistic boundary conditions for the lifting body struts by incorporating the section of the hull where the lifting body struts are connected.

3.2 FE Model Development

A 33.4-foot section of the SES 200 hull is built at the location of the strut-hull interface and is illustrated in Figure 3.1a-b. A scale of 1:1 is used for the model with the base unit of measure in inches. For the purpose of combining the SES 200 hull section model with the lifting body model, the global coordinate system of the SES 200 corresponds with the location of the global coordinate system of the lifting body model, which is the point where the port strut leading edge intersects the port hull. Though no composite panels are utilized in the SES 200 hull model, linear layered, 8-node, shell elements are used to maintain consistency with the lifting body model.

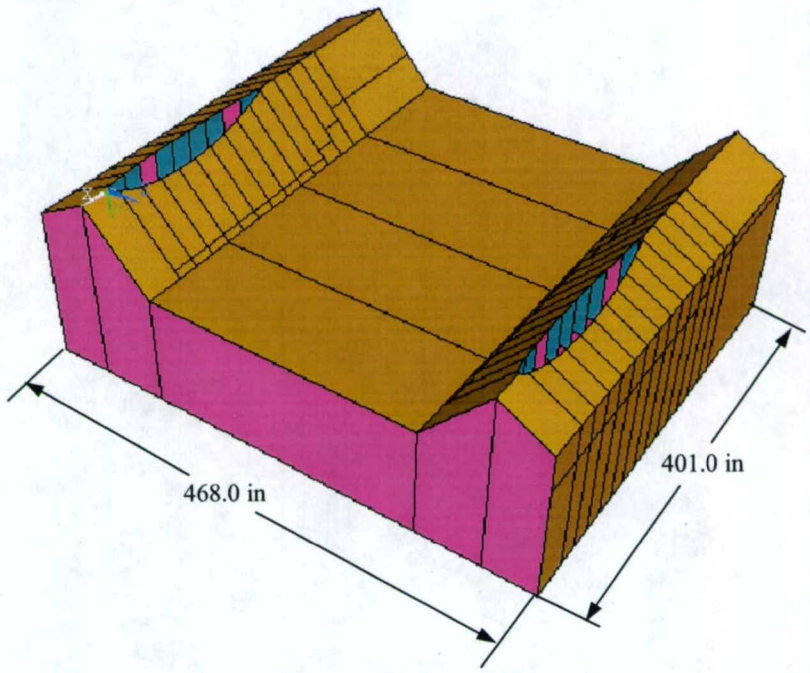

Figure 3.1a – SES 200 Hull Section

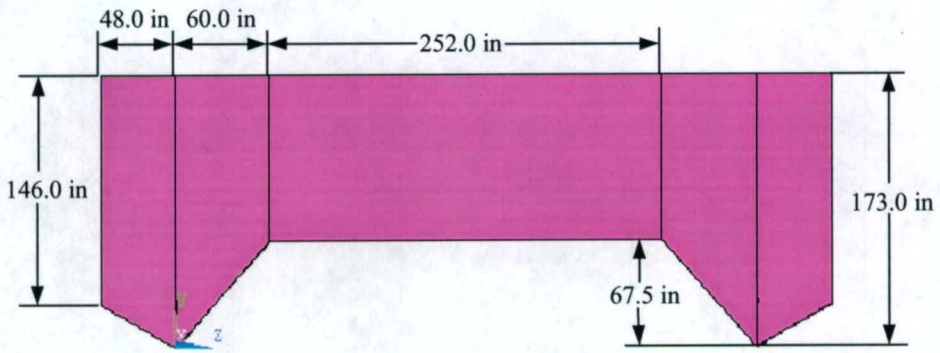

Figure 3.1b – SES 200 Hull Section

The dimensions for the hull, bulkhead and gusset locations and material properties are based on data obtained from the SES 200 FE model provided by CETEC Consultancy Ltd[1]. Because the primary purpose of the hull section model is to provide realistic boundary conditions for the lifting body struts, the level of detail in the model is kept to a minimum to reduce model size. All framing and stiffeners for the bulkheads and panels are omitted with the exception of the keel plates and gussets at the strut-hull interface. To compensate for removed structural detail orthotropic plate theory is used to generate equivalent material properties for the bulkheads and panels. Figure 3.2 illustrates the hull-framing scheme used for the model.

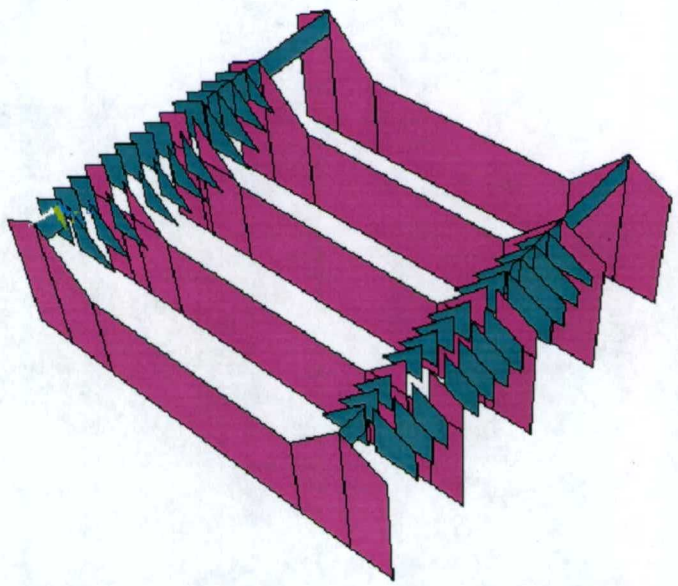

Figure 3.2 – SES 200 Hull Section Framing Scheme

3.3 Material Systems

Aluminum, 6061-T6, is used for the entire SES 200 hull. However, the hull plating and bulkheads are normalized to a uniform plate thickness of one-inch and the material properties are modified using orthotropic plate theory to represent the actual stiffened panels. The gussets surrounding the strut interface, and the keel in each hull consist of a 1/2-in aluminum plate. Table 3.1 summarizes the material models incorporated in the SES 200 hull section.

Table 3.1 – Material Properties

Material System	Properties								
	Ex ksi	Ey ksi	Ez ksi	G_{xy} ksi	G_{yz} ksi	G_{xz} ksi	nu_{xy}	nu_{yz}	nux_z
Aluminum	10,000	10,000	10,000	3,760	3,760	3,760	0.33	0.33	0.33
Orthodtropic Bulkheads	19.5	335,300	10,000	962	962	962	---	---	---
Orthodtropic Hull Plates	335,300	305.4	10,000	3,800	3,800	3,800	---	---	---

4. Complete Model: Lifting Body Combined with SES 200 Hull Section

4.1 Overview

The complete FE model, illustrated in Figure 4.1, combines the lifting body model with the SES 200 hull section model and consists of 24,119 elements, 192,952 nodes, and approximately 416,400 degrees of freedom. The global origin is maintained at the same location as the global origin for each individual model; On the leading edge of the port strut, at the strut-hull interface. With a successful model built various loading scenarios, boundary conditions and composite material systems can be investigated.

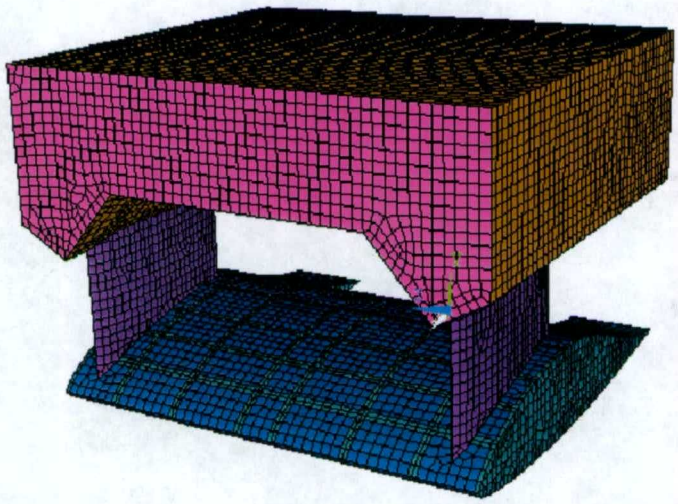

Figure 4.1 – Lifting Body Assembled with SES 200 Hull Section

4.2 Lifting Body and SES 200 Hull Connection

The struts of the lifting body extend 62.0-in into the SES 200 hull section and are reinforced with ½-in aluminum gussets on 20-in centers. Figure 4.2 illustrates the strut-hull interface of the port strut. To constrain the struts in the hull coincident nodes were created and constrained in all six degrees of freedom between the struts and hull. The constrained nodes correspond to the locations where the hull gussets and hull plating are joined to the struts. The purpose of this constraint method is to create a simple connection that is representative of welding the hull gussets to the struts.

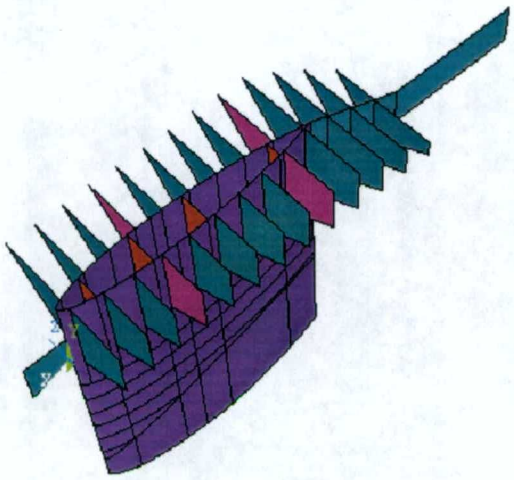

Figure 4.2 – Port Side Strut and SES 200 Strut Gussets

4.3 Boundary Conditions

The model boundary conditions are imposed on the perimeter of the forward most and aft most bulkheads of the SES 200 hull section, as shown in Figure 4.3. Two methods of constraining the perimeter nodes of the bulkheads are used; the primary method is to constrain the nodes in all six degrees of freedom. The second method utilizes analytically rigid beam links to connect the perimeter nodes to the approximate center of buoyancy of the lifting body. The primary purpose of tying the nodes to the center of buoyancy is to create a single reaction point for the model to aid in applying realistic hydrostatic and dynamic pressure loads. Further detail pertaining to the application of the pressure loads is discussed in Section 4.4.

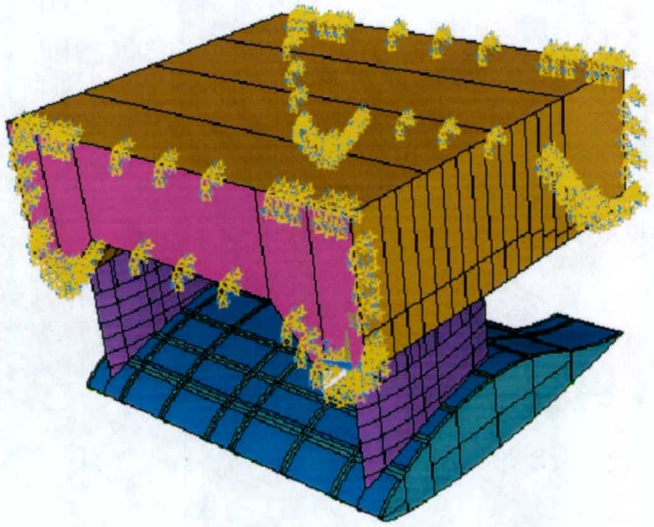

Figure 4.3 – Location of Bulkhead Perimeter Boundary Conditions

4.4 – Load Cases

Currently, four load cases have been examined with the existing model configuration: hydrostatic pressure load, dynamic pressure load, resultant drag load and resultant docking load. All load values utilized in the model are based on the loads document provided by NAVATEK and are available in Appendix A. Additional load scenarios may be examined in future efforts such as grounding, vertical load, nose-up and nose-down moments, and flap loads; however, current work has emphasized establishing a realistic pressure distribution on the lifting body.

The hydrostatic pressure load is based on the maximum draft of the lifting body, which is approximately 18.8 feet. A specific weight of 64.0 lb/ft^3, for seawater at 60^oF, is used to calculate the hydrostatic pressure gradient, which results in a maximum pressure of 8.5 psi at maximum draft and a pressure of 5.5 psi at the shallowest point on the top surface of the lifting body. Hydrostatic load is only applied to the top and bottom surface of the lifting body, with the pressure gradient illustrated in Figure 4.4. Hydrostatic load is not applied to the struts because the strut surfaces offer no net buoyant force to the model and are not areas of interest for composite panel locations. Additionally, the model does not include the port and starboard lifting body end caps, leaving no realistic method to apply pressure loads to the terminating bulkheads.

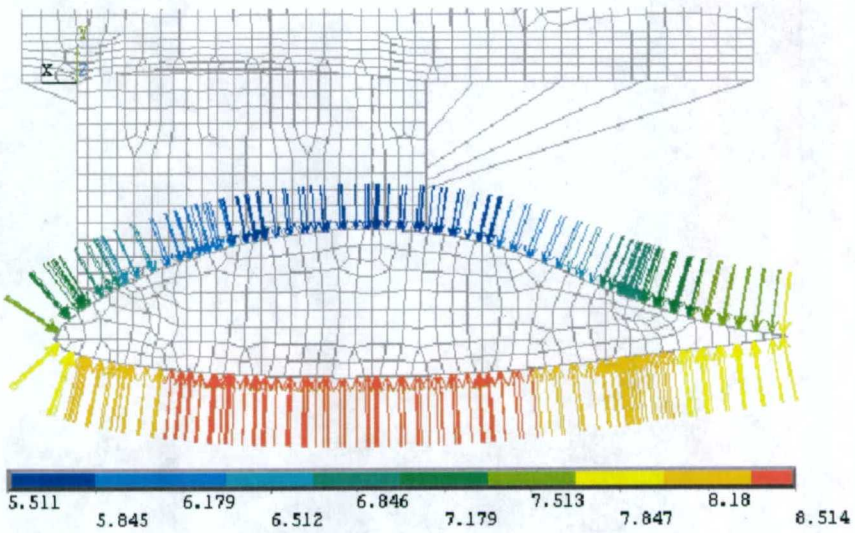

Figure 4.4 – Hydrostatic Pressure Load Applied to Lifting Body

The dynamic pressure load is based on the CFD results from the NAVATEK loads document, available in Appendix A, and corresponds to the pressure distribution at 35 knots. To apply the pressure distribution to the lifting body model data points from the CFD plots were graphed in Excel, and polynomial curve fits were generated for both the top and bottom surface. Figure 4.5 illustrates the top surface and bottom surface pressure distributions plotted as a function of the global x-position. A sixth order polynomial is fit to the top surface pressure data,

$$p = 1.009 \cdot 10^{-12} \cdot x^6 + 1.186 \cdot 10^{-9} \cdot x^5 + 5.172 \cdot 10^{-7} \cdot x^4 + 1.040 \cdot 10^{-4} \cdot x^3 + \ldots$$
$$\ldots + 1.096 \cdot 10^{-2} \cdot x^2 + 0.07398 \cdot x + 12.42$$

and a fourth order polynomial is fit to the lower surface pressure distribution,

$$p = -2.898 \cdot 10^{-9} \cdot x^4 - 2.720 \cdot 10^{-6} \cdot x^3 - 6.854 \cdot 10^{-4} \cdot x^2 - 6.436 \cdot 10^{-2} \cdot x - 7.644$$

where 'p' is pressure in psig and 'x' is the position on the lifting body in the global x-direction. The two dynamic pressure distribution equations are added to the hydrostatic pressure to produce one equation for each surface of the lifting body. Subsequently, the complete pressure distribution on the lifting body at 35 knots and maximum depth of 18.8 feet is represented in the model and is illustrated in Figure 4.6.

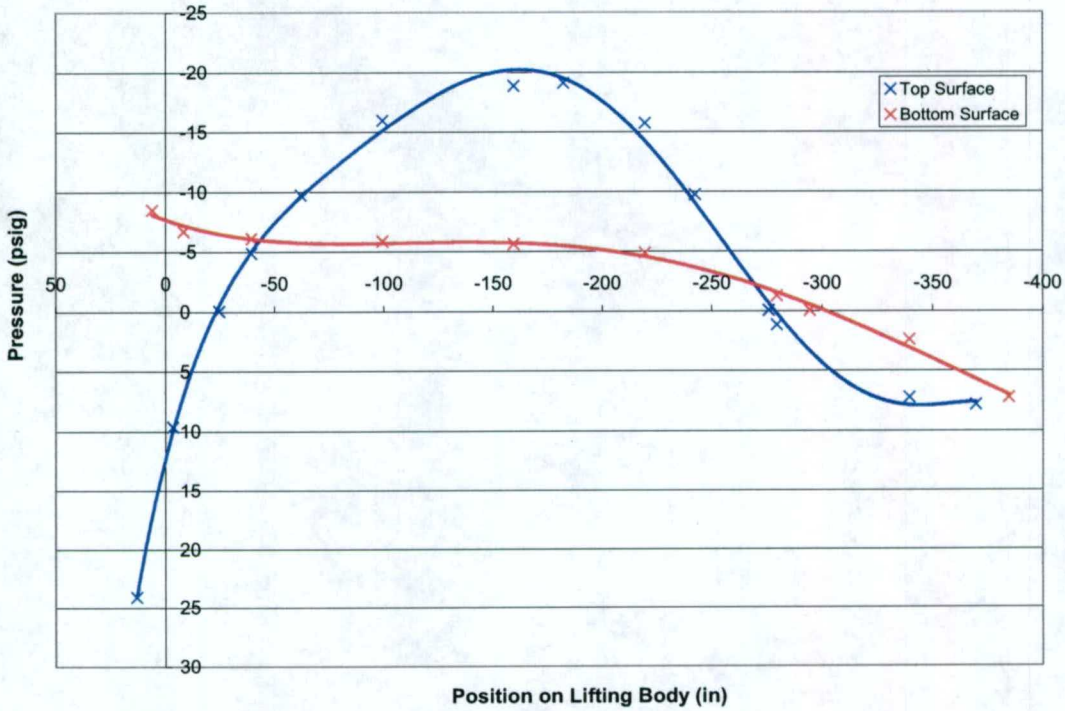

Figure 4.5 – Dynamic Pressure Distribution at 35 Knots

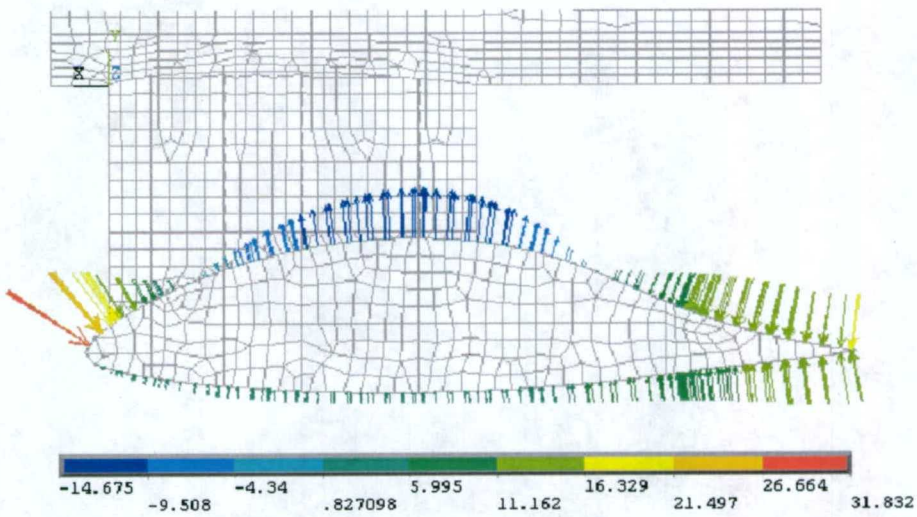

Figure 4.6 – Total Pressure Distribution at 35 Knots and 18.8 ft Draft

The drag load is approximated in the loads document (Appendix A) as a concentrated load of 40 LT at the center of gravity. To minimize stress concentrations in the FE model resulting from a drag load applied at a single node, the drag load is evenly distributed over the entire leading edge of the lifting body, as illustrated in Figure 4.7. Because the resultant drag load is moved approximately 12-in deeper and 75-in forward of the center of gravity, the moment generated at the strut-hull interface will increase. However, the area of interest for this effort revolves around establishing realistic loads and analysis techniques for composite panels and joints on the lifting body, not the structural design of the ship-hull interface. Therefore, the approximation of the drag load along the leading edge is a more practical and realistic loading scenario than applying a concentrated load on one node at the center of gravity.

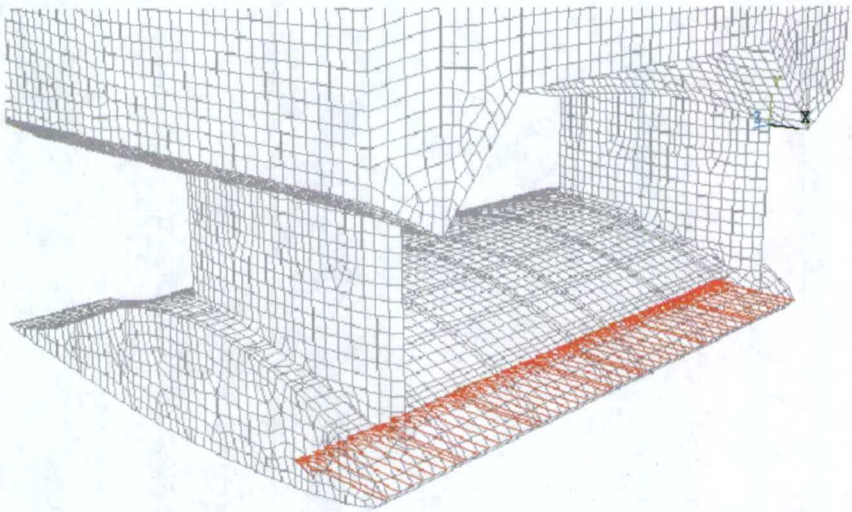

Figure 4.7 – Drag Load Distributed Along Lifting Body Leading Edge

The 170 LT docking load is distributed along the deepest transverse bulkhead on the port side as shown in Figure 4.8. A location for the docking load is not specified in the loads document, so the deepest transverse bulkhead appeared to be the most practical location to apply the load and minimize local stress concentrations. If further analysis is necessary pertaining to the application of docking loads then greater detail is necessary about the location of the docking loads and if the nature of these loads are impact loads, or quasi-static loads.

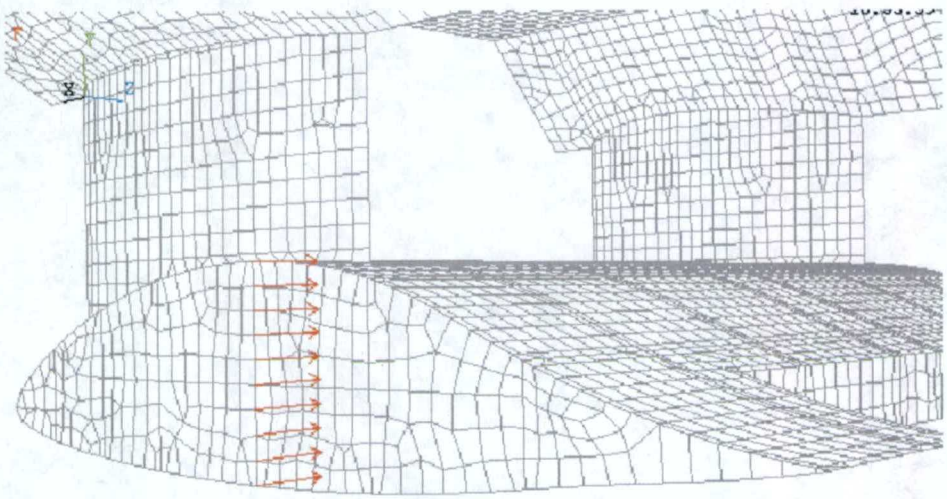

Figure 4.8 – Distributed Docking Load On Transverse Bulkhead

5. Baseline Aluminum Panel Model

5.1 Model Purpose

The purpose of the aluminum panel model is to generate a baseline FE model with equivalent panel stiffness to that of the existing aluminum H-body designed by Nigel Gee and Associates. The results of this model are used to aid in the evaluation of the composite panel system.

5.2 FE Model Development

The aluminum panel model is virtually identical to the composite panel model presented in Section 2, with the exception of the material system utilized for the lifting body surfaces. The existing lifting body panel design incorporates ¼-inch, 6061 T6 aluminum plate with five-inch by ¼-inch aluminum blade stiffeners on 12-inch centers. To incorporate the stiffened panels into the FE model, orthotropic plate theory is used to generate equivalent material properties to represent the stiffened plates using a uniform, one-inch thick panel. The equivalent properties for the blade stiffened, aluminum panels are summarized in Table 5.1. The primary reason for using orthotropic material properties in place of physically modeling the blade stiffeners is to maintain a manageable FE model size. Additionally, the goal of this model is to capture the panel stiffness on a global scale, not to perform a detailed panel analysis.

Table 5.1 – Panel Material Properties

Material System	Properties					
	Ex ksi	Ey ksi	Ez ksi	G_{xy} ksi	G_{yz} ksi	G_{xz} ksi
Orthotropic Panels	581	130,200	10,000	3,270	3,760	3,760

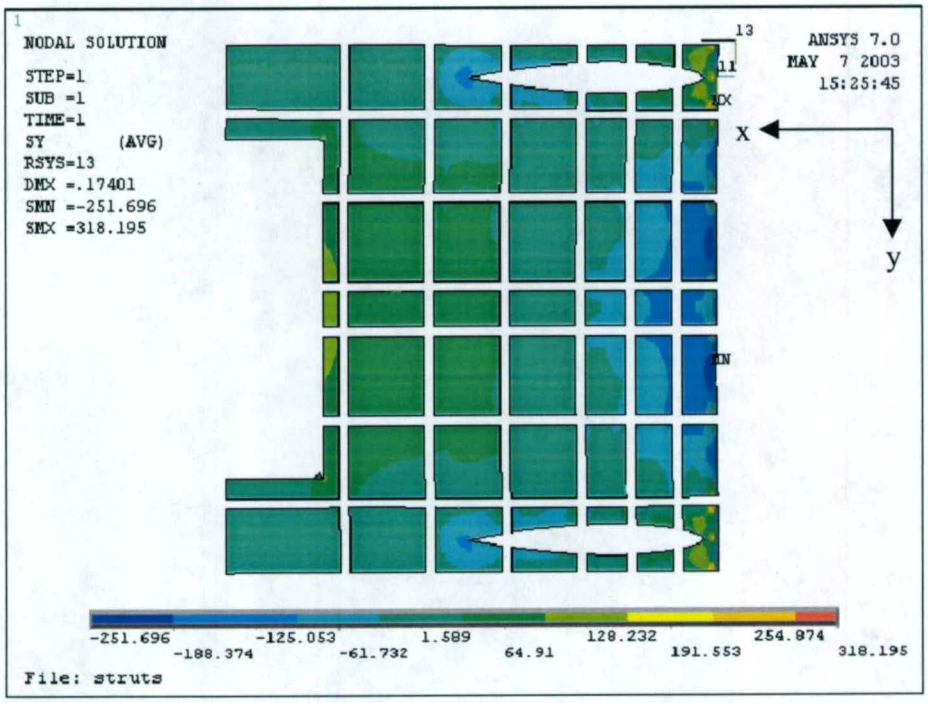

Figure 5.1 – Top Surface y-direction Stress Distribution, Layer Two

5.3 FE Model Results

The load case examined with the aluminum panel model is the total pressure distribution (hydrostatic pressure plus dynamic pressure) at 35 knots. Because the panels are modeled using equivalent orthotropic plate properties to represent the blade stiffened panels the stress distribution for the panels is not presented. However, the goal of this model is to develop a stiffness criterion for the composite panels based on the existing SES 200 lifting body, not perform a detailed structural analysis.

Figure 5.2 illustrates the global deflection of the entire model and Figures 5.3a-b illustrates the global and local deflection of the panels on the top and bottom surface of the lifting body.

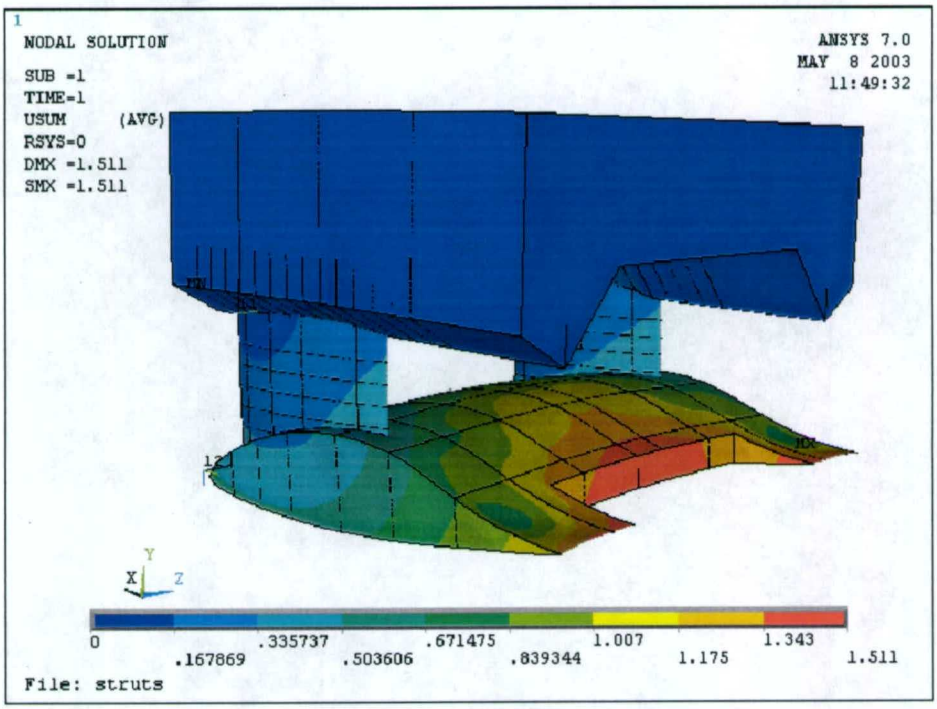

Figure 5.2 – Global Deflection Under Total Pressure Load at 35 Knots

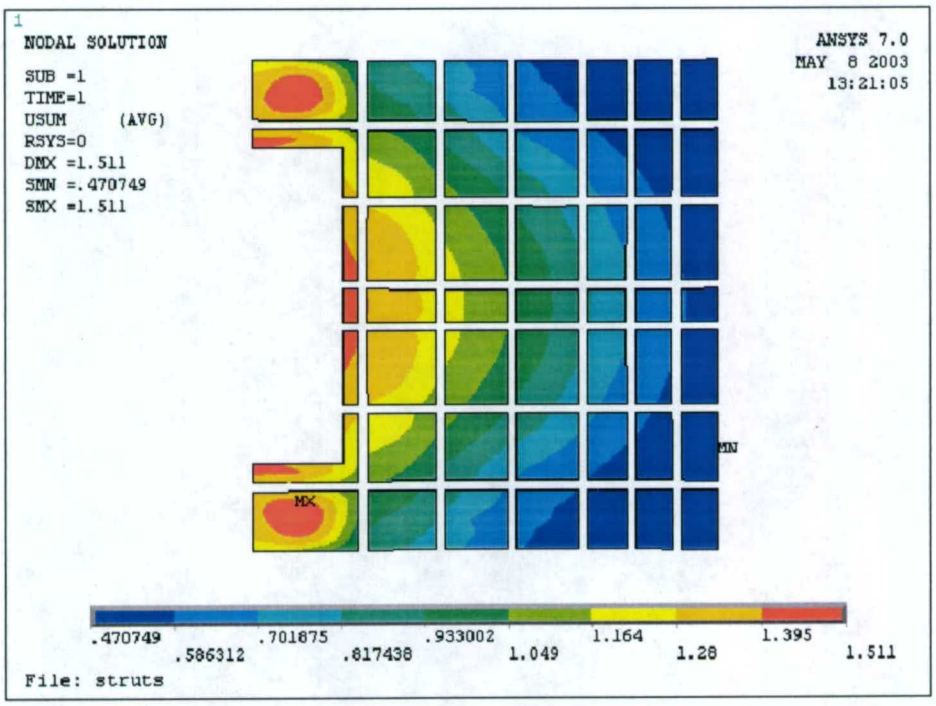

Figure 5.3a – Bottom Surface Deflection

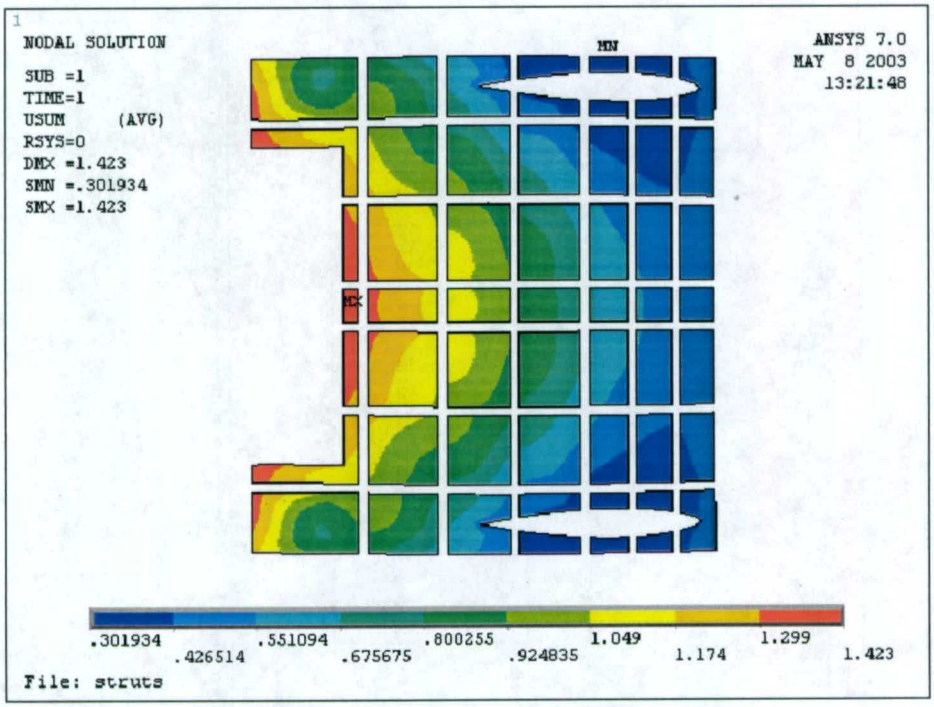

Figure 5.3b – Top Surface Deflection

6. FE Results for the Composite/Aluminum Hybrid System Using Sandwich Panels

6.1 Model Purpose

This section summarizes the results of the lifting body model utilizing an e-glass vinyl ester sandwich panel scheme in conjunction with the aluminum sub-frame. The results of this analysis are used to facilitate the design and analysis of hybrid joints at the University of Maine and were used to develop a full scale, hydrostatic panel testing system, discussed in Sections 11 through 13. Though the current models do not incorporate a detailed connection scheme for the panels, Section 8 summarizes a method to model the non-linear response of the hybrid joints. Additionally, this model is also utilized to evaluate the Von Mises stress in the aluminum sub frame to determine if lighter weight bulkheads are feasible.

For the purpose of achieving better resolution and clarity with the FE results the composite panels are removed from the aluminum sub frame after the analysis is performed, which permits evaluating the results of the aluminum sub frame and panels separately. The maximum in-plane stress and through-thickness shear stress of the core is presented in a predefined local element coordinate system; with the orientation displayed in all of the contour plot figures. The composite material system, summarized in Section 2, consist of 13 layers, which includes a two-inch core. Layer one corresponds to the outboard layer of the laminate, while layer 13 corresponds to the inboard layer of the laminate for all composite panels on the lifting body. All stress values in this section are presented in units of lb/in^2 and all displacement values are displayed in inches.

6.2 Hydrostatic Pressure Results

The maximum in-plane stress in the element local x-direction occurs at the outer most layers of the laminate, layers one and 13. Figures 6.1a-b illustrates the results for layer 13, however, the results for layer one are similar in magnitude with the exception of a sign change for most of the panels due to local panel bending. The maximum in-plane stress in the local y-direction occurs at layers two and 12. The outer most layer of the laminate does not carry the highest stress in the y-direction due to the laminate schedule;

layers one and 13 are 0^{o} layers, while layers two and 12 are oriented at 90^{o} with respect to the element local x-direction. Figures 6.2a-b illustrates the maximum in-plane stress in the element local y-direction for layer 12.

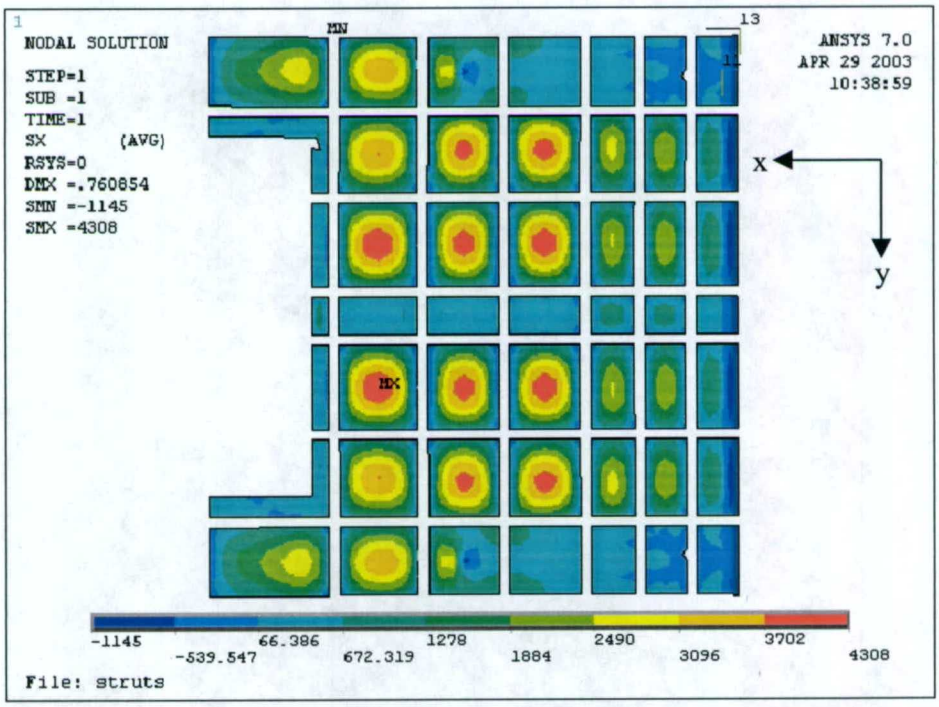

Figure 6.1a – Bottom Surface x-direction Stress Distribution, Layer 13

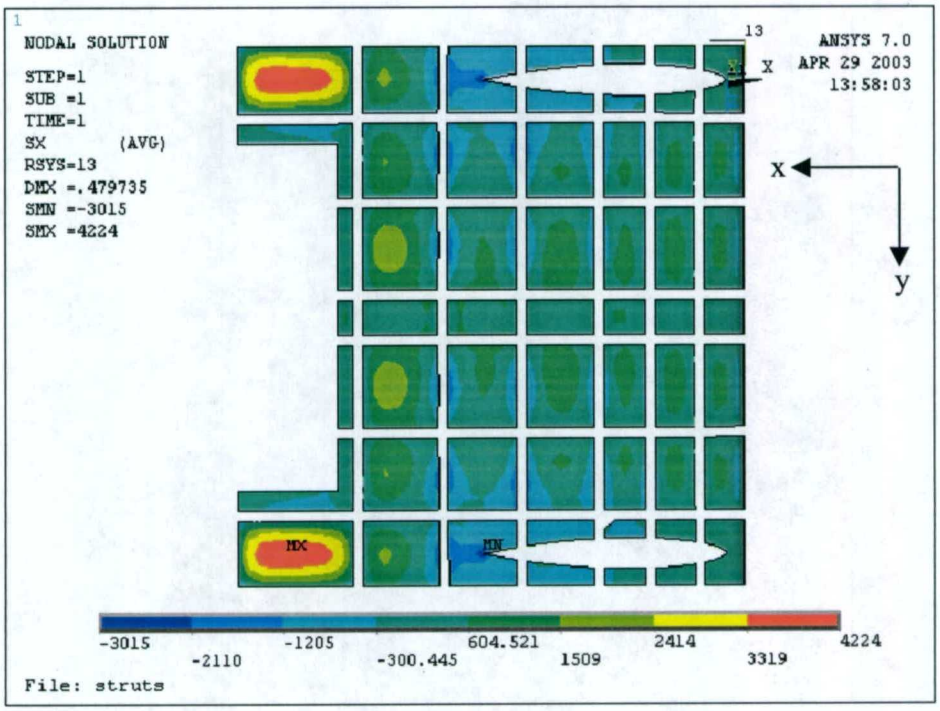

Figure 6.1b – Top Surface x-direction Stress Distribution, Layer 13

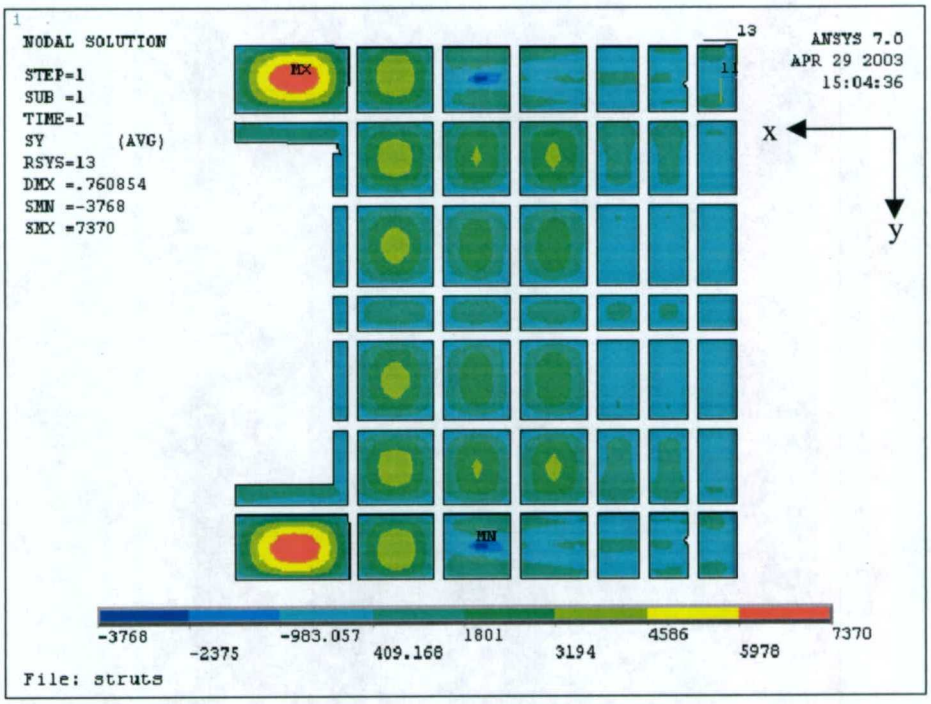

Figure 6.2a – Bottom Surface y-direction Stress Distribution, Layer 12

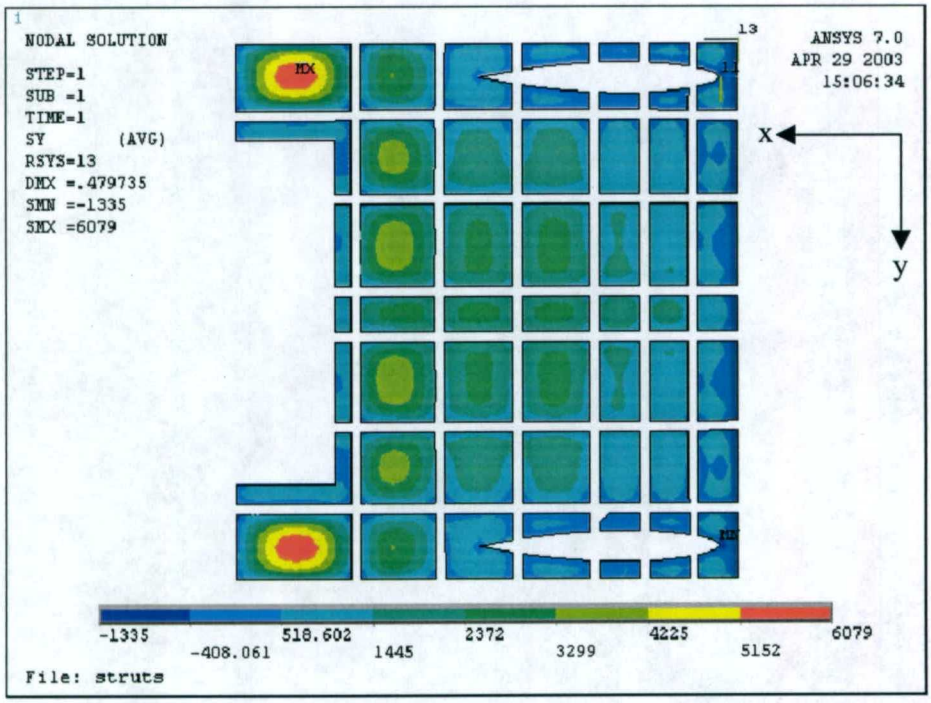

Figure 6.2b – Top Surface y-direction Stress Distribution, Layer 12

The maximum in-plane shear stress in the element local coordinate system occurs on the outer most layers, layers one and 13, and is approximately ±1580-psi. Figure 6.3a-b illustrates the in-plane shear stress for layer one. The shear stress for the core is also low, with maximum values of ±11-psi for in-plane shear and maximum values of ±14-psi for the through-thickness shear stress.

The maximum local panel deflection and global deflection of the lifting body occur on the bottom surface of the lifting body and are illustrated in Figure 6.4. While only the panels are shown in Figure 6.4, the maximum global deflection is based on the maximum deflection of the bulkheads, which is approximately 0.4-in.

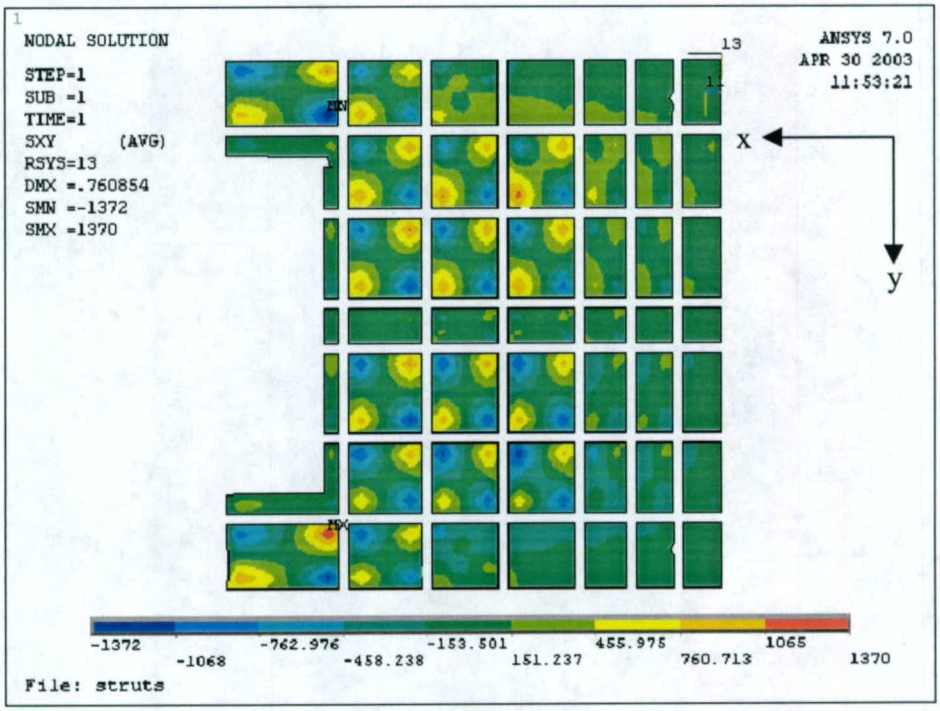

Figure 6.3a – Bottom Surface In-plane Shear Stress, Layer One

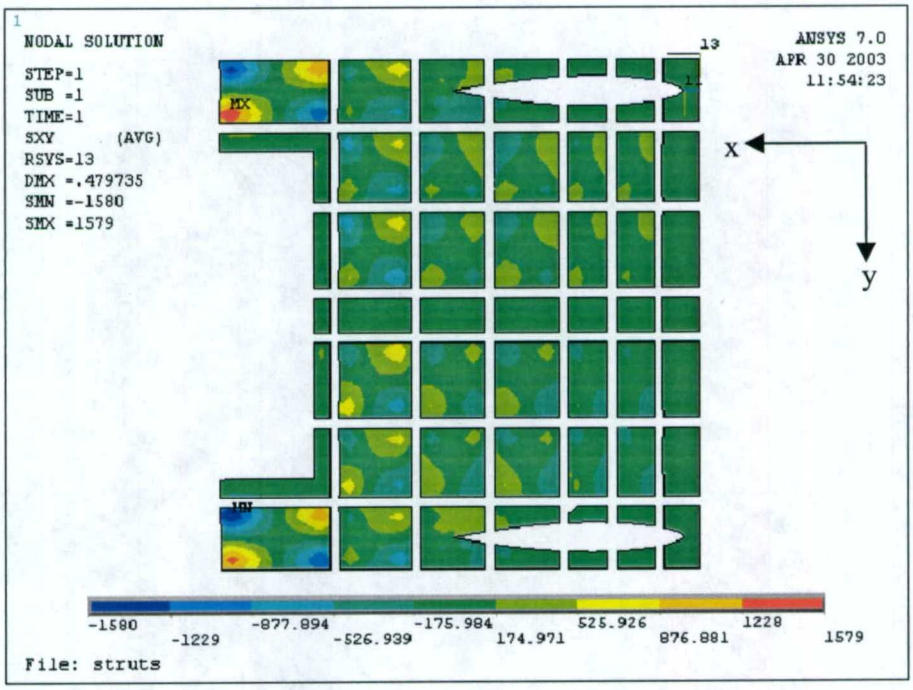

Figure 6.3b – Top Surface In-Plane Shear Stress, Layer One

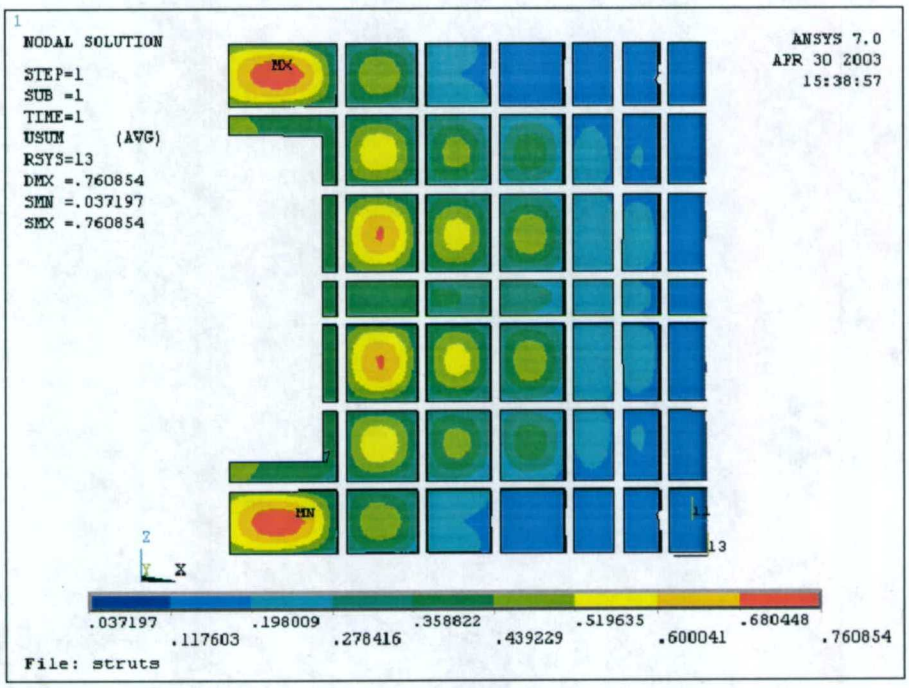

Figure 6.4 – Bottom Surface Deflection

6.3 Total Pressure Results at 35 Knots

The results in this section pertain to the resultant total pressure distribution on the lifting body at maximum depth and speed of 35 knots, as described in Section 4.4. The maximum in-plane stress in the element local x-direction occurs in layers one and 13. The stress distribution in the x-direction is illustrated in Figure 6.5a-b for layer one, which has slightly higher maximum stress values than layer 13. Due to the laminate schedule, as described in Section 6.1, the maximum in-plane stress in the element local y-direction occurs in layers two and 12. Figure 6.6a-b illustrates the y-direction stress distribution for the top and bottom surface of the lifting body for layer 12, which has slightly higher maximum stress values than layer 2.

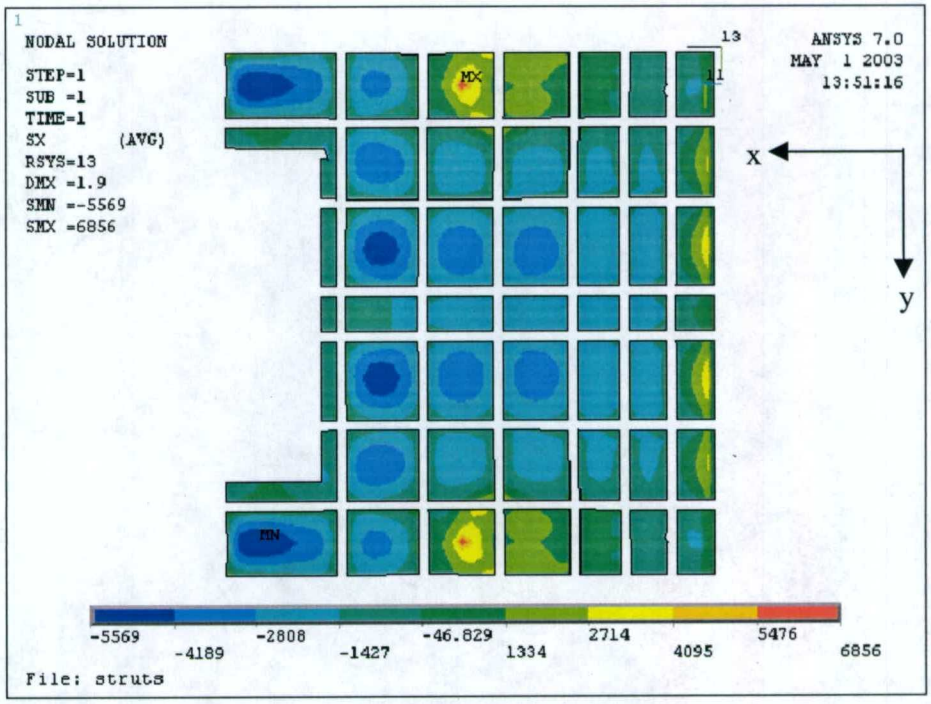

Figure 6.5a – Bottom Surface x-direction Stress Distribution, Layer One

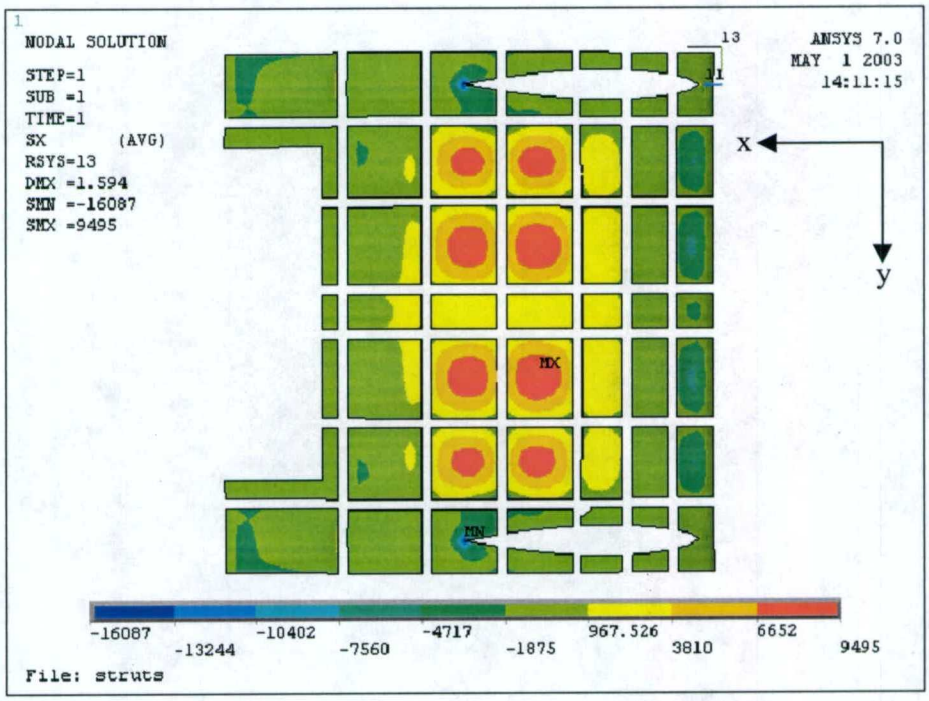

Figure 6.5b – Top Surface x-direction Stress Distribution, Layer One

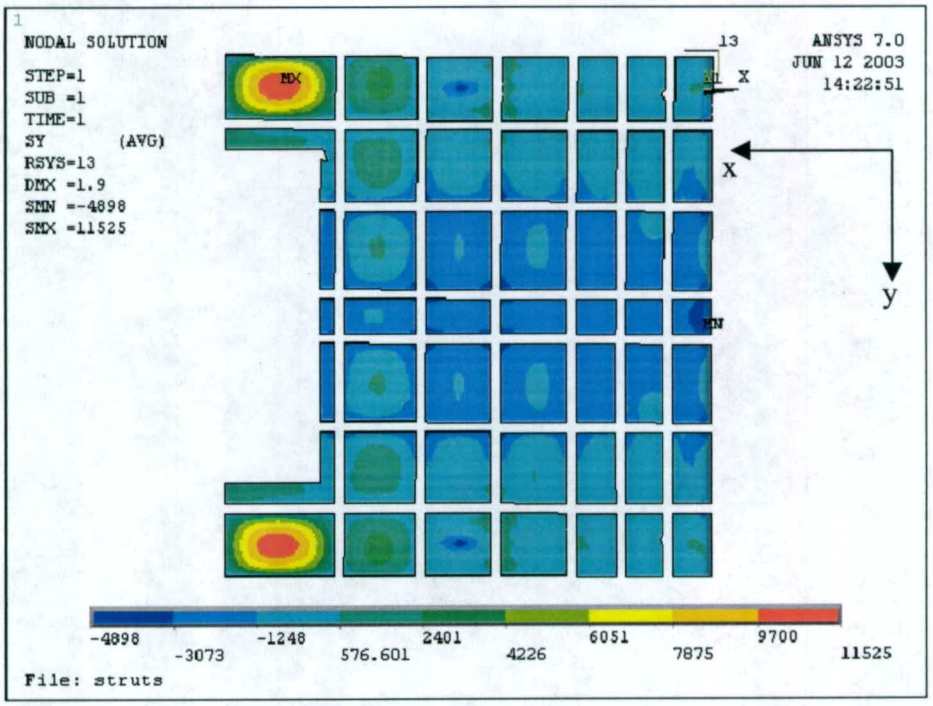

Figure 6.6a – Bottom Surface y-direction Stress Distribution, Layer 12

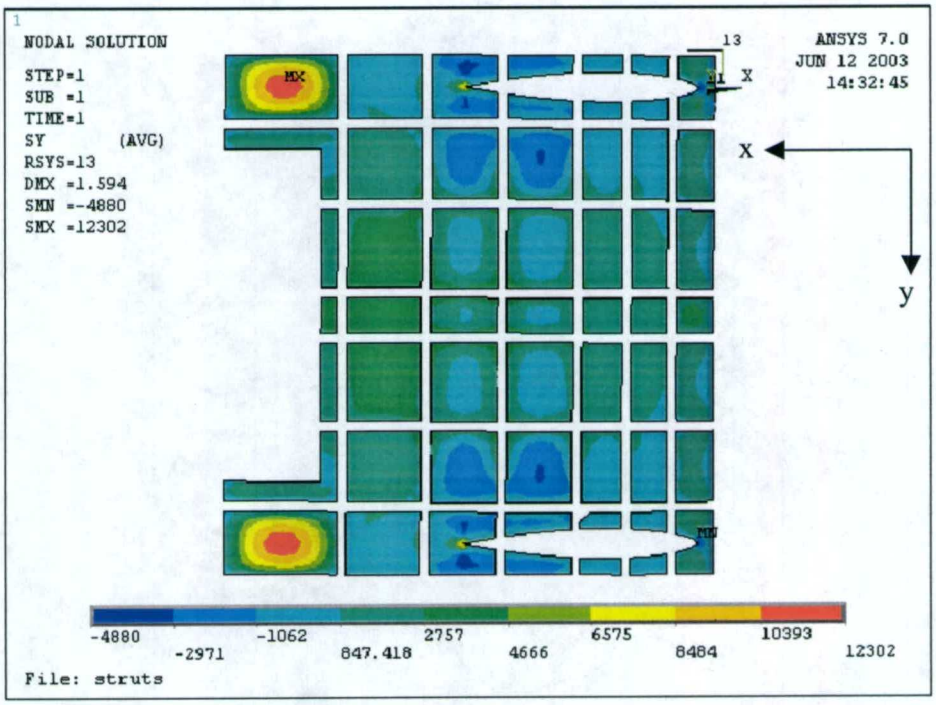

Figure 6.6b – Top Surface y-direction Stress Distribution, Layer 12

The maximum in-plane shear stress in the element local coordinate system occurs in the outer most layers of the composite panels, layers one and 13, with the results for layer 13 illustrated in Figures 6.7a-b. The in-plane shear stress and the through-thickness shear stress for the core is low, with maximum values of ±38-psi and ±52-psi respectively.

Similar to the hydrostatic load case, maximum panel deflections occur on the bottom surface of the lifting body, and are illustrated in Figure 6.8. However, the negative pressure distribution that occurs on a large area of the lifting body top surface results in an outward local deflection of several panels on the top surface. Figure 6.9 illustrates the local panel deflection at the top surface of the lifting body. The maximum global deflection is approximately 1.5-in. and occurs on the aft sections of the two center longitudinal bulkheads.

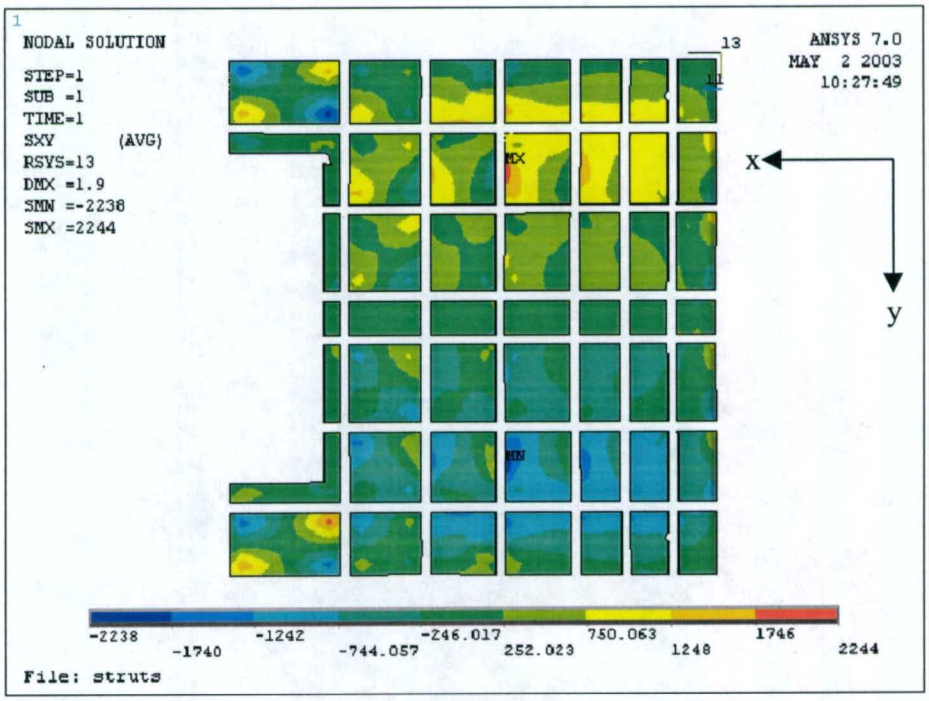

Figure 6.7a – Bottom Surface In-plane Shear Stress, Layer 13

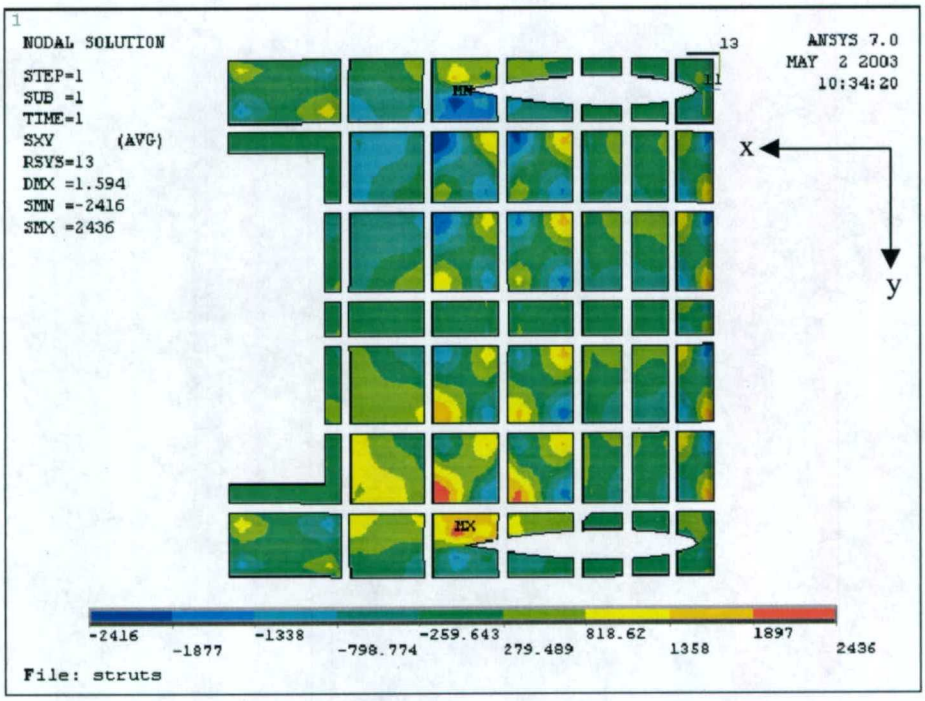

Figure 6.7b – Top Surface In-plane Shear Stress, Layer 13

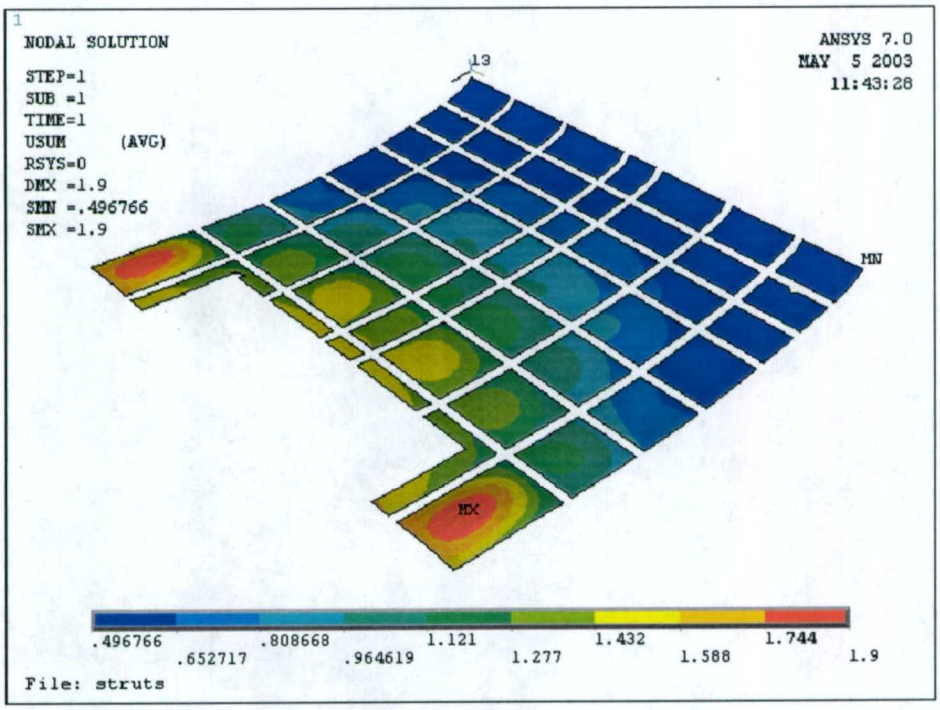

Figure 6.8 – Bottom Surface Deflection

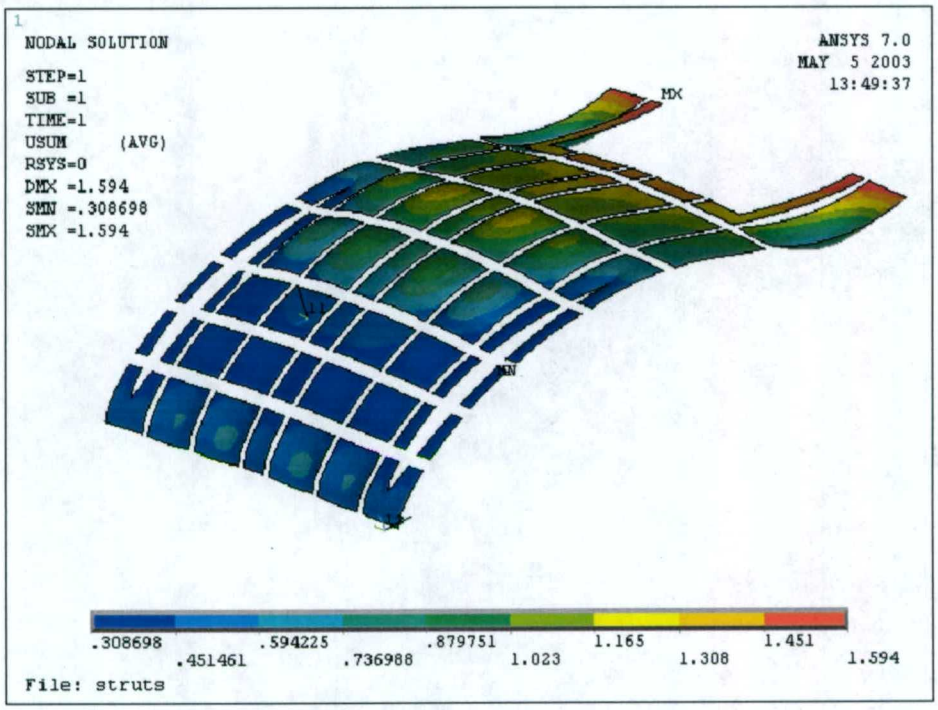

Figure 6.9 – Top Surface Deflection

The Von Mises stress in the aluminum sub frame of the lifting body is illustrated in Figure 6.10. The higher stress values of approximately 34,000-psi are only present in some of the riders on the corners of the transverse bulkhead cutouts, as illustrated in Figure 6.11. These higher stress concentrations are likely due to the relatively course mesh for the size of the rider radius. However, for a global FE model of large magnitude stress concentrations of this nature are expected. Additional mesh refinement has not been initiated because the details of the existing aluminum sub frame are not considered a priority at this point in time.

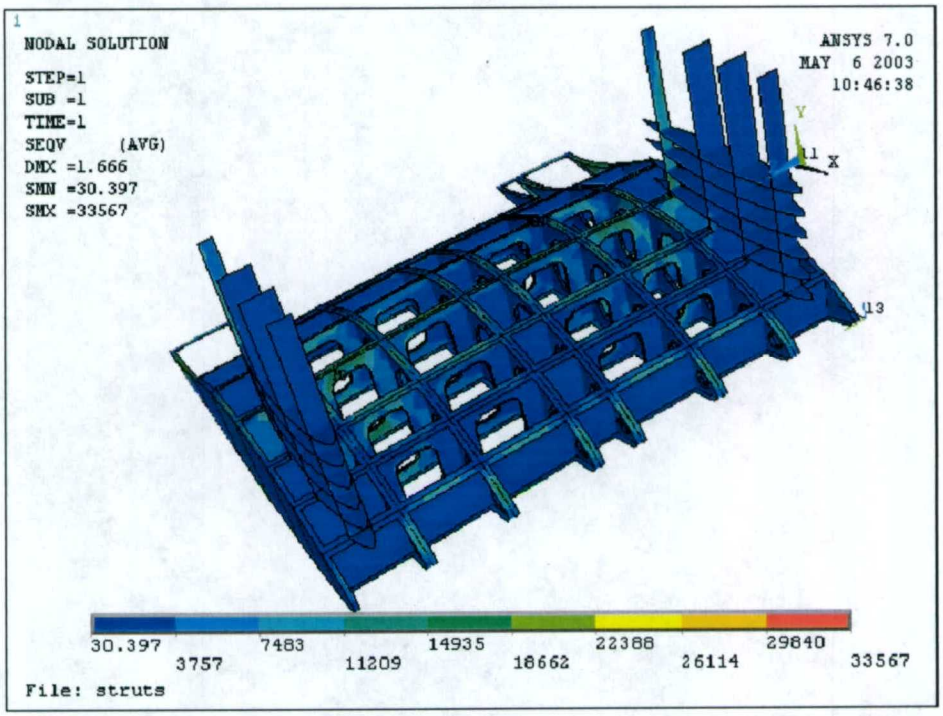

Figure 6.10 – Von Mises Stress in Lifting Body Frames

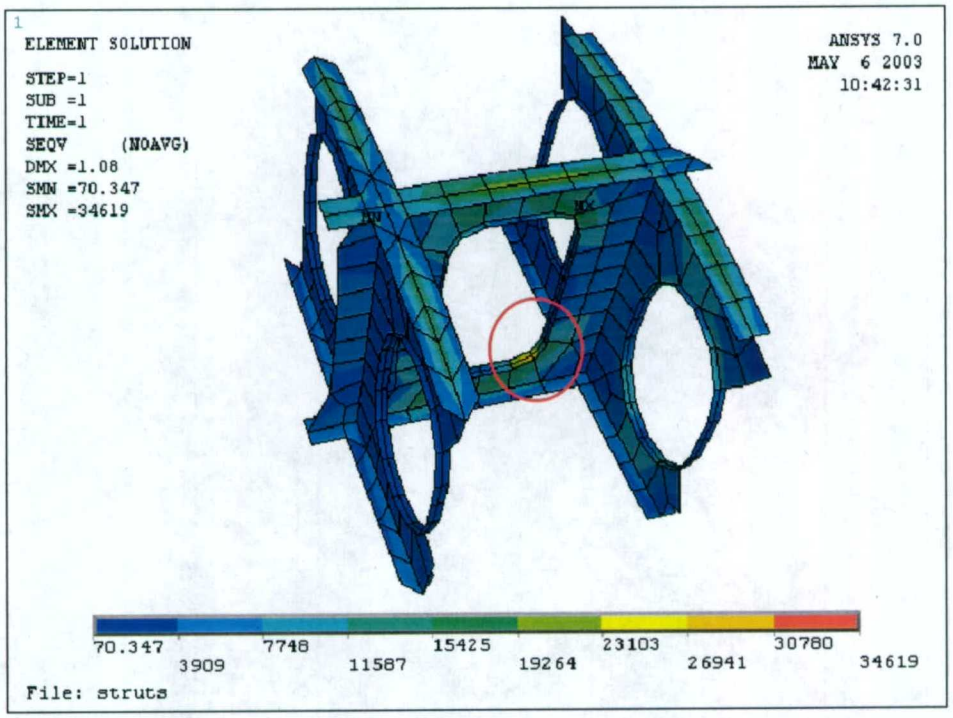

Figure 6.11 – Detail of High Stress Area, Von Mises Stress

6.4 Docking Load Results

The 170 LT docking load applied to the port side of the lifting body results in a maximum global deflection of approximately 1.9-in and is illustrated in Figure 6.12. The stresses generated in the composite panels are relatively low with the maximum stress values occurring on the top surface of the lifting body in the vicinity of the strut-lifting body interface. Figure 6.13 illustrates the in-plane stress for layer 13 in the element local x-direction, and Figure 6.14 illustrates the in-plane stress for layer 12 in the local y-direction. The maximum in-plane shear stress occurs in layer one and 13 on the top surface of the lifting body and is illustrated in Figure 6.15 for layer 13. The maximum Von Mises stress for the aluminum sub frame occurs in the struts, at the strut-hull interface and the strut-lifting body interface as shown in Figure 6.16.

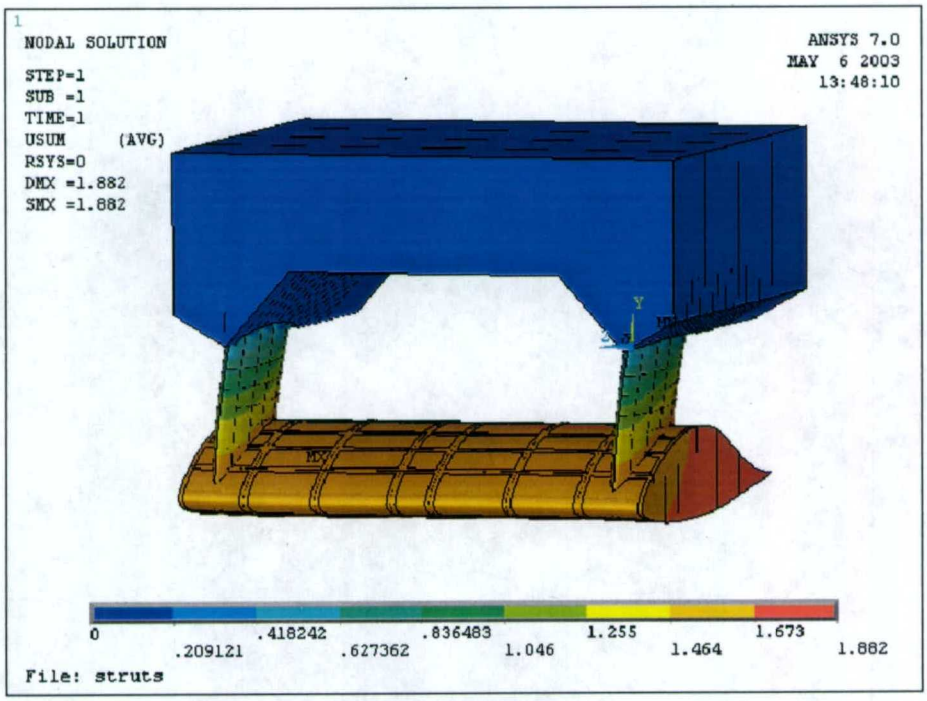

Figure 6.12 – Global Deflection Under 170 LT Docking Load

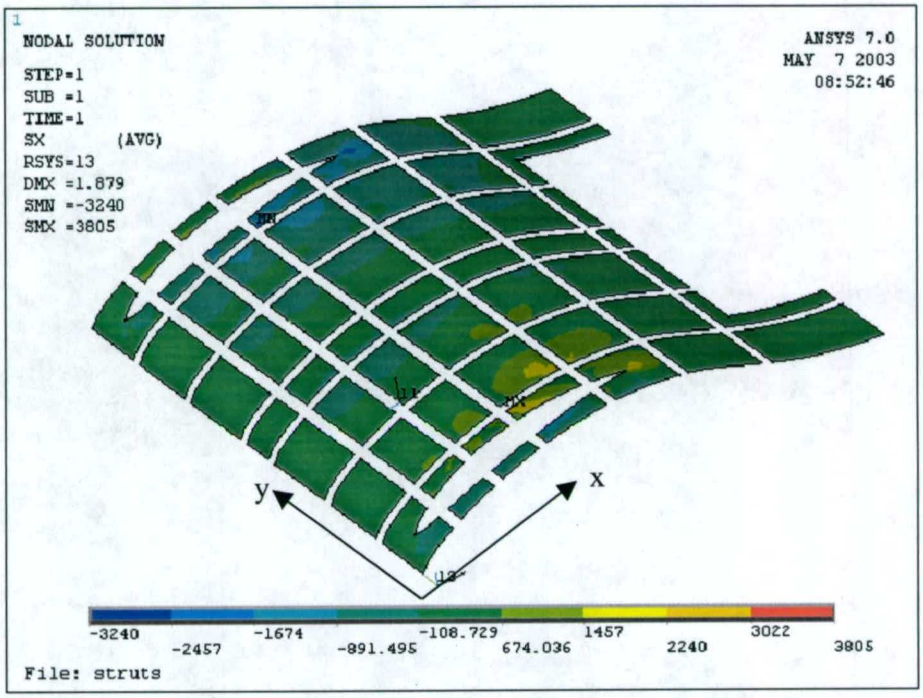

Figure 6.13 – Top Surface x-direction Stress Distribution, Layer 13

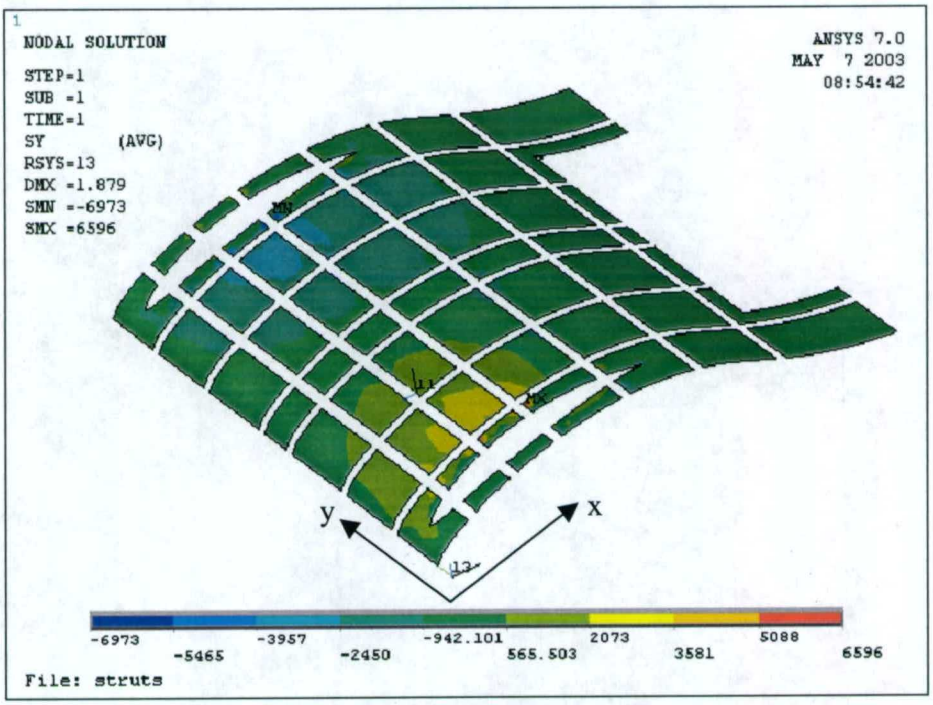

Figure 6.14 – Top Surface y-direction Stress Distribution, Layer 12

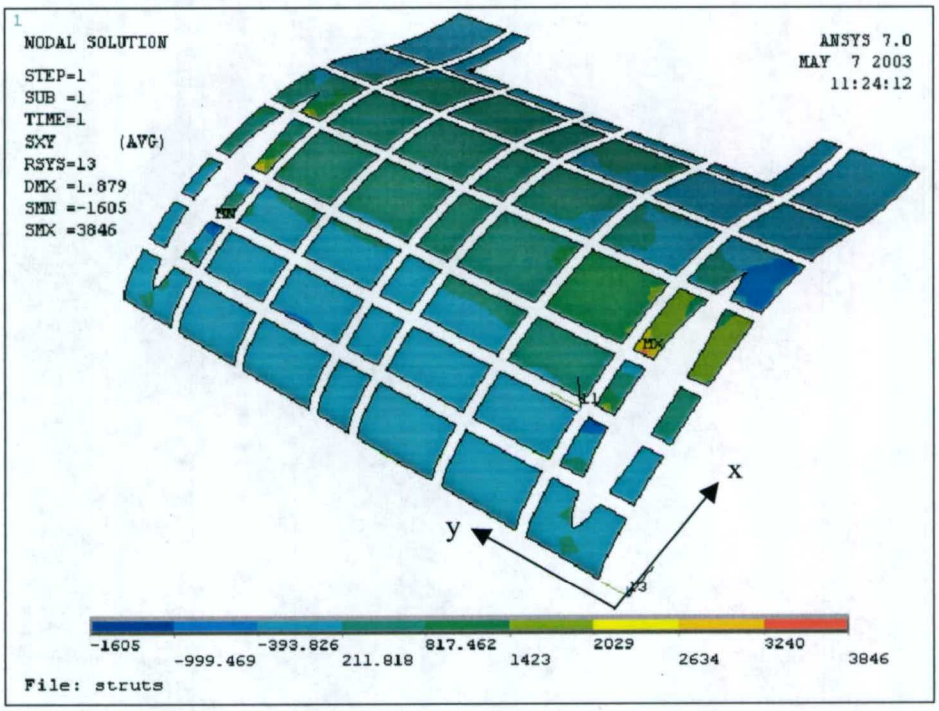

Figure 6.15 – Top Surface In-plane Shear Stress, Layer 13

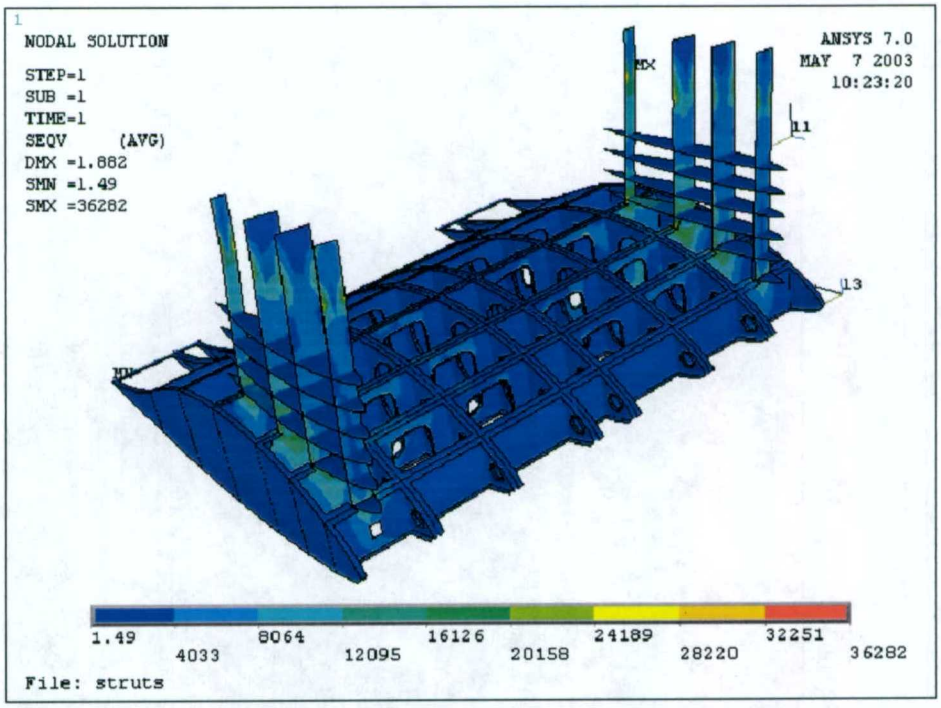

Figure 6.16 – Von Mises Stress in Aluminum Sub Frame

6.5 Drag Load Results

The 40 LT drag load applied to the leading edge of the lifting body results in very low stress values for both the composite panels and aluminum framing. The global deflection of the model is illustrated in Figure 6.17. Because the maximum stress values are consistently low for all composite panel layers, only the stress distributions where the maximum stress values occur in the x and y element local coordinate system are presented and illustrated in Figures 6.18 and 6.19. The maximum Von Mises stress in the aluminum sub frame is approximate ±1,200-psi, while the maximum through thickness shear stress in the core is only 3-psi.

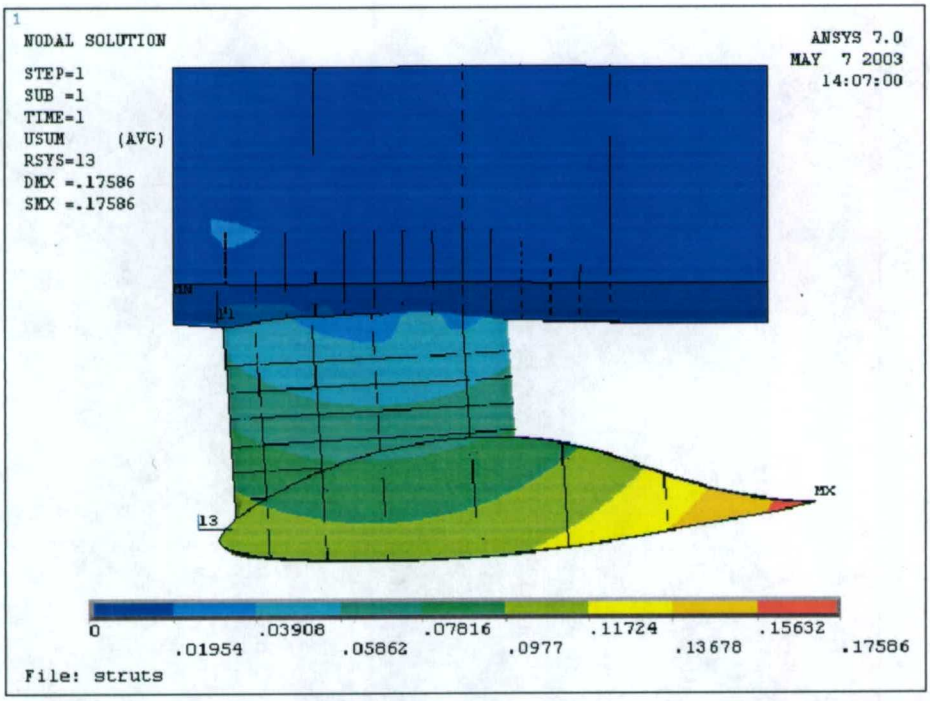

Figure 6.17 – Global Model Deflection Under 40 LT Drag Load

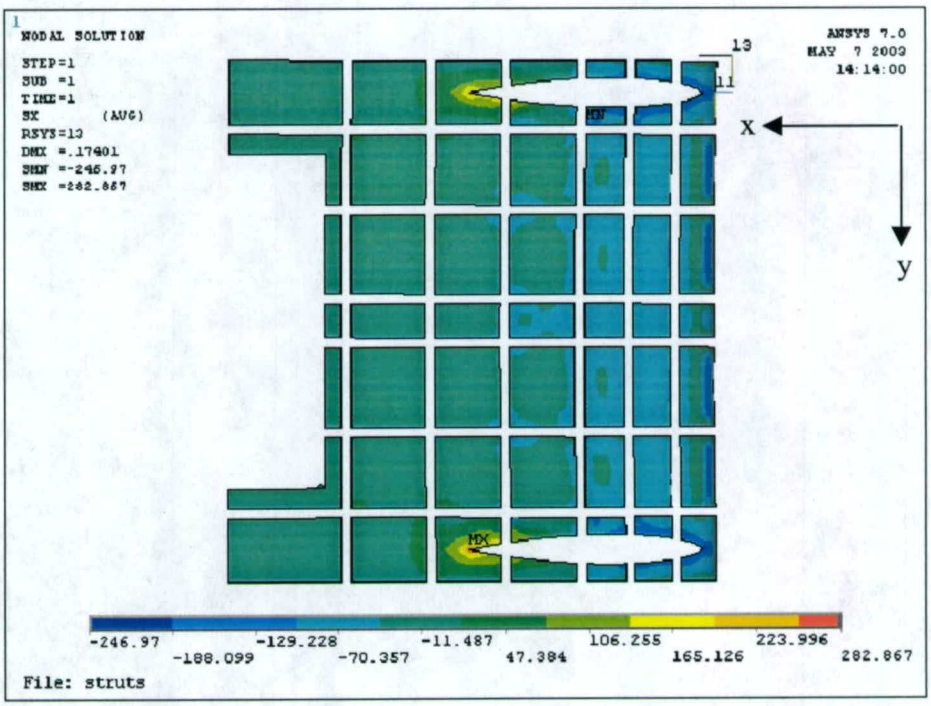

Figure 6.18 – Top Surface x-direction Stress Distribution, Layer One

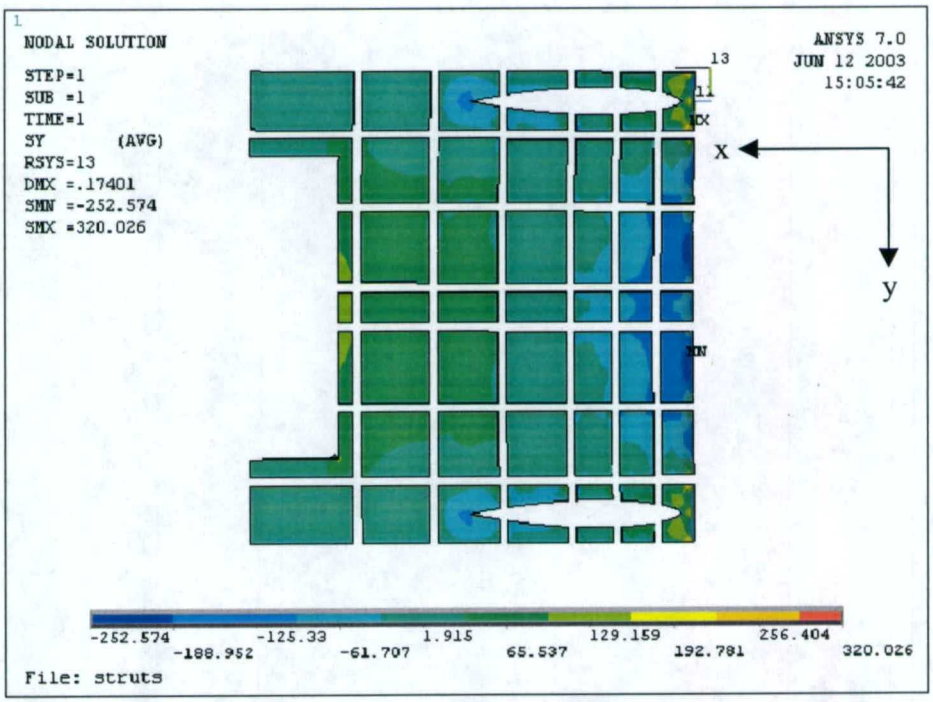

Figure 6.19 – Top Surface y-direction Stress Distribution, Layer Two

7. Composite Panel Optimization for Strength and Weight Reduction

7.1 Purpose of the Model

The purpose of this section is to detail efforts to determine the effects of panel lay-up, materials and panel stiffener configuration on the weight per square foot of panel. Additionally, efforts to determine the effects of frame/bulkhead spacing and weight on the overall structural weight will be presented and discussed.

7.2 Panel Finite Element Models

Figure 7.1 shows a typical finite element model constructed for this work. The finite element method was chosen to evaluate panel performance, as deflection under a given uniform load was the design criteria chosen. The finite element method gives us the ability to evaluate local, between stiffeners, panel deflections as well as global deflection. Other analytical methods smear the stiffeners to produce an effective panel rigidity and local panel effects cannot be evaluated properly.

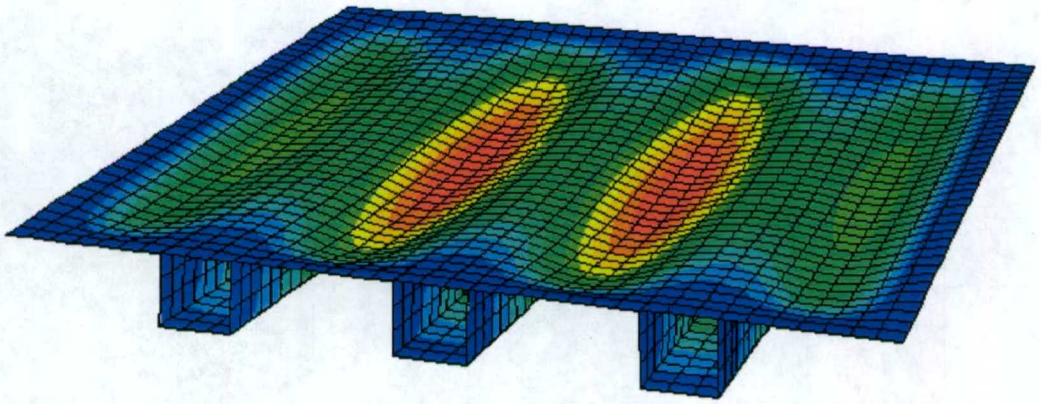

Figure 7.1 – Typical Finite Element Model Showing Three Equally Spaced Stiffeners

The panels considered for this effort are square, flat and simply supported. A uniform pressure of 10 psi was applied to the top face of the model. The peak deflection allowed in the panels is 0.08 inches. This criterion was established by evaluating an existing aluminum stiffened panel from the current lifting body. The base panel is ¼ inch aluminum plate stiffened with 5-inch deep ¼ inch thick blade stiffeners 1 foot on center.

7.3 Panel Configurations

The material system considered in this study is e-glass/vinyl ester, chosen for its current cost effectiveness and wide spread use in the marine industry. The panels considered are 4, 6, 8 and 10 feet square monocoque, hat stiffened monocoque and balsa-cored panels. A variety of stiffener configurations were considered in this work. The stiffener dimensions were varied from 6, 9, 12, and 15 inches square. There was no attempt to optimize the shape of the stiffeners; they were kept as squares for simplicity. The number of equally spaced stiffeners varied from 1 to 6 depending on panel and stiffener size.

7.4 Sub-frame Weight Estimate

Figure 7.2 shows the sub-frame of the existing lifting body design. The longitudinal bulkheads are labeled L1 through L3. The transverse bulkheads are labeled T1 through T6. To estimate the average weight per foot of this framework the distance along the perimeter of each section was measured using ANSYS™ Pre/Post. The weight of each section was determined using ANSYS by applying a gravity load to each section. The results are tabularized in table 7.1.

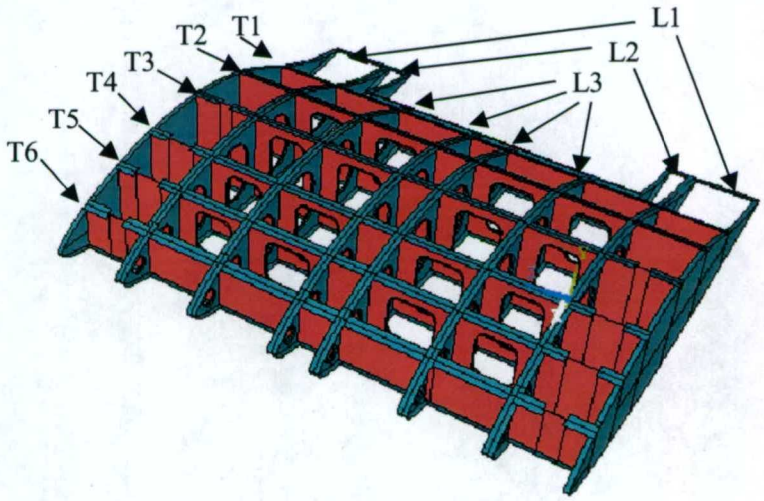

Figure 7.2 – Existing Lifting Body Bulkhead/Frame Assembly

Table 7.1 - Bulkhead Weight and Perimeter Dimensions

Description	Quantity	Weight	Perimeter	Sub-Total Weight	Sub-Total Perimeter
L1	2	1197 lbs.	68.8 ft.	2394 lbs.	137.6 ft.
L2	2	1138 lbs.	68.8 ft.	2276 lbs.	137.6 ft.
L3	4	1028 lbs.	56.2 ft.	4112 lbs.	224.8 ft.
T1	1	1357 lbs.	72 ft.	1357 lbs.	72 ft.
T2	1	1904 lbs.	72 ft.	1904 lbs.	72 ft.
T3	1	2078 lbs.	72 ft.	2078 lbs.	72 ft.
T4	1	1942 lbs.	72 ft.	1942 lbs.	72 ft.
T5	1	1635 lbs.	72 ft.	1635 lbs.	72 ft.
T6	1	1394 lbs.	72 ft.	1394 lbs.	72 ft.
			TOTAL	19092	932
			lb/ft	20.5	

The average weight per foot of the existing bulkhead/framing is 20.5 lb/ft.

7.5 Results and Discussion

The panel study was conducted based on the maximum local deflection criteria. The lifting body was designed using ¼ inch aluminum plate stiffened with 5-inch deep ¼ inch thick blade stiffeners 1 foot on center. A uniform pressure of 10 psi was applied to the top face of the simply supported finite element model. The peak local deflection of the aluminum panel was 0.08 inches. The maximum local deflection of each of the composite panels presented in this study did not exceed 0.08 in. Figures 7.3 through 7.6 present the results of the panel study for the 4', 6', 8', and 10' square panels respectively. The study suggests that when possible an odd number of stiffeners should be used. The odd number of stiffeners places a stiffener at the mid-span of the panel. Additionally, the stiffener width dimension should produce equally spaces "blades" created by the height component of the stiffeners. This is demonstrated in Figure 7.7a-b showing the 4' and 6' panel dimensions schematically viewed from the end of the panel.

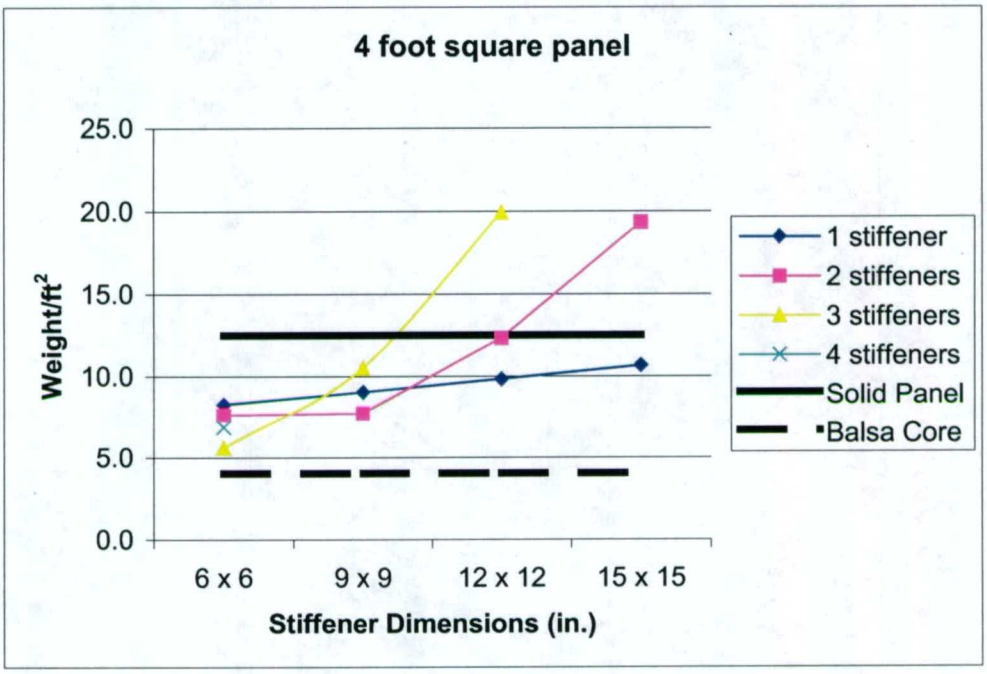

Figure 7.3 – Four Foot Square Panel Study

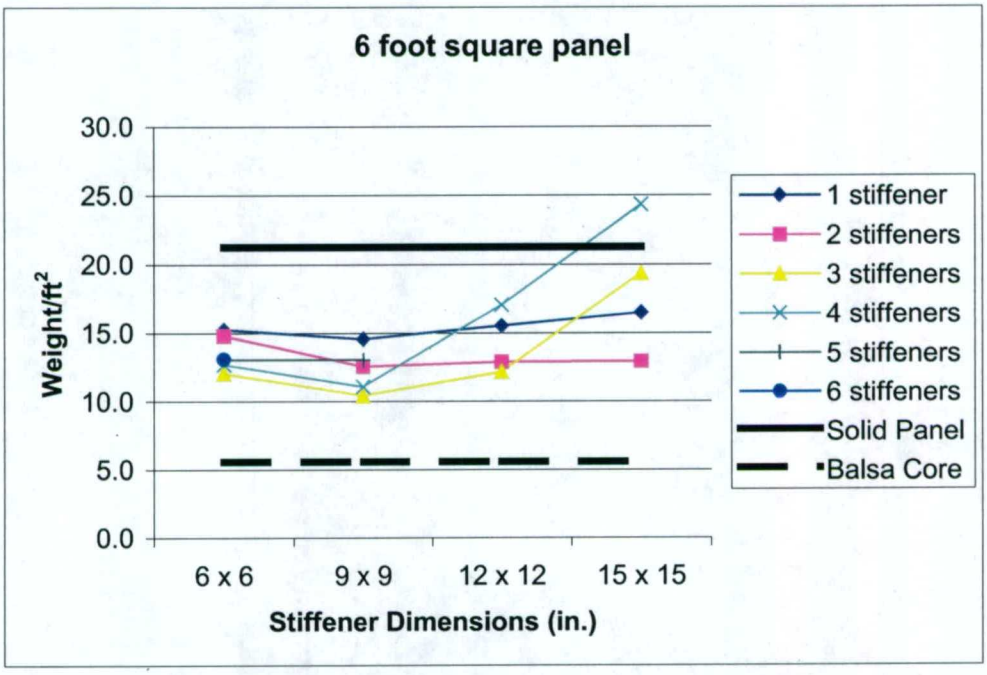

Figure 7.4 – Six Foot Square Panel Study

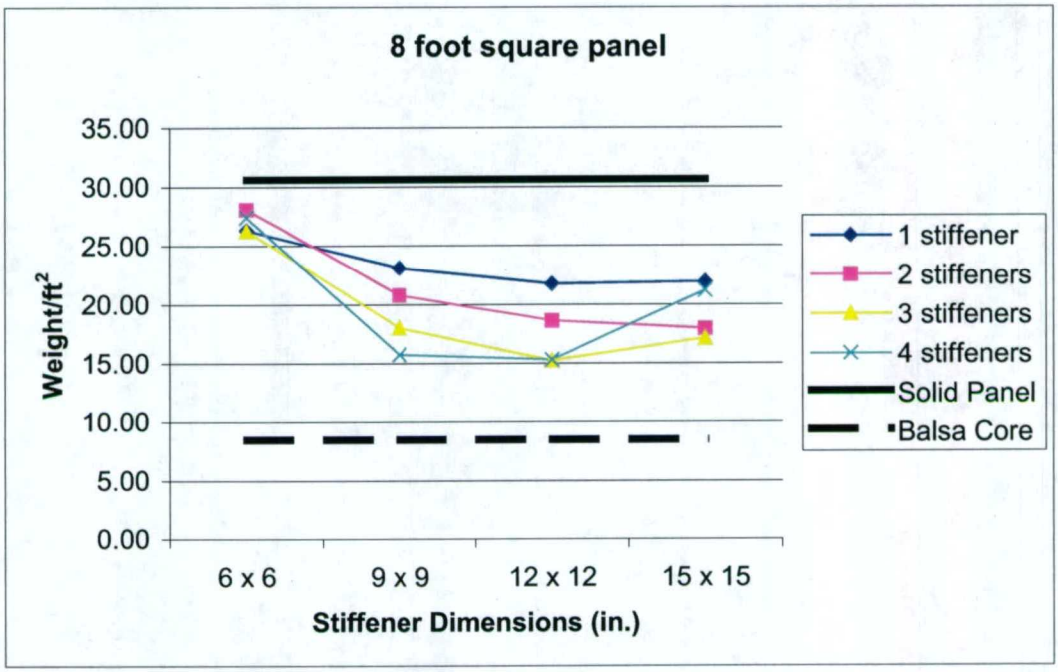

Figure 7.5 - Eight Foot Square Panel Study

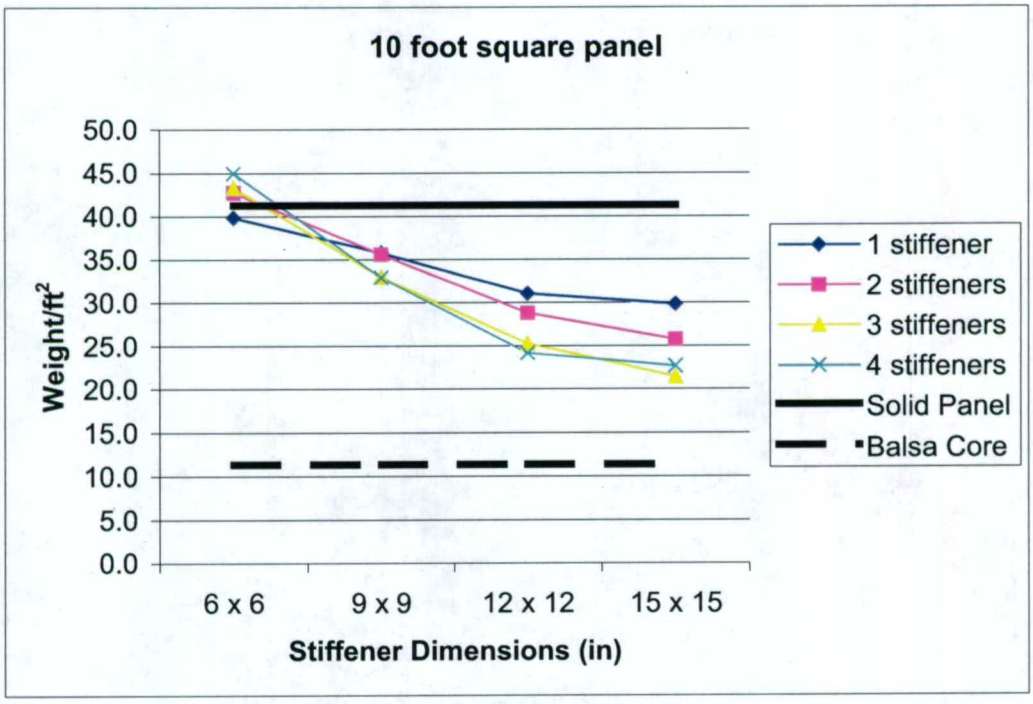

Figure 7.6 - Ten Foot Square Panel Study

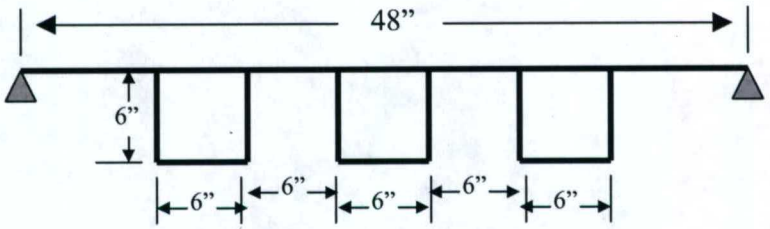

(A)

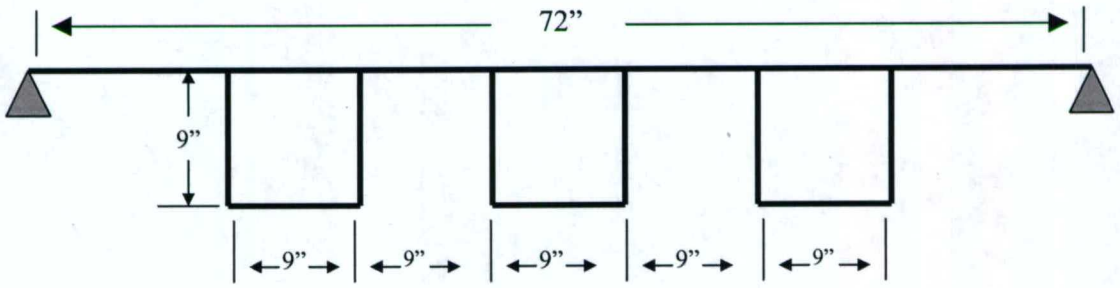

(B)

Figure 7.7 – Four Foot and Six Foot Square Panels

Minimum weights for each of the hat stiffened square panels were recorded and shown in Figure 7.8. A power function curve fit demonstrates how the weight of hat stiffened composite panels would increase over a practical range of panel framing for ship construction.

From a total weight stand point one must consider the location and weight of the framing as well as the panel weight. An "effective" weight per square foot of the panel system can be determined by:

- Measure the length around the perimeter of the square panel
- Multiply the weight per foot of the stiffener by the length of the perimeter above
- Divide this weight by 2 (two adjacent panels will use the same stiffener)
- Add the stiffener weight to the weight of the panel (Effective total weight)
- Divide the Effective total weight by the area of the plate (Effective weight per sq. ft.)

For the lifting body under consideration it was previously approximated that the aluminum bulkhead/frame weight per linear foot was approximately 20 lb/ft. Figure 7.9 presents the effects of frame weight combined with the panel weight. The curve marked with the triangles (20 lb/ft) shows the current lifting body configuration. As can be seen from this curve an optimal frame spacing for weight consideration would be 5 feet, which is approximately the lifting body design.

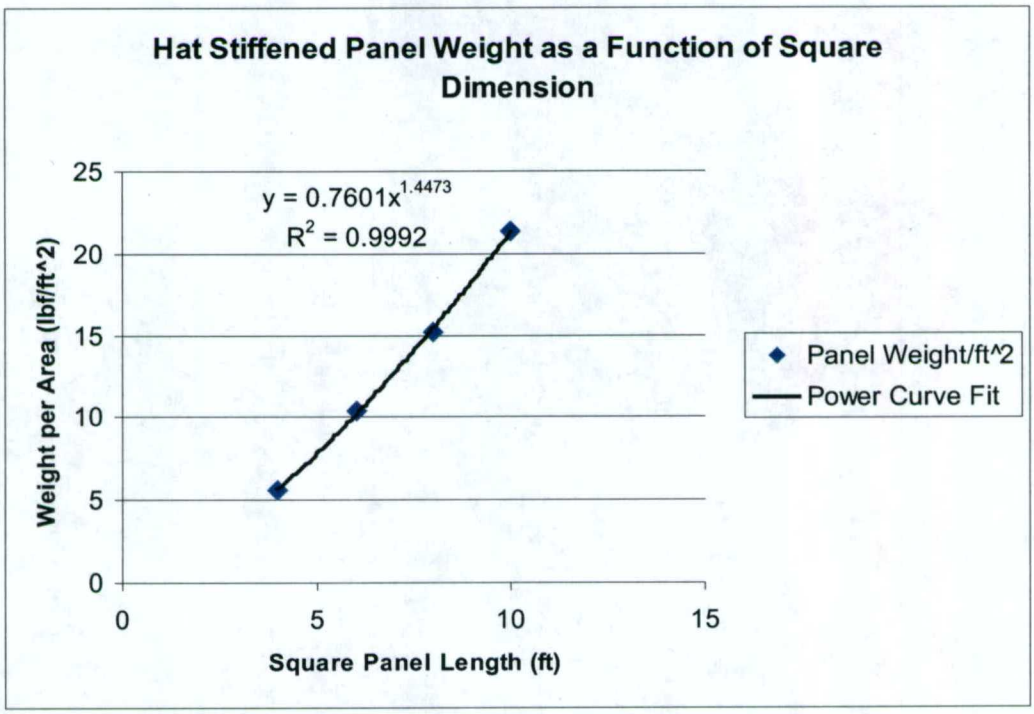

Figure 7.8 - Hat Stiffened Panel Weights as a Function of Panel Size

The 0, 10, 30 and 40 lb/ft frame weights are to demonstrate the effects of the frame weight the "effective" total weight of the frame and panel structural system. As can be seen from the curves shown in Figure 7.9 the right side of the graph shows that the panel weight as the dominating effect, while the left side of the graph shows the framing weight as the dominating effect. The design point for this trade would be where the slope of the curve approaches zero, a local minimum.

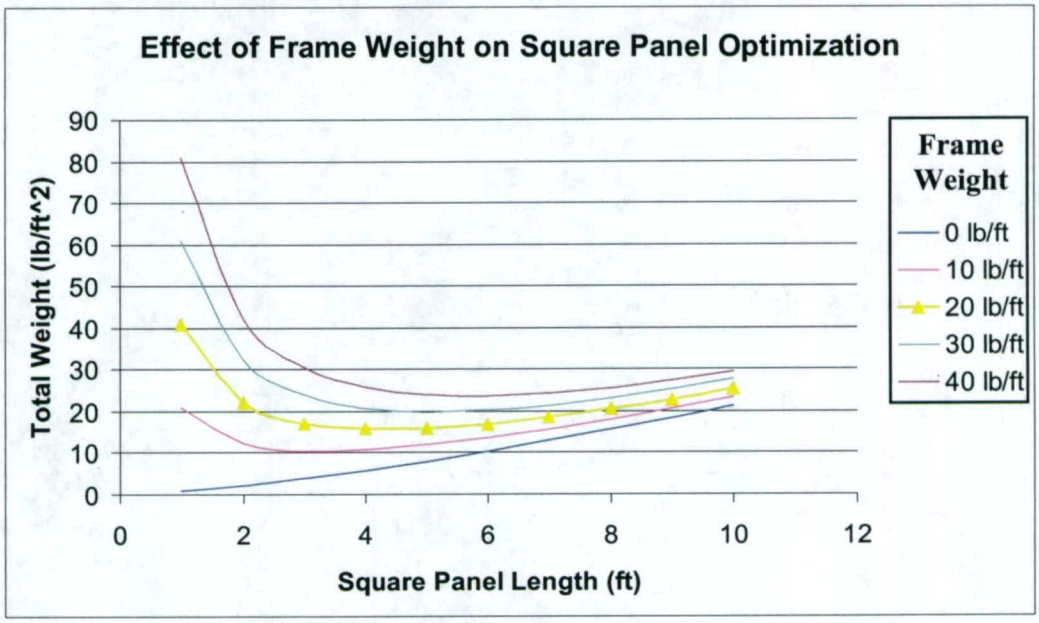

Figure 7.9 - Effect of Framing Weight

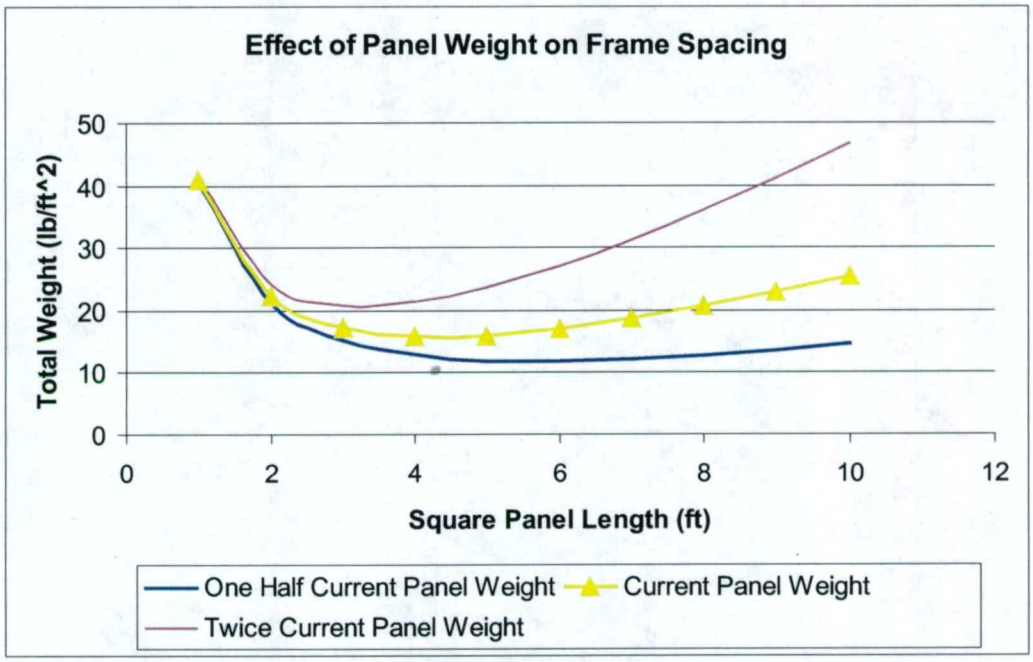

Figure 7.10 - Effects of Panel Weight

Figure 7.10 shows the effect of panel weight on the frame spacing. The curve annotated with the triangles shows our current weight panel as a function of square panel length with a 20 lb/ft frame. If for some reason one were required to make design changes that doubled the panel weight, the top curve in Figure 7.10 indicates that the design choice would be to increase the number of frame stiffeners effectively decreasing the panel size to approximately 3.5 ft square. Then conversely, if the panel weigh could be halved, the design choice would be to make panel dimensions of approximately 7 square feet. For completeness, one should consider the effects of frame location and weight on a fixed panel weight.

Figure 7.11 shows the effects of frame location and weight on a panel. A fixed panel weight of 17 lb/ft^2 was selected as both an 8-foot square hat stiffened monocoque panel and a ½ inch steel plate would weigh approximately 17 lb/ft. The results of this are obvious, the heavier the framing the heavier the "effective" panel weight will be and the curve drops similar to 1/X.

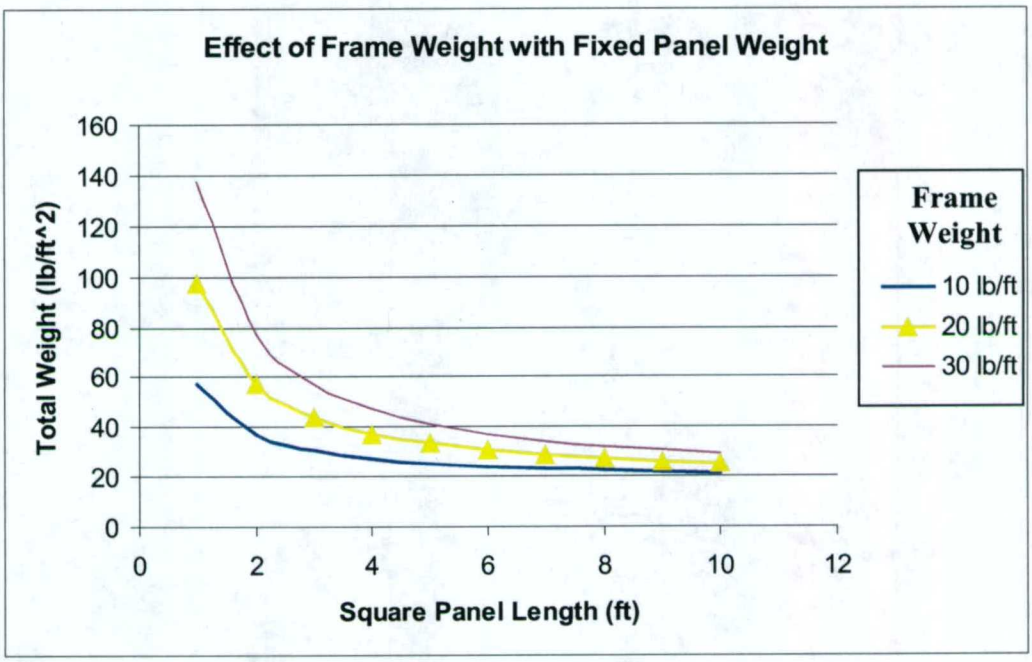

Figure 7.11 - Effects of Frame Weight

8. Nonlinear Connection Model and Response

8.1 Purpose of the Model

As a result of the hydrostatic load shown in Figure 4.4 and the hydrostatic plus dynamic load shown in Figure 4.6, the panels on the top of the lifting body are expected to experience surface pressure differentials that will cause the panel to bend out of plane in both directions. Therefore the connection must be capable of withstanding out of plane bending in both the positive and negative direction.

Figure 8.1 shows a test specimen undergoing downward load, during this type of loading the composite panel is pressed into the metallic substructure resulting in a simple rotation

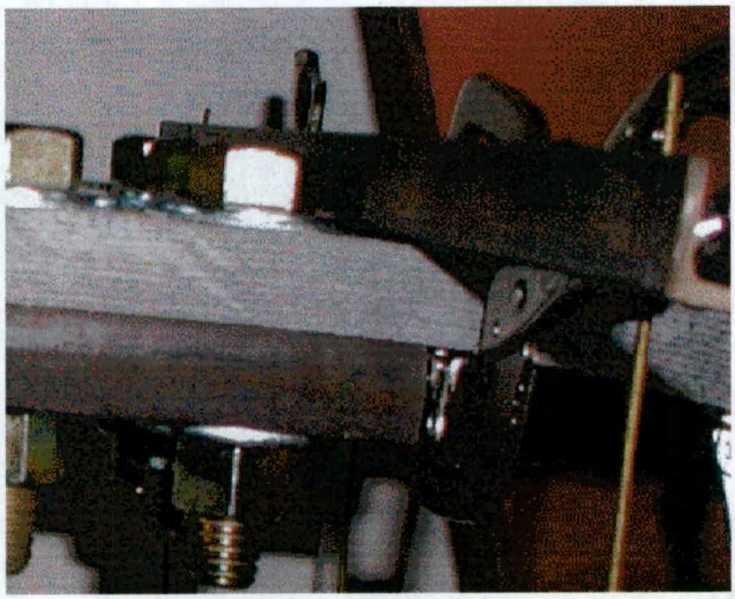

Figure 8.1 Cruciform Test with Load Pushing

along the line of contact between the substructure and the composite panel.

Figure 8.2 shows the same test specimen undergoing an upward load, during this type of load a gap develops between the composite panel and the substructure as well as a

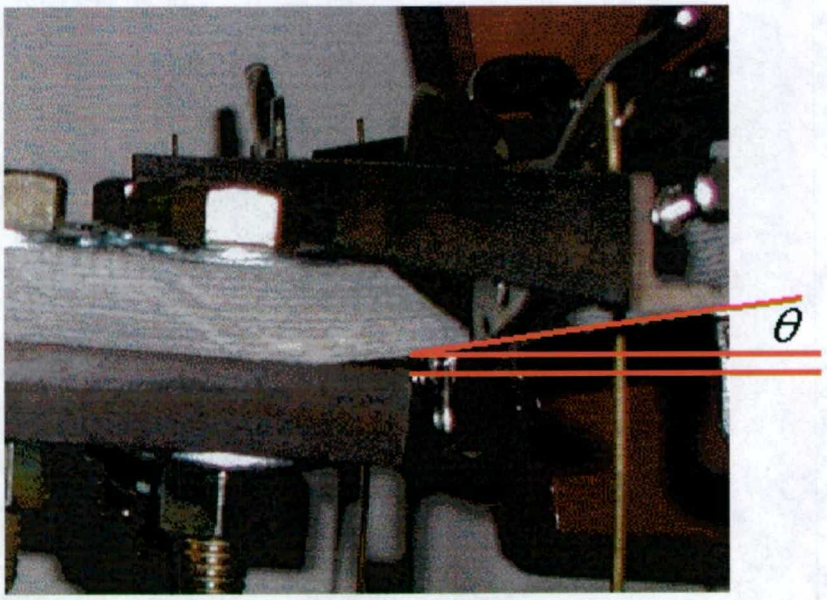

Figure 8.2 Cruciform Test with Load Pulling Upward

rotation. This results in a non-linear connection response. These nonlinear connection effects should be considered for study in the global lifting body model. A Simplified method is required so that the connection properties can be analyzed in the global model.

8.2 Connection Model Development

A simple shell model shown in Figure 8.3 was developed using Ansys™ to simulate the hybrid joint experiments conducted at the University of Maine. The model consists of

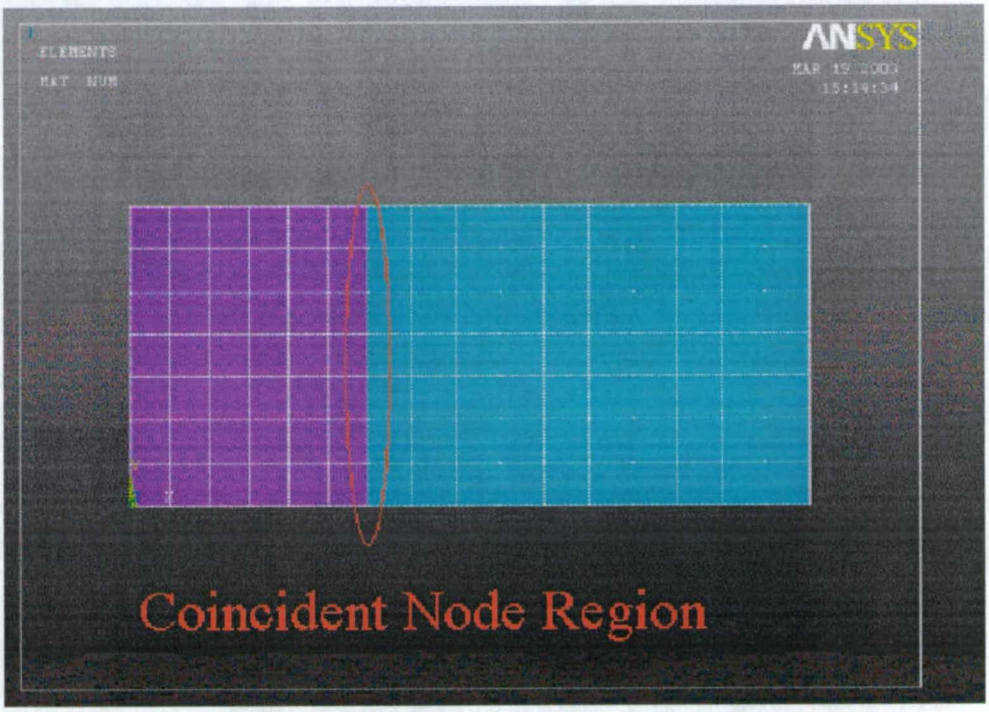

Figure 8.3 Cruciform Test Model

112 shell elements, 16 piecewise non-linear spring elements, and 144 nodes. The violet colored elements shown in Figure 8.3 are ¾" metal plates while the light blue colored elements are ¾" quasi-isotropic e-glass/vinyl ester. A built-in boundary condition is enforced on the nodes at the far left edge of the steel plate. The line that is encircled in Figure 8.3 is a region of coincident nodes, which results in two nodes occupying the same space, one node from the metal elements and one node from the composite elements. Two piecewise nonlinear spring elements are connected between the coincident nodes. One of the spring elements are a translational spring in the Z direction, the other is a rotational spring about the Y-axis. The coordinate system is shown in the lower left corner of the model in Figure 8.3. The spring connection is shown schematically in Figure 8.4.

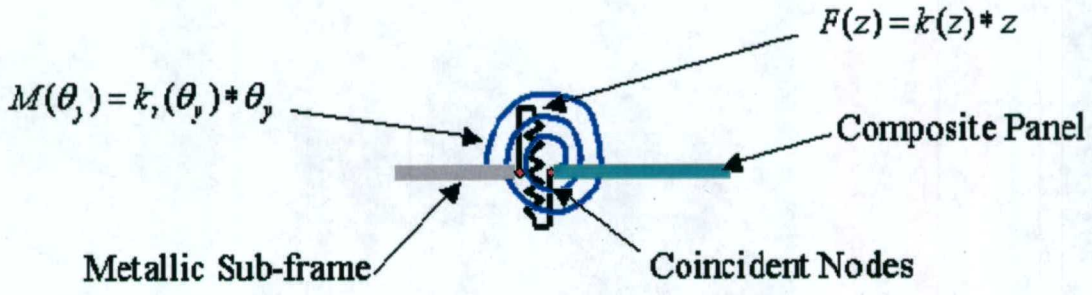

Figure 8.4 - Connection Schematic

8.3 Results and Discussion

Using data from a bolted connection test provided by the University of Maine, peak loads recorded from the data were applied to the model on the right edge nodes, shown in Figure 8.3, as a distributed load. Multiple nonlinear analyses were conducted by "tweaking" the translational and rotational spring stiffness to match the analytical force and displacement results with force and displacement data from the experiment. Figure 8.5a shows the final force/displacement curves that represent the translational spring stiffness and 8.5b shows the final moment/rotation curves that represent the rotational spring stiffness. Figure 8.6 shows the calibrated finite element results compared with experimental data. This method shows promise as an effective technique for including nonlinear connection mechanisms in a global finite element model.

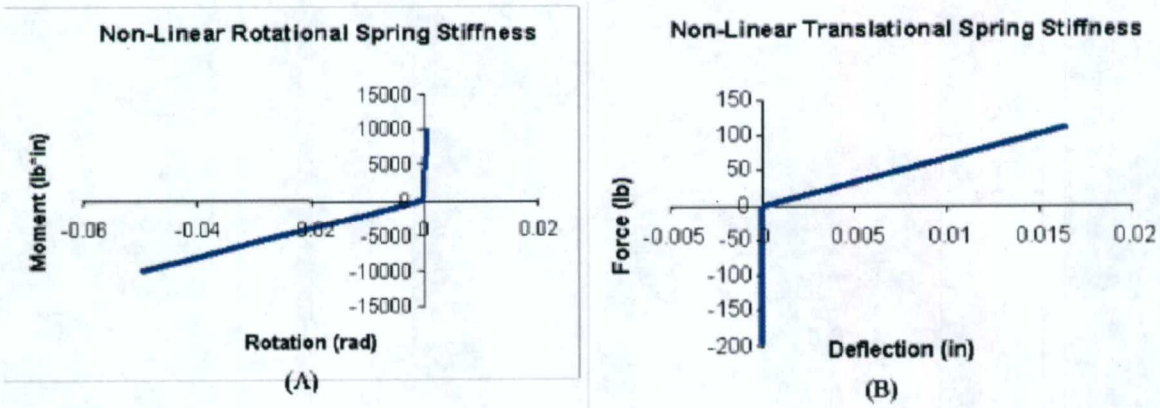

Figure 8.5 - Representative Spring Stiffness

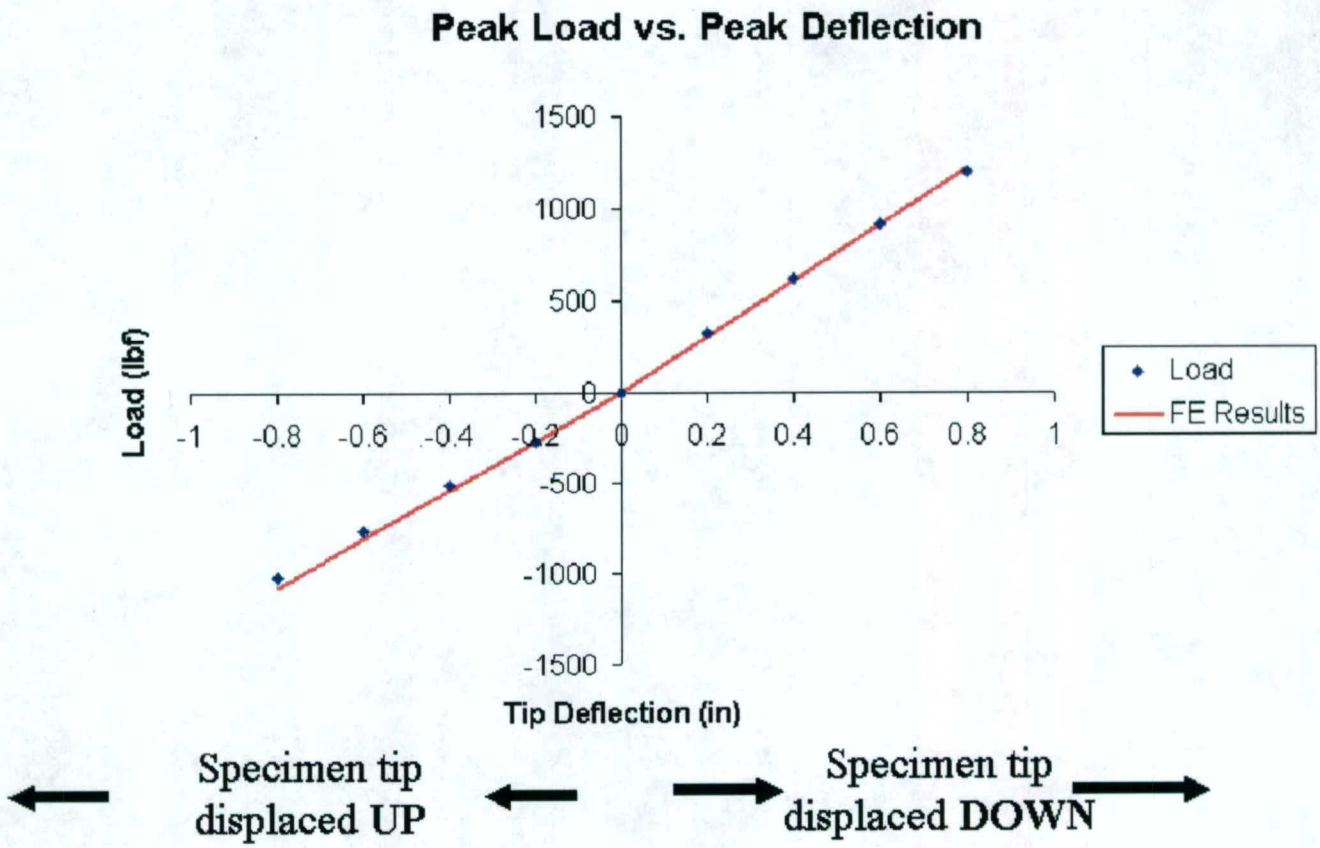

Figure 8.6 - Comparison of Analytical and Experimental Results

9. Bolted Joint Design

9.1 Model Purpose

The purpose of the finite element models that are presented in this chapter was to determine the maximum bolt spacing allowed to insure the watertight integrity of the joint. Since the intended application for this joint is at or below the water line, watertight integrity is imperative. In order to insure a watertight integrity significant contact pressure must maintained in the joint surfaces at all times. Presented are two models, an axisymmetric model which supported the creep test plan and served as an initial estimate for bolt spacing and 3 dimensional finite element model, which incorporates contact and viscoelastic material properties to model the long-term effects of bolt relaxation on the connection.

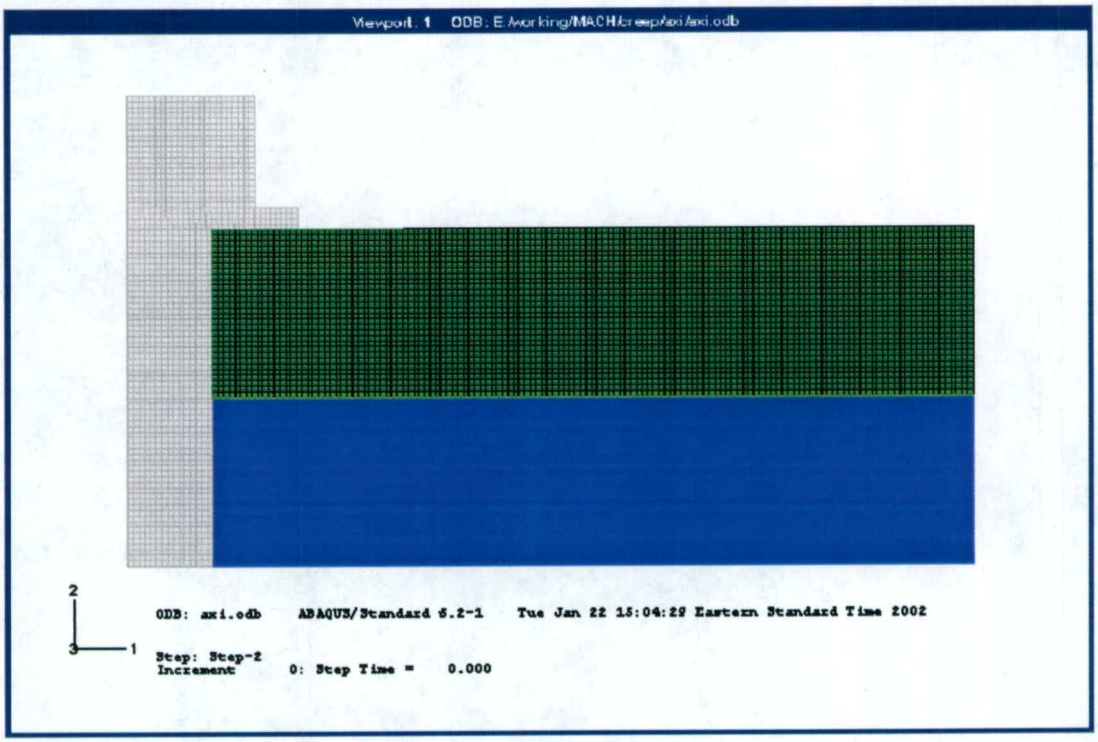

Figure 9.1 - Axisymmetric Finite Element Model

9.2 2-D Finite Element Model

Figure 9.1 shows an axisymmetric finite element model that simulates a single bolt, shown in gray, passing through an e-glass/vinylester composite panel, shown in green,

and a steel plate, shown in blue. Contact surfaces exist between the composite and steel plates, immediately under the bolt head and between the bolt shank and both the metallic and composite plates. The bolt tension was simulated as a pressure load applied to the bottom surface of the bolt. Displacement boundary conditions were applied to the bottom of the steel plate, which prevents rigid body motion of the model. Figure 9.2 shows the

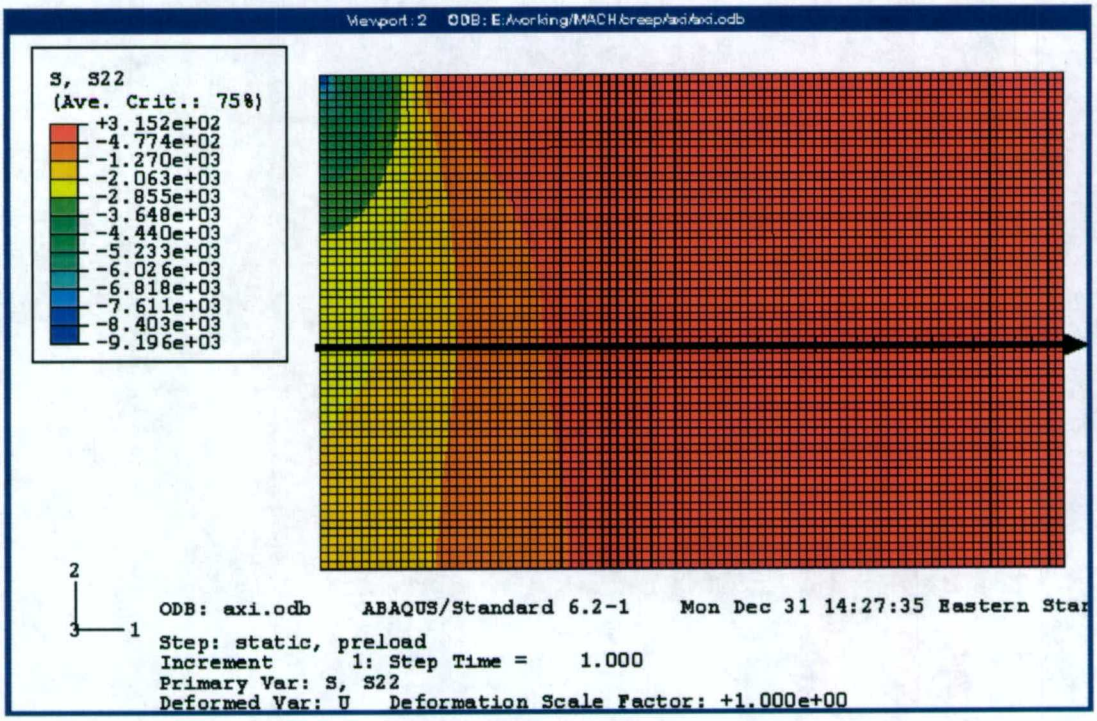

Figure 9.2 - Vertical Stress in the Composite and Metallic Components

vertical component of the stress due to bolt tension. As can be seen in Figure 9.2 the region of bolt tension influence drops off rapidly. The area shown in red represents zero pressure. The black arrow in Figure 9.2 represents the contact surface between the composite and metallic sections. Figure 9.3 shows the contact elements between the composite and metallic sections and is represented as a line. The contact pressure drops off abruptly at approximately 1.5 bolt diameters away form the center of the bolt.

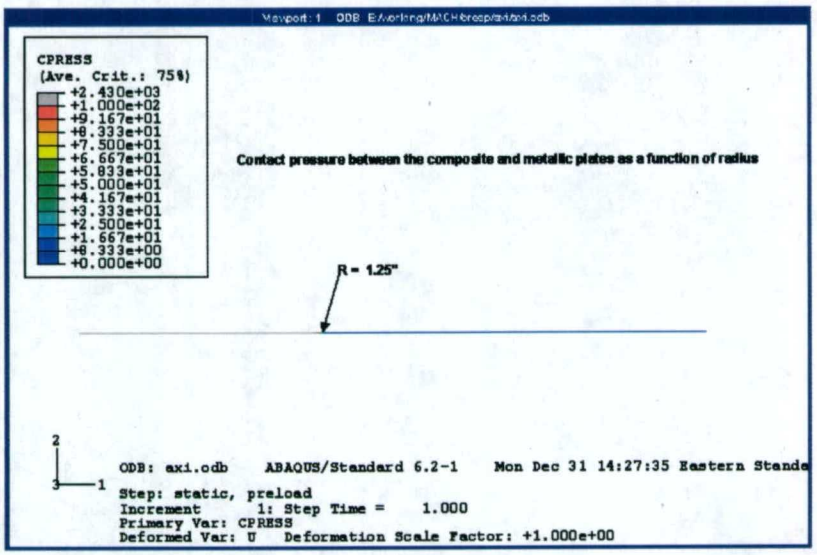

Figure 9.3 - Contact Pressure Elements

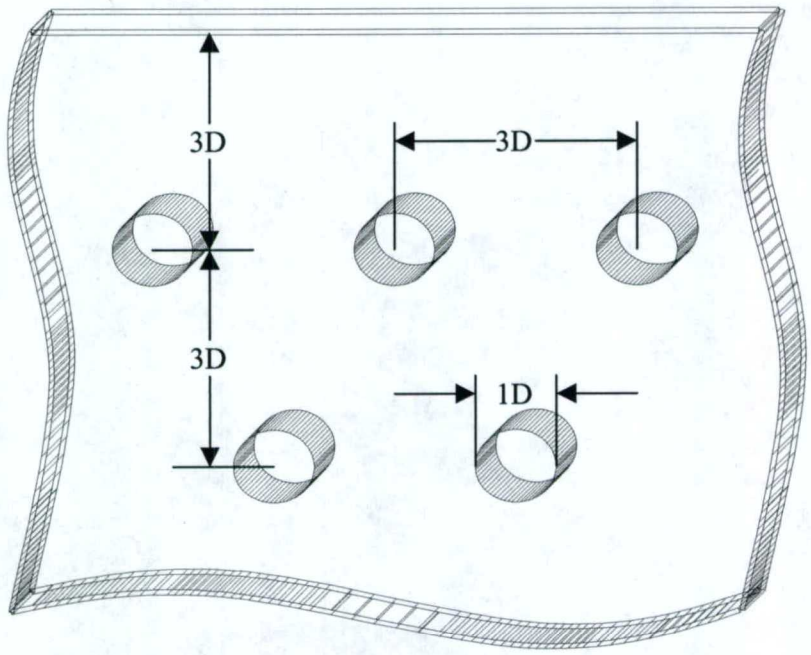

Figure 9.4 - Bolted Connection Under Consideration

9.3 3-D Finite Element Model

A three dimensional finite element model was developed to support the design of a bolted joint. Since the anticipated use of this connection is below the waterline the ability

of the joint to maintain watertight integrity is paramount. Figure 9.4 shows bolted connection under consideration. Figure 9.5 is a representative section of the bolted joint

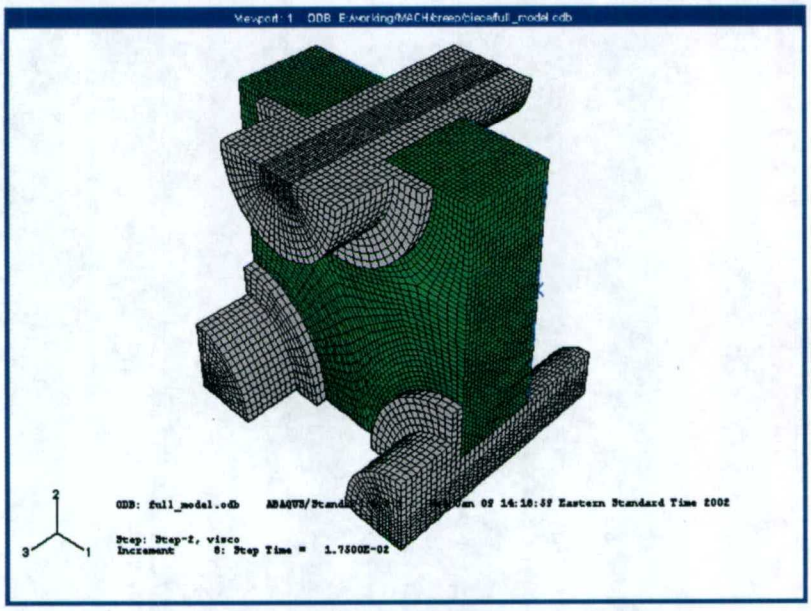

Figure 9.5 – Finite Element Model of the Bolted Connection Under Study

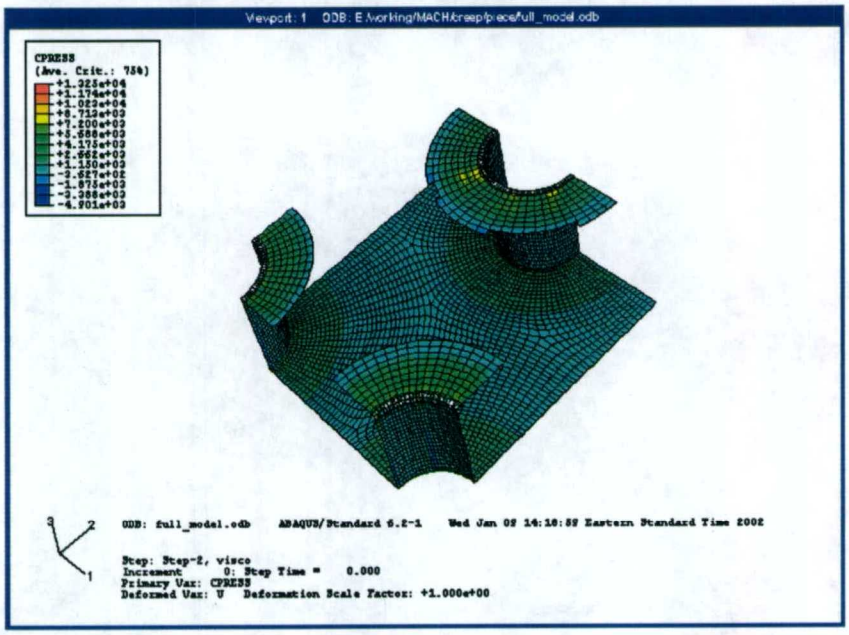

Figure 9.6 - Contact Surfaces

under study. The elements shown in green are the viscoelastic composite material, while the elements that are gray represent the bolts. Contact is modeled on the surfaces under the bolt heads and along the shaft. The metallic plate which the specimen is bolted to is modeled as an analytical rigid surface. Figure 9.6 shows the contact surfaces. The model has 80,224 3D solid elements and 295,382 degrees of freedom.

A nonlinear static analysis calculates the displacement along and around the bolt due to tensioning and created the initial contact stress between the composite material, the metallic plate and the bolts. Bolt forces are simulated by applying pressure to the bottom surface of the bolt. Figure 9.7 shows the contact stress developed in the region between the composite material and the backing plate, the results shown the dark blue region between the boltholes represents a contact pressure of 100-psi. This should generate sufficient clamping force to insure watertight integrity for the joint.

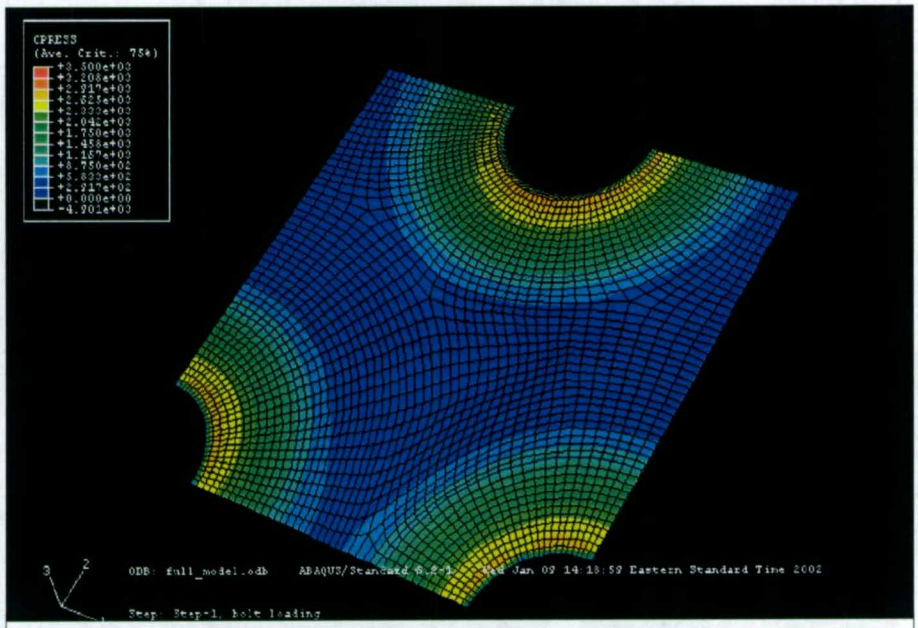

Figure 9.7 - Contact Pressure

10. Hydrostatic Panel Testing Purpose

The primary purpose of developing a full-scale, hydrostatic panel testing apparatus is to evaluate the performance of the MACH concept utilizing the hybrid joints that have been developed and tested for this effort. Fourteen different joint configurations were tested at the University of Maine utilizing a double cantilever test apparatus, illustrated in Figure 10.1. The next logical step in the MACH effort was to take the data and results from the sub-component, hybrid joint tests combined with the results of the SES 200 lifting body FE model efforts, Figure 10.2, to generate and test full-scale hybrid panels.

Figure 10.1 – Double Cantilever Test Apparatus

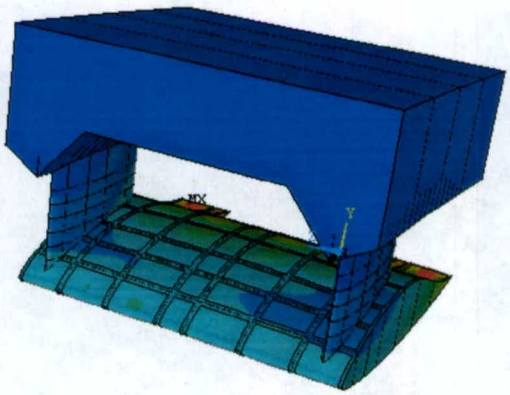

Figure 10.2 – SES 200 Lifting Body FE Model

Researchers[2-5] have utilized several methods of simulating hydrostatic and aerodynamic loads for panel testing. ASTM D6416 documents a pressure bladder approach for applying distributed flexural loads on panels in conjunction with a traditional load frame. Though the water bladder method could be adapted for larger scale panels, watertight integrity of the connections cannot be evaluated with this panel test concept. Another approach considered for the MACH effort is the D-Box Test Fixture developed by Lockheed Aeronautical Systems and later adapted by NASA Langely Research center[2,3] . The D-box fixture utilizes a sealed box pressurized with air or other inert gas to generate true flexural loading on full-scale curved panels. The fixture also incorporates in-plane loading by using movable boundary conditions connected to hydraulic actuators. Though this method proved to be an effective test apparatus for Lockheed and NASA, the technique is not well suited for testing to failure. The complexity and cost associated with

the D-Box fixture also outweigh the technique's benefit for the MACH effort. Another technique that is utilized in the aeronautics field is multiple point loading with pads bonded to the aircraft skin. Due to the nature of multiple point loading, it is difficult to achieve a realistic distributed panel load that does not require an extensive system of hydraulic actuators and load points. Additionally, this method will not permit evaluating the watertight integrity of the joint.

Assessing the current techniques for testing composite panels and the applications of the MACH concept for large ship structures, the need for a true hydrostatic test apparatus to evaluate the performance of the hybrid-paneling concept is realized. By utilizing water as the testing medium an evaluation of both the structural integrity of the paneling concept as well as the watertight integrity of the hybrid joint can be accomplished without generating potentially dangerous situations associated with high volumes of compressed air.

Figure 10.3 is a photograph of the test tank near the end of completion and illustrates the first panel configuration of four panels connected by structural beams to simulate bulkheads. It should be noted that the panel configuration in Figure 10.3 is upside-down and will be flipped over for final assembly. The current configuration of the test system permits quasi-static testing of composite panels or composites panel systems of 10-feet by 11 feet in size up to 50-psi. Though only one panel configuration is presented in this report, the design of the test tank permits numerous different panel configurations. The test tank and pressure control system is also capable of 100-psi test pressures to accommodate a future low-level, dynamic testing retrofit.

Figure 10.3 – Photograph of the Hydrostatic Test Tank at the University of Maine

11. Hydrostatic Panel Testing Scheme

In an effort to accurately represent the panel and hybrid joint boundary conditions a multiple panel test system incorporating simulated structural bulkheads is designed. The geometry of the test panels is based on the bulkhead spacing of the SES 200 lifting body. The test section selected consists of four panels on the lower, aft section of the lifting body, illustrated in Figure 11.1. The panels outlined in Figure 11.1 represent a region of slight curvature and are the most highly stressed panels on the lifting body. Due to the complexity of building a test system to accommodate and test curved panels, and the relatively flat nature of the lifting body panels our test apparatus design efforts focused on flat panels. This multiple panel configuration generates a connection region of four panels that is located away from the stiff, fixed edge boundary conditions of the test tank. The dimensions of the chosen four-panel region is approximately 10-ft by 11-ft, which permits utilizing the existing reaction frame grillage at the Hybrid Structures Lab at the University of Maine.

Figure 11.2 illustrates the individual overall test panel dimensions. To simulate the bulkheads the panels are connected to wide flange I-beams utilizing the short doubler connection. The I-beam configuration is illustrated in Figure 11.3 and incorporates one 124-inch W14 x 53 and two 69-inch W8 x 31 beams.

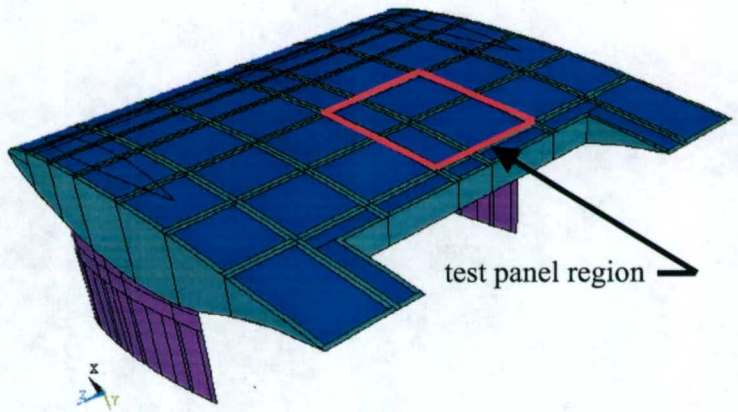

Figure 11.1 – Test Panel Location on SES 200 Lifting Body FE Model

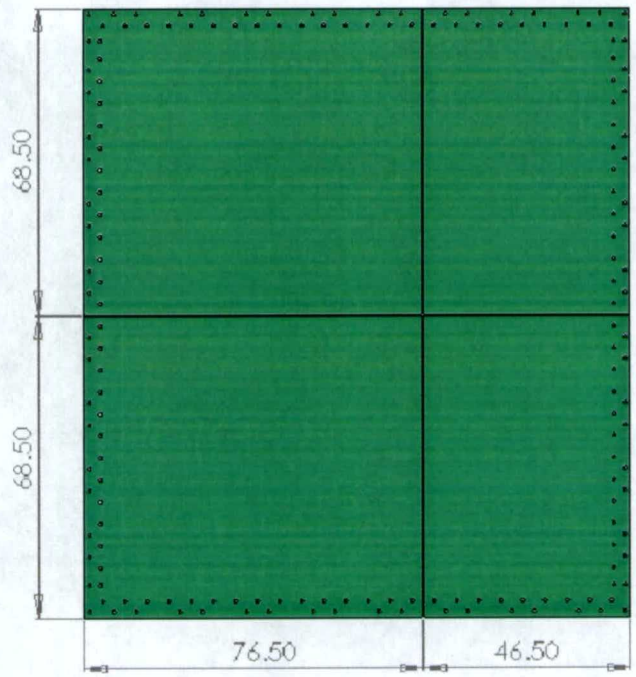

Figure 11.2 – Test Panel Dimensions

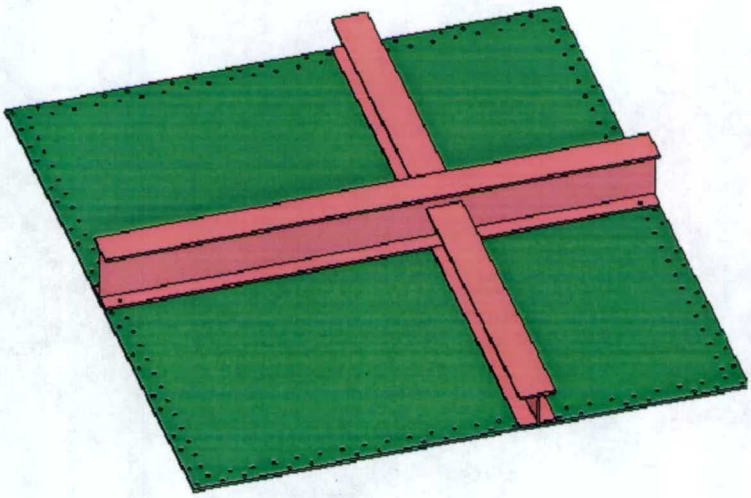

Figure 11.3 – I-beam Bulkhead Simulation

11.1 Panel Design Loads

The test panel design loads are based on the hydrostatic, dynamic, and combined pressure loads associated with the SES 200 lifting body. Load data is based on the loads document provided by NAVATEK and is available in Appendix A. The total gage pressure is determined by the sum of the dynamic loads at 35 knots and the hydrostatic pressure at maximum draft of 18.8-ft, illustrated in Figure 11.4. On the aft region of the lifting body in proximity to where the test panels are located, the pressure ranges from approximately 5-12 psig. The upper limit of 12 psig is selected for the panel and hybrid joint deign load, with the stipulation that the safety factor for the panel design be limited to no more than three times the design load to insure failure loads can be attained with the test system.

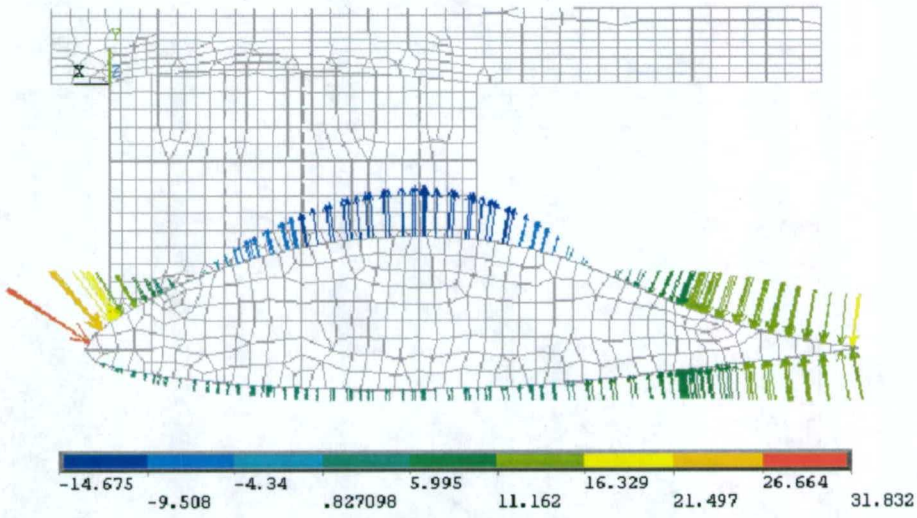

Figure 11.4 – Total Pressure Distribution at 35 Knots and 18.8 ft Draft

11.2 – Test Panels and Connection Detail

The panel design is based on the panel optimization studies summarized in Section 7. For panel sizes in the range of four feet to six feet, the optimum number of stiffeners for a quasi-isotropic, e-glass/vinyl ester panel was determined to be three. The optimum stiffener dimensions in the study for the four-foot to six-foot range were six-inches by six-inches. The optimization study was developed as a design guide and because there are additional design considerations, such as panel thickness and connection scheme, deviations from the study to meet the design criteria are expected.

The two small 68 ½ x 46 ½-in. panels incorporate three, 3-in. deep tapered hat stiffeners aligned along the short dimension of the panel with a base width of 4-in. and a top width of 2-in. Figure 11.5 is a cross section that illustrates the details of the tapered edge of the small panels and the connections to the tank and bulkhead stiffeners. The panel thickness tapers from 1-in. from the panel edges to ½-in. in the center.

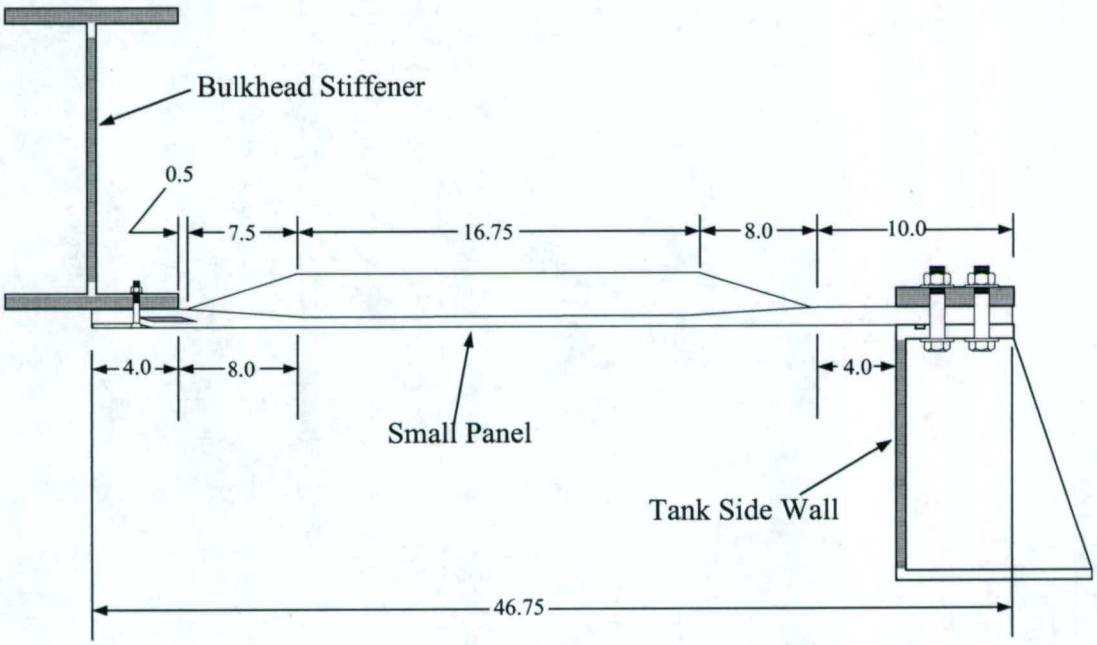

Figure 11.5 – Cross Section of the Small Panels and Connection, Dimensions in Inches

The two large 68 ½ x 76 ½-in. panels incorporate three, 6 ½-in. deep tapered hat stiffeners aligned along the short dimension of the panel with a base width of 6.5-in. and a top width of 4.5-in. Figure 11.6 is a cross section that illustrates the details of the tapered edge for the large panels. The connections to the tank and bulkhead beams are not shown however, the connections are identical to those illustrated for the small panels in Figure 11.5. The panel thickness for the large panels also have the same thickness and taper as the small panels.

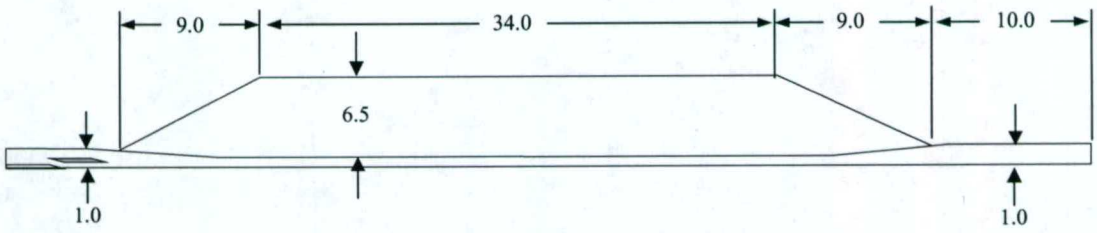

Figure 11.6 – Cross Section of the Large Panels, Dimensions in Inches

Based on the results of the hybrid joint tests conducted by the University of Maine the short doubler, bolted connection scheme was chosen as the first connection to be tested with the hydrostatic test apparatus. The short doubler connection provides a relatively simple bolted connection scheme utilizing a single bolt row for each panel edge while providing good moment transfer through the joint. Figure 11.7 illustrates how the short doubler joint is utilized to create the connection between the composite panels and the I-beam bulkheads. The composite panel is sandwiched between the I-beam flange and ¼-in. thick doubler plates. Applying a thin layer of RTV silicone between the doubler plates and the panels forms the watertight seal. The small seam between the panels, which is approximately 1/8-in wide, is also filled with RTV silicone. A photograph of the final assembly illustrating the wet side of the panels is shown in Figure 11.8.

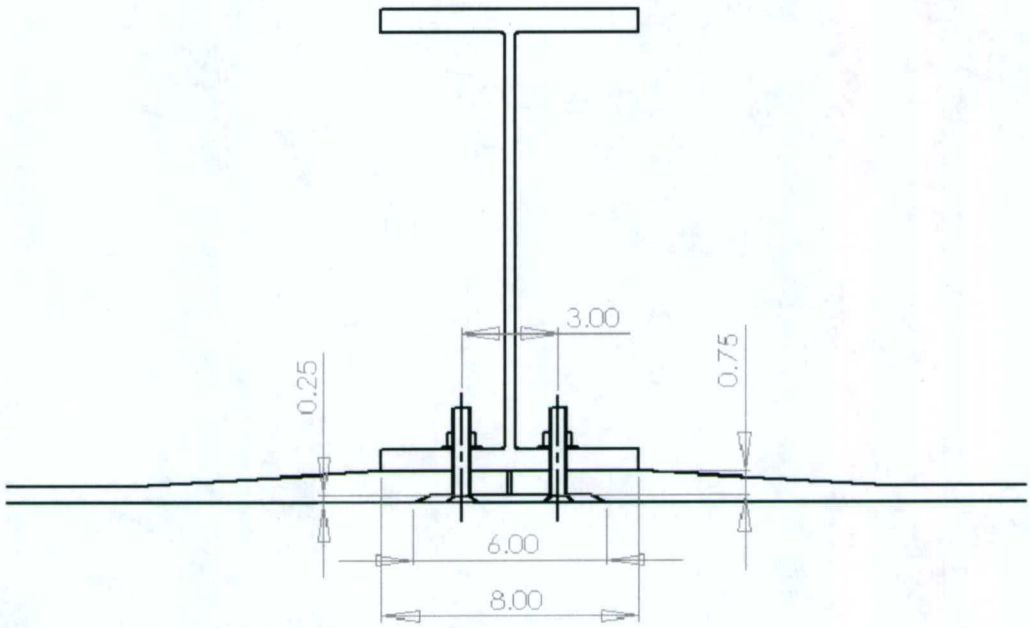

Figure 11.7 – Short Doubler Connection Detail

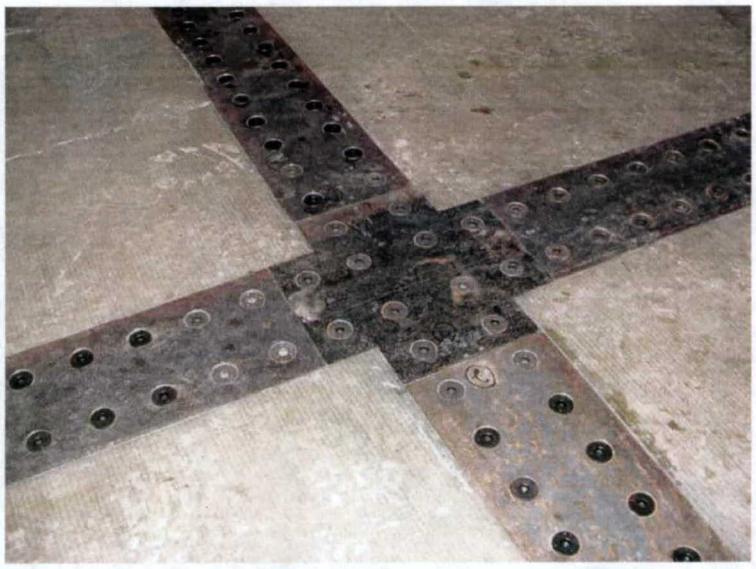

Figure 11.8 – Final Assembly of the Short Doubler Connections

12. Test Tank and Pressure Control

The hydrostatic test system consists of two principal parts: a test tank that the composite panels are bolted to, and a pressure vessel that is used to pressurize the test tank. Figure 12.1 is a simplified schematic of the test system that illustrates how building supply air is safely utilized to impart hydrostatic load on the test panels.

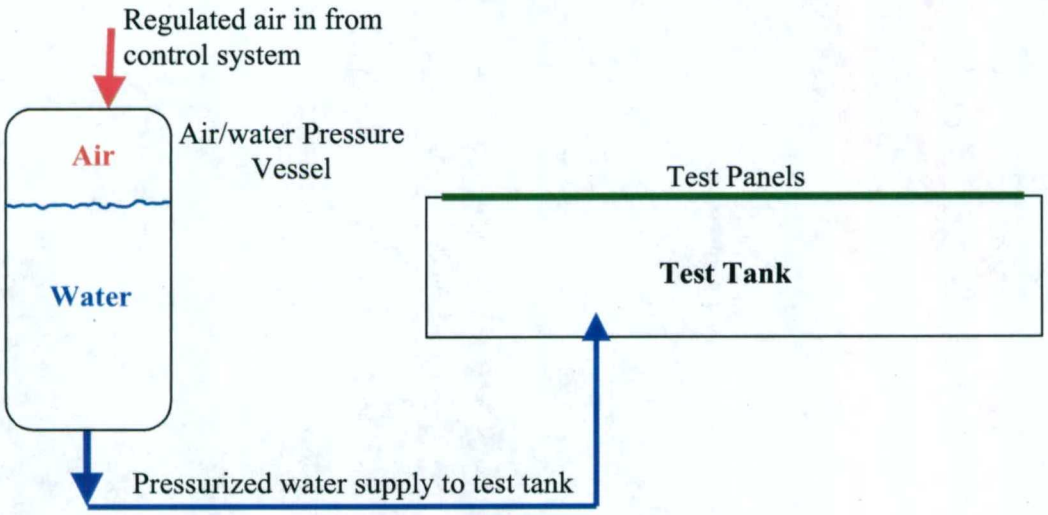

Figure 12.1 – Simplified Hydrostatic Test System Schematic

12.1 Design Requirements

The design requirements of the test tank are primarily based on the desired panel size, panel design loads, and space constraints of the 300-kip reaction frame located at the Hybrid Structures Lab at the University of Maine. Additional design considerations are also made to facilitate future modifications of the test tank for hydrodynamic pressure testing.

Based on a panel design load of 12-psi, with a maximum safety factor of three, a minimum test pressure capability of 36-psi is established. To insure that the panels can be sufficiently loaded to failure, the initial test system design was established as 50-psi. A final design load of 100-psi is established based on plans to utilize the test tank for future low level dynamic testing. The most critical portion of the test tank design are the

walls, which must withstand the maximum test pressure and the reaction loads of the test panels while maintaining water-tight integrity. The total load that the tank must react at 100-psi is approximately 1.4 million pounds.

12.2 Test Tank Design

The test tank consists of four custom laser welded, 13.25-inch deep steel asymmetric C-sections to form the walls of the tank and 1-½ inch steel plate to form the bottom of the tank. Half-inch thick web stiffeners are welded to the C-sections on 15-inch centers to provide adequate stiffness for the top and bottom flanges. Figure 12.2 illustrates a typical C-section with stiffeners and Figure 12.3 is a dimensioned cross sectional detail. The channels are bolted through the tank base plate and the W36-300 grillage, as shown in Figure 12.4, to form the assembled tank illustrated in Figure 12.5. The overall dimensions of the tank are illustrated in Figure 12.6. Three access covers are located in the tank base plate for assembly purposes and a future low level dynamic testing retrofit. Detailed drawings of the entire tank are available in Appendix B.

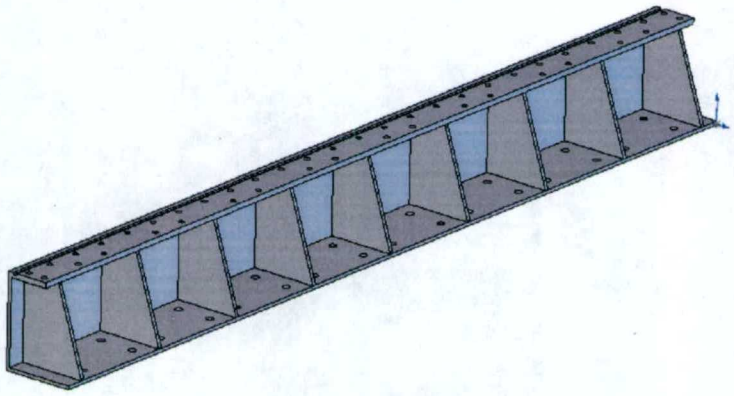

Figure 12.2 – Typical Tank Wall C-section with Stiffeners

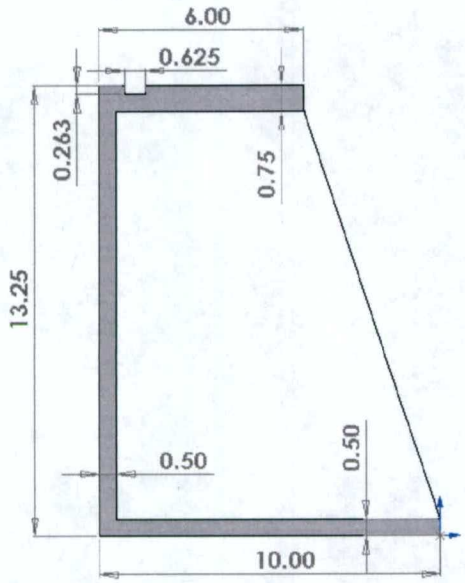

Figure 12.3 – C-section Detail, in Inches

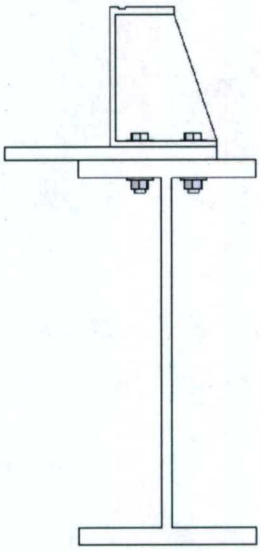

Figure 12.4 – Detail of Tank Base Connection

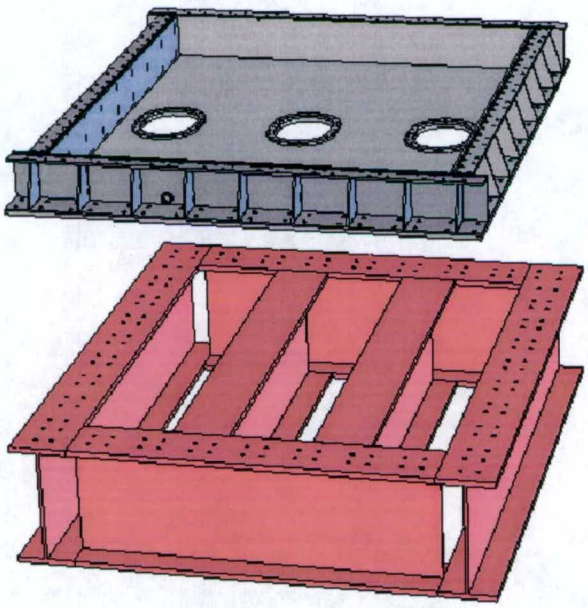

Figure 12.5 – Assembled Test Tank and W36 X 300 Grillage

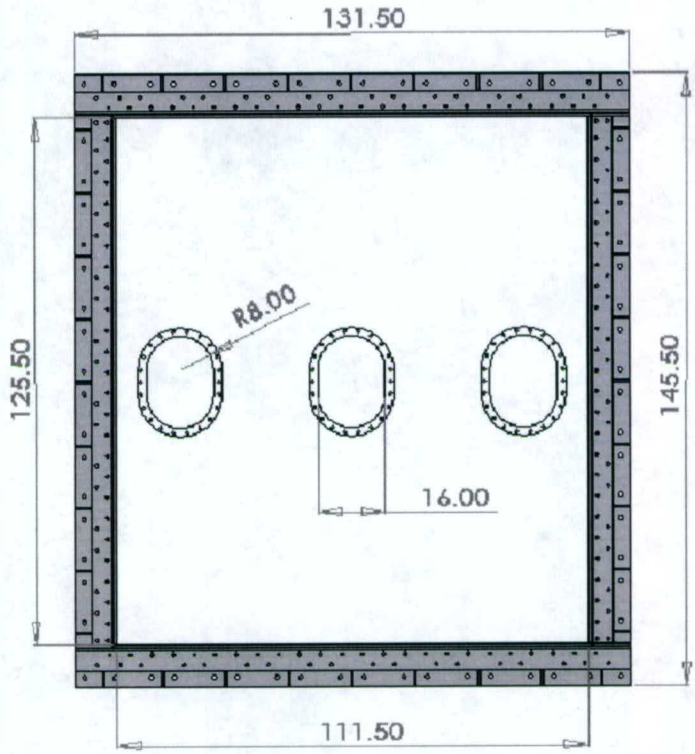

Figure 12.6 – Overall Test Tank Dimensions, in Inches

The composite test panels are connected to the test tank by sandwiching the panels between the top flange of the tank and a one-inch thick steel backing plate, shown in Figure 12.7. A watertight seal is created with a 3/8-inch square rubber O-ring located in a 0.625 x 0.263 inch deep gland on the top flange of the tank inside the first bolt row. The first bolt row consists of ¾-inch grade five bolts on five-inch centers. The second bolt row also utilizes ¾-inch grade five bolts, but on an irregular pattern or two bolts on five-inch centers, centered between the tank stiffeners, which is illustrated in Figure 12.6.

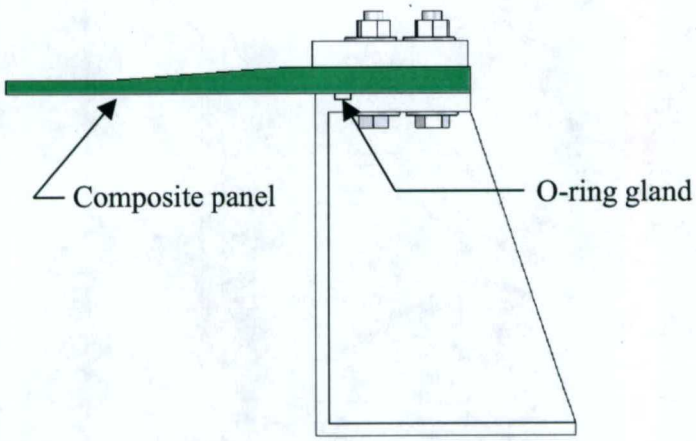

Figure 12.7 – Test Panel Connection to Tank

12.3 Laser Welded Channels

The four custom C-sections that comprise the test tank walls were fabricated at Applied Thermal Sciences, Inc. Laser Processing Facility in Sanford Maine. The facility features a 25-kW CO2 laser, shown in Figure 12.8a-b, capable of welding sections up to 30-ft long. To provide maximum flexibility in choice of materials, the ATS welding system can operate in any of three modes: autogenous, cold wire filler-added, and Laser Assisted-Gas Metal Arc Welding (GMAW) or "hybrid" welding procedures. Quality control of the weld is insured by a breakthrough process control and quality assurance (PC/QA) system that features pre-weld joint scanning, weld pool monitoring, post-weld joint scanning and real-time process control. By utilizing this advanced fabrication technique for the test tank, it was possible to create custom beams, shown in Figure 12.9, with minimal distortion to insure water-tight integrity of the tank and composite panel connections.

Figure 12.8a – ATS Laser Processing Facility

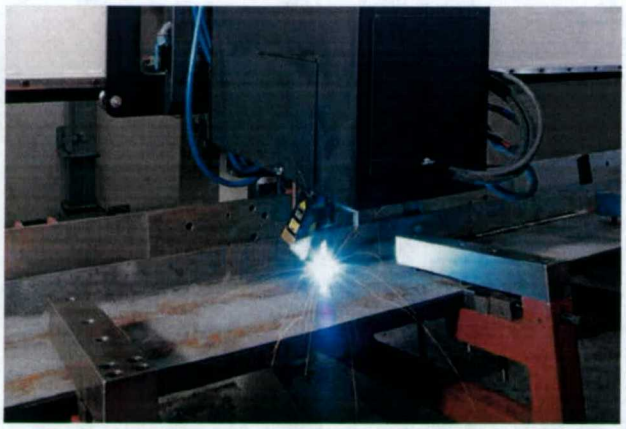

Figure 12.8b – ATS Laser Processing Facility

Figure 12.9 – Laser Welded C-section for Test Tank

12.4 Tank FE Model

A linear, static FE model of the test tank was constructed to identify any problem areas that may develop in the design. Due to the asymmetric bulkhead scheme utilized for the test panel configuration the entire tank was modeled. The model was built with ANSYS 8.0 and consists of 10,755 8-node structural shell elements with 168,594 degrees of freedom and is illustrated in Figure 12.10. The connection detail between the composite panels and the test tank, and the connection between the composite panels and the bulk head beams is not incorporated in the model, as the primary purpose of the model is to evaluate the global response of the test tank custom channels to the resulting load transferred from the test panels. As a result of leaving this detail out, artificially high stresses are present in the bulkhead beams due to significantly lower bending rigidity in the flanges. The stiffness of the composite panels is approximated by using equivalent orthotropic material properties.

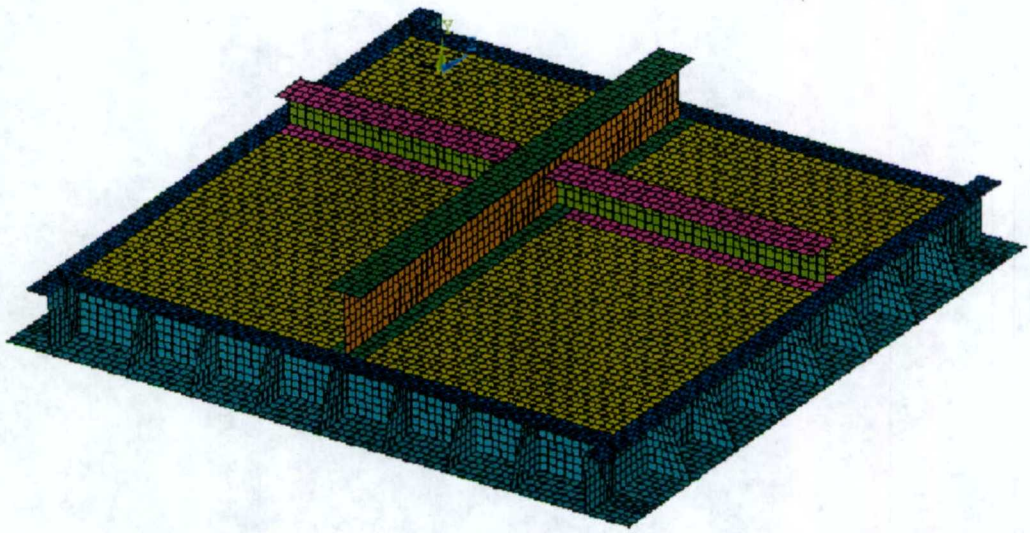

Figure 12.10 – Test Tank Finite Element Model

Figure 12.11 illustrates deflection magnitude of the test tank, with the panels and bulkhead framing removed for clarity, subjected to a 50-psi load, which is approximately 4.2 times larger than the panel design loads. Figure 12.12 illustrates the Von Mises stress in the tank channels and bulkhead frames. The area of interest here is the tank web stiffener directly below the W14 x 53 bulkhead beam. With the design shown in Figure 12.10 a significant amount of load is transferred through the stiffeners located directly below the bulkhead framing. To better distribute the load from the bulkhead frames to the test tank, ¾" steel gussets are added to the ends of the beams, as shown in Figure 12.13. The gussets also help stabilize the beams and prevent significant twisting due to the asymmetric framing scheme.

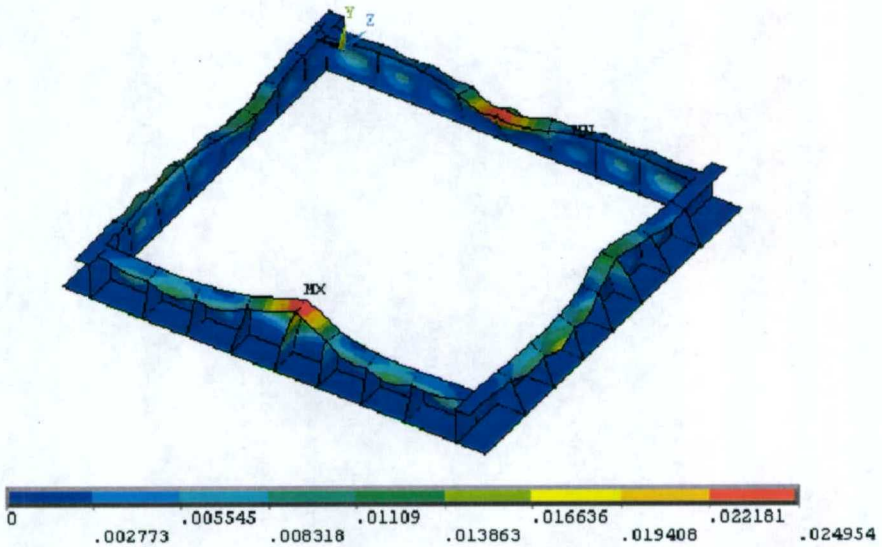

Figure 12.11 – Deflection Magnitude of Tank Walls Subjected to a 50-psi Load

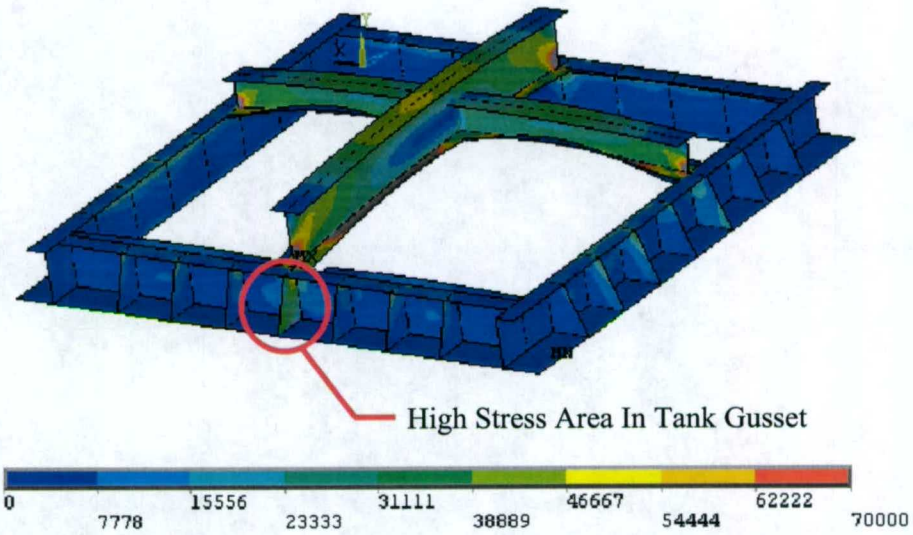

Figure 12.12 – Von Mises Stress for Test Tank Under 50-psi Load

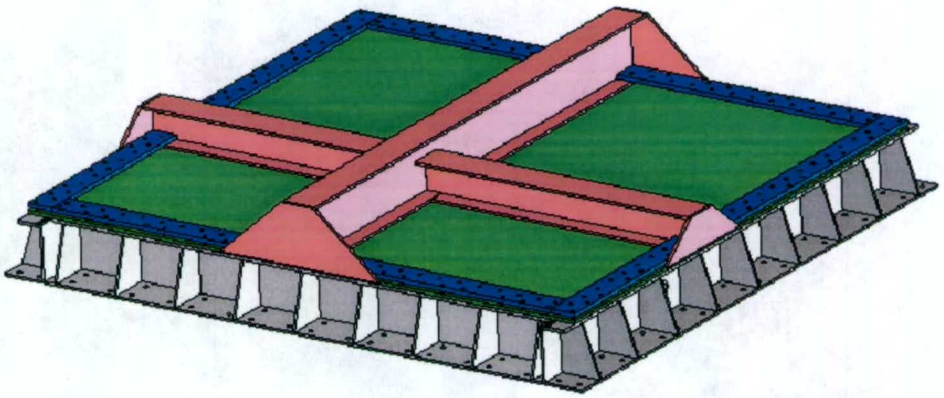

Figure 12.13 – Test Tank with Gussets Welded to the Bulkhead Frames

12.5 Pressure control

A critical portion of the hydrostatic panel testing system is this ability to accurately control and regulate the tank pressure. Numerous pressure-regulating methods were evaluated including:

- Recirlculating pump with pressure regulating valves and a separate water make-up tank
- Direct connection with 80-psi building water supply using a commercially available water regulating valve
- A large piston-cylinder arrangement driven by a hydraulic actuator
- Air over water system utilizing 120-psi building supply air

For static testing the air over water system is chosen based on design simplicity and cost, the availability of commercial, precision manual and electronic PID regulators and an available 260-gallon, 200-psi certified pressure vessel, shown in Figure 12.14. The future dynamic testing retrofit will likely incorporate a large piston cylinder arrangement.

Figure 12.14 – Air/Water Pressure Vessel

The air over water pressure control system regulates the test tank water pressure by using the 260-gallon pressure vessel as an interface between the test tank and compressed air. Figure 12.15 is an as-built schematic illustrating how the system works. The pressure vessel sits next to the test tank and is filled with water to a height equal to the top of the test tank to insure no initial hydrostatic pressure is developed. As the control regulator increases air pressure in the pressure vessel, the water pressure in the test tank subsequently increases. The initial volume of water in the pressure vessel, approximately 173-gallons, provides the additional volume of water required as the test panels deform.

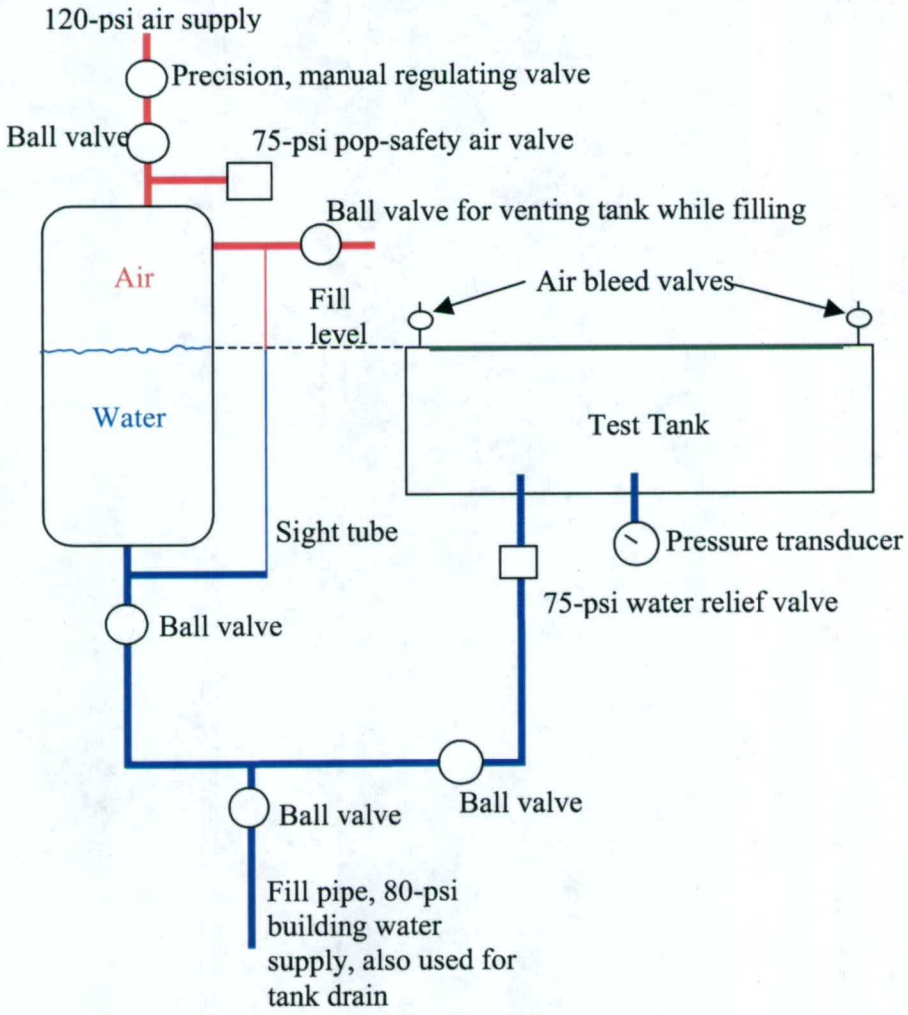

Figure 12.15 - As-Built Panel Test Apparatus Schematic

The existing test system incorporates a Control Air, Inc. Model 700 precision air pressure regulator, which requires each pressure step during a test to be manually dialed in. Though this method will work fine for the first panel test and proof of concept, it is desirable in any structural test system to have automated load control. The next system update will incorporate an electronic PID regulator, Tescom model ER3000, combined with a high flow booster to provide full automated, feedback control of the tank pressure. The Tescom system will permit user defined time-pressure profiles to be programmed with a conventional PC using RS485 serial protocol.

13. Summary and Conclusion

The objective of this effort was to develop and evaluate a panelized, hybrid structural hull system capable of withstanding the requirements for below waterline marine applications. By performing a case study of the existing aluminum SES 200 lifting body design a baseline was established for the hybrid structural system design. All structural aspects: global lifting body deformations, local panel deflections and strength, of the hybrid structural system meet or exceeded the baseline design. The major tasks accomplished in this work were as follows:

1) Analysis of a representative SES 200 ship section
2) Analysis of baseline aluminum lifting body structure
3) Analysis of the panelized lifting body design.
4) Optimal preliminary detailing of composite panels including connection details
5) Design and implementation of a hydrostatic test system to study the structural performance and watertight integrity of hybrid marine structures.

A systematic approach was used to progress from the conceptual MACH ideas to the final design and testing of a full-scale panelized system, shown in Figure 13.1. An overview of the roll Applied Thermal Sciences (ATS) played in the MACH evolution is illustrated graphically in Figure 13.2; As the University of Maine progressed with hybrid joint research ATS was able to provide the necessary research and design support to integrate one of the optimum hybrid joint designs into a full-scale panelized system design and develop a hydrostatic test system capable of testing the panelized system. By developing FE models of the SES 200 hull section and lifting body a baseline aluminum model could be used to establish the allowable deflections and required strength for the panelized lifting body design. The global finite element model of the hybrid lifting body was utilized to determine the worse case (highest deflection and stress level) scenario for the MACH panels. Combining the results from the hybrid lifting body and the results from generic panel and frame spacing studies two different size MACH panels were designed incorporating hybrid joints. This effort culminated in the successful testing of the panelized system, which were conducted at the Hybrid Structures Lab at the University of Maine during the month of December 2004.

Figure 13.1 - Hybrid Test Panel

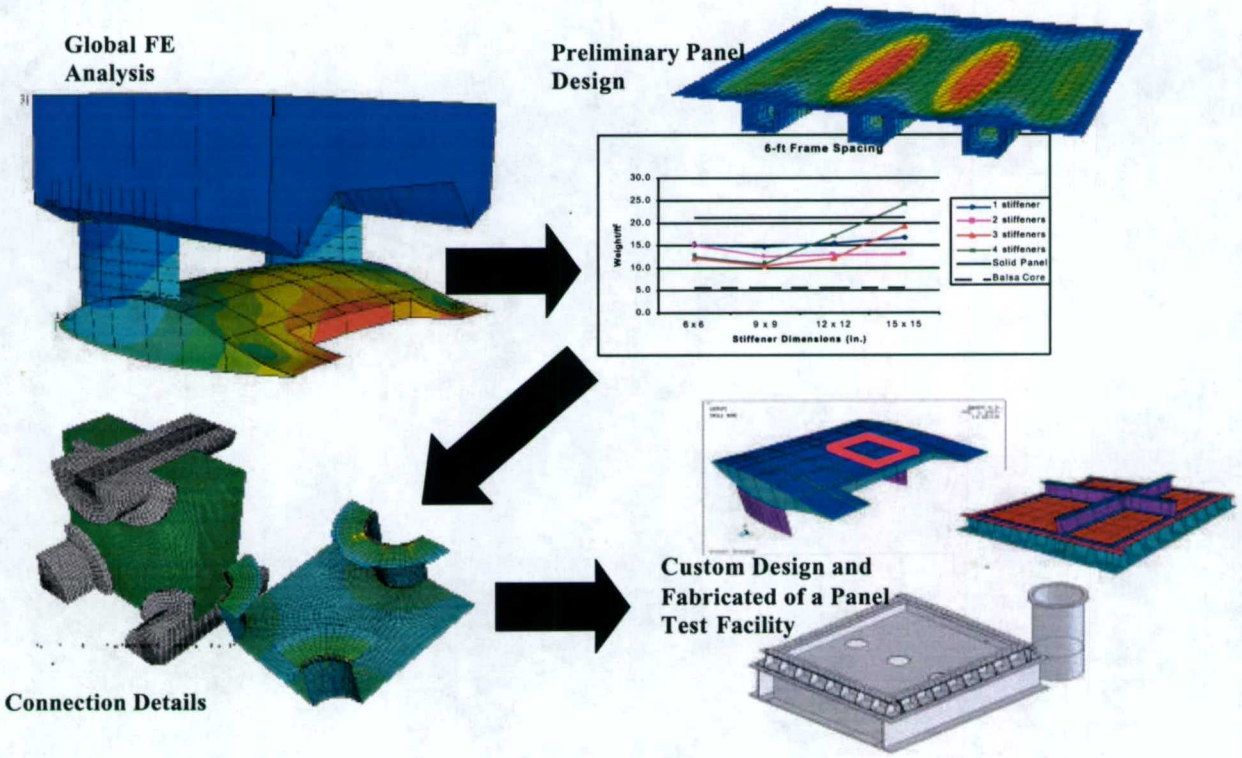

Figure 13.2 - Schematic of the Major Tasks Accomplished in the MACH Program

14. References

1. Pollard, M.R., "SES-200 Global Finite Element Analysis Report", CETEC Consultancy Limited, Romsey Hampshire, England, Report No. CET/0617/R/01 20pp. 2001.
2. Arbur, D. R., Gerro, J. A., Dickson, J, "D-Box Fixture for Testing Stiffened Panels in Compression and pressure", Journal of Aircraft, vol. 32 No. 6, November – December 1995.
3. Arbur, D. R., Sikora, J., Maguire, J. F., Winn, P. M., "Development of a Pressure Box to Evaluate Reusable-Launch-Vehicle Cryogenic-Tank Panels", AIAA Paper No. 96-1640-CP, 1996
4. Black, S., *Technical Editor*, "Static and Fatigue Testing Prove Out Durability", High Performance Composites, January, 2003, pp. 26 – 31.
5. Rouse, M., Arbur, D. R., "Fuselage Response Simulation of Stiffened Panels Using a Pressure-Box Test Machine", AIAA Paper No. 95-12362, April 10-13, 1995.
6. Ansys Release 8.0 Documentation, 2003 SAS IP, Inc.

15. Appendix A – SES 200 Loads Document Provided by NAVATEK, Honolulu, HI

SES 200

DESIGN SPEED – 35 KNOTS

AHFID OPERATION MAX SPEED 30 KNOTS
OPERATE IN SEA STATE 5 AT 20 KNOTS (operational restriction)

MAX FULL DISPLACEMENT – 340 LT

OPERATION HOURS – 5000 HOURS

FLAP EXCURSION - +/- 20 DEG @ SPEEDS LESS THAN 20 KNOTS
- +/- 12 DEG @ SPEEDS GREATER THAN 20 KNOTS

MAX FLAP RATE – 20 DEG/SEC

MAX FLAP LOADS

HINGE MOM. (FT-LT)	LIFT (LT)	DRAG (LT)
+200	-110	+10
+86	+40	-35
+ LE up	+ up	- fwd

FLAP HINGE @ 6.63 FT FROM TRAILING EDGE

FLAP CYCLES 9,000,000
ASSUMING +/- 5 DEG DEFLECTION

HINGE MOM. (FT-LT)	FLAP LIFT (LT)	FLAP DRAG (LT)
- 159	+4	-5
- 60	- 72	-25
+ LE up	+ up	- fwd

H-BODY MOM. (FT-LT)	H-BODY LIFT (LT)	H-BODY DRAG (LT)
-140+/-70	220 +/-85	20+/-8

SURFACE PRESSURES ON H-BODY

POSITIVE PRESSURE MAX. = ?gh + .5?V^2

NEGATIVE PRESSURE MIN. = 35 lb/ft^2

H-BODY STRUT SIDE LOAD – 55 LT PER STRUT (see figure for location)

H-BODY SIDE LOAD (hydrodynamic) – 5 LT (centroid)

H-BODY SIDE LOAD (docking) – 170 LT

H-BODY DRAG MAX. – 40 LT (centroid)

H-BODY NOSE DOWN MOMENT – 5000 FT-LT

H-BODY NOSE UP MOMENT – 1500 FT-LT

H-BODY INERTIAL LOADS – 0.5 g's in all directions

H-BODY MAXIMUM VERTICAL LOAD – 510 LT

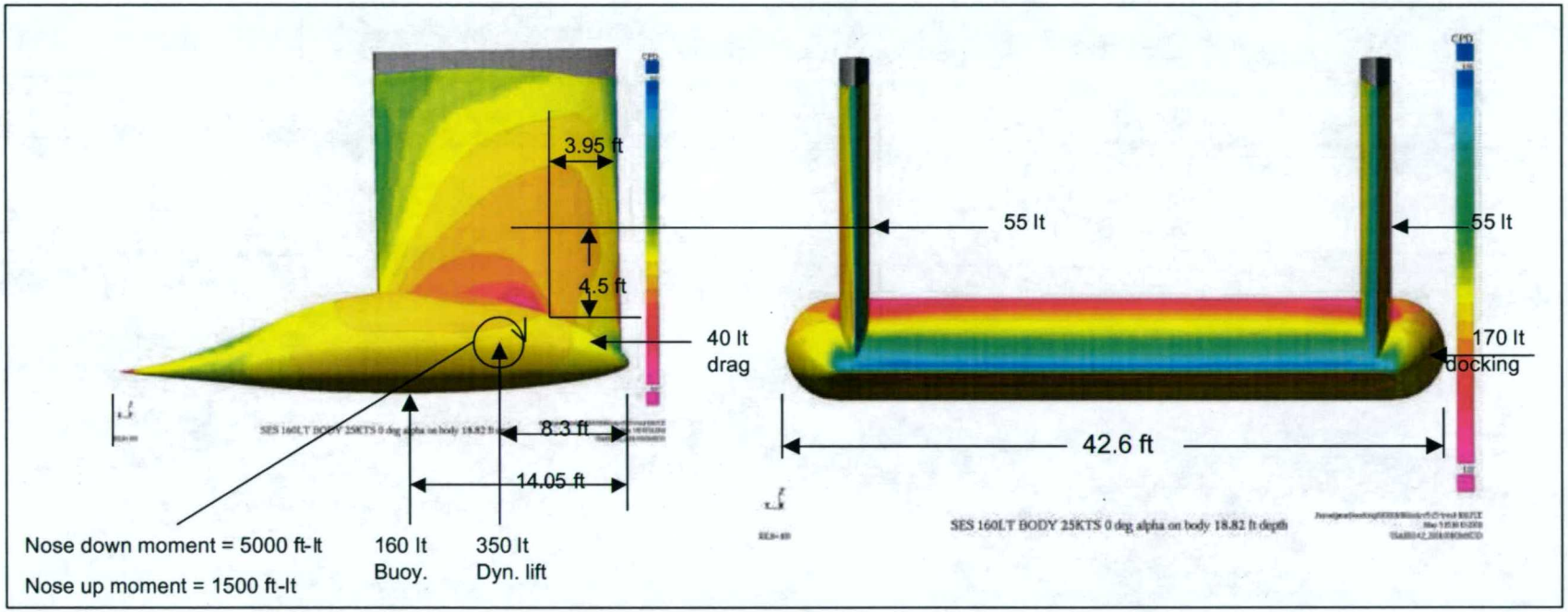

Figure 15.1 – Resultant Loads for the H-Body

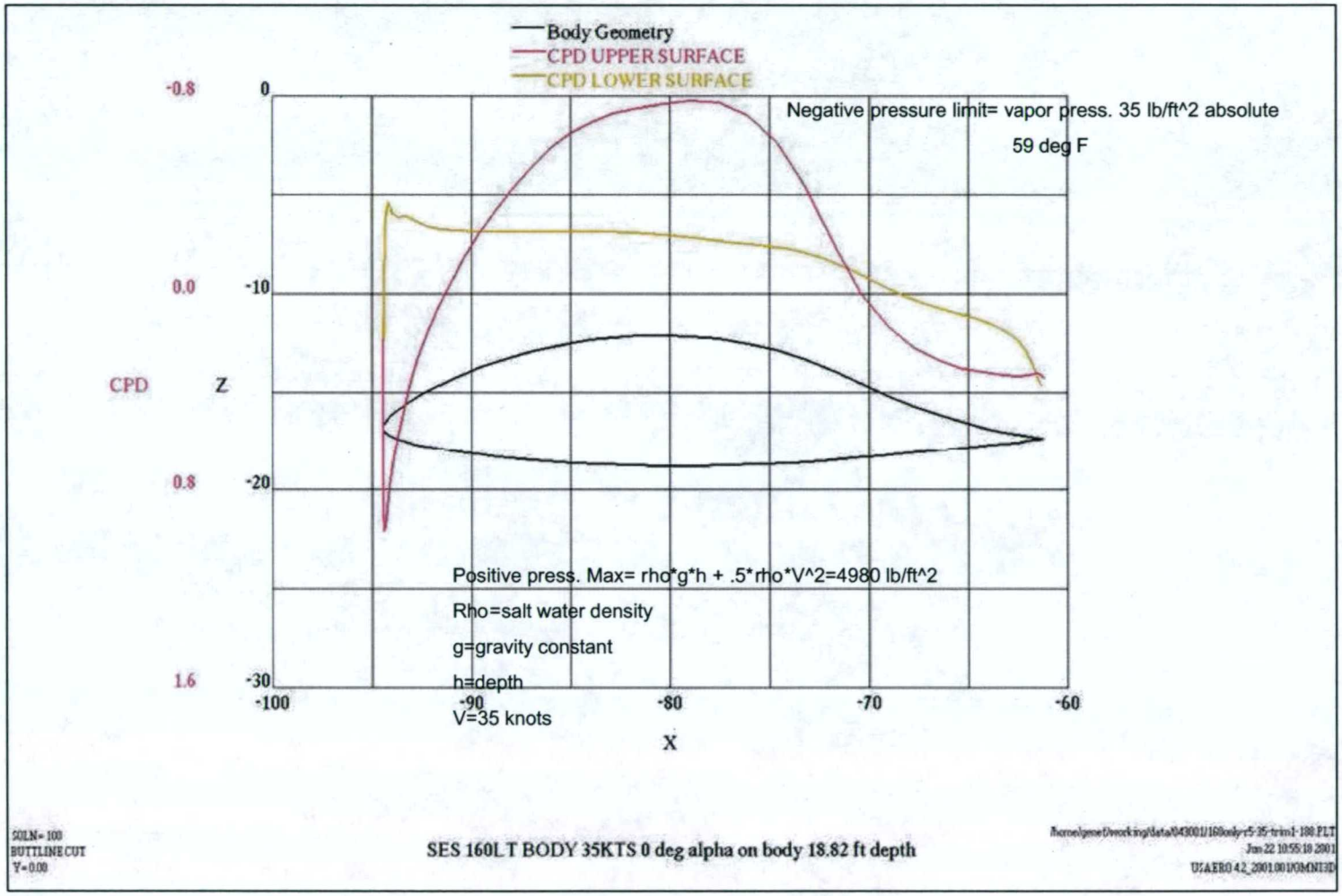

Figure 15.2 – CFD Results at 35 Knots

REVISIONS				
ZONE	REV.	DESCRIPTION	DATE	APPROVED

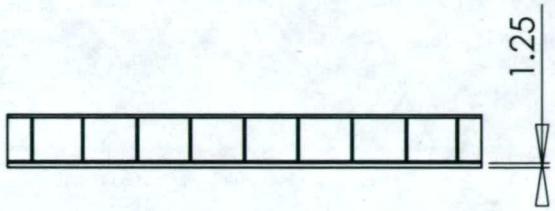

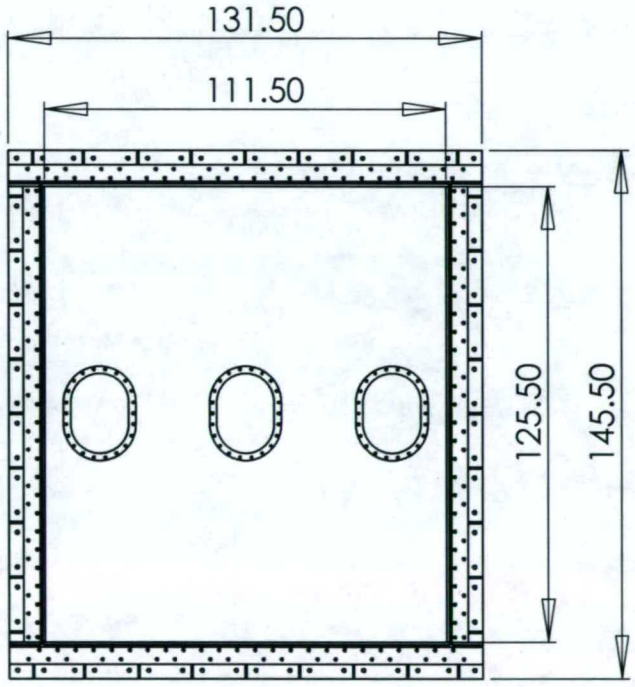

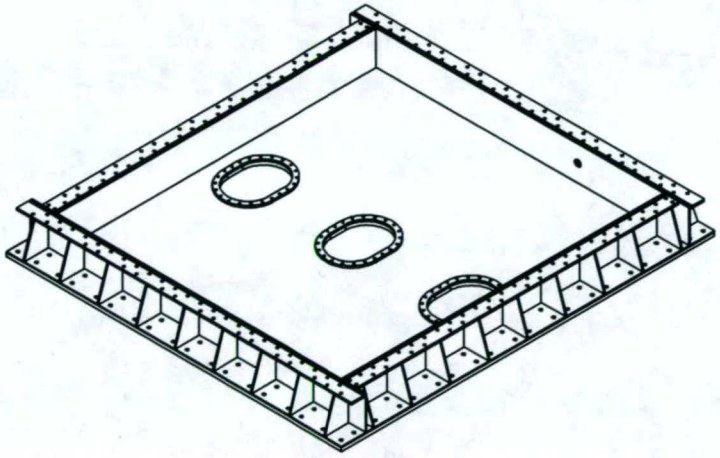

North

NEXT ASSY	USED ON
APPLICATION	

DIMENSIONS ARE IN INCHES
TOLERANCES:
FRACTIONAL ±
ANGULAR: MACH ± BEND ±
TWO PLACE DECIMAL ±
THREE PLACE DECIMAL ±

MATERIAL ---

FINISH ---

DO NOT SCALE DRAWING

	NAME	DATE
DRAWN	J.W.	8/11/03
CHECKED		
ENG APPR.		
MFG APPR.		
Q.A.		

COMMENTS:

Applied Thermal Sciences, Inc

SIZE	DWG. NO.	REV.
A	Tank Assembly	1
SCALE:1:50	WEIGHT:	SHEET 1 OF 7

REVISIONS				
ZONE	REV.	DESCRIPTION	DATE	APPROVED

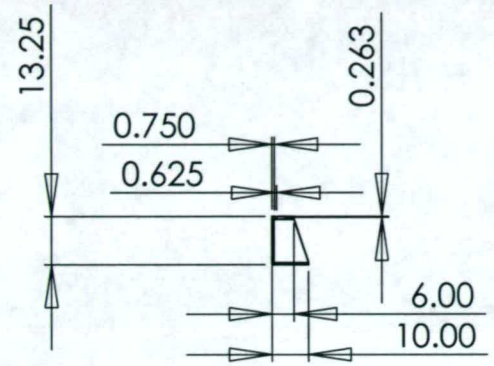

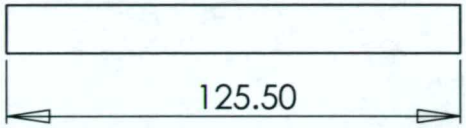

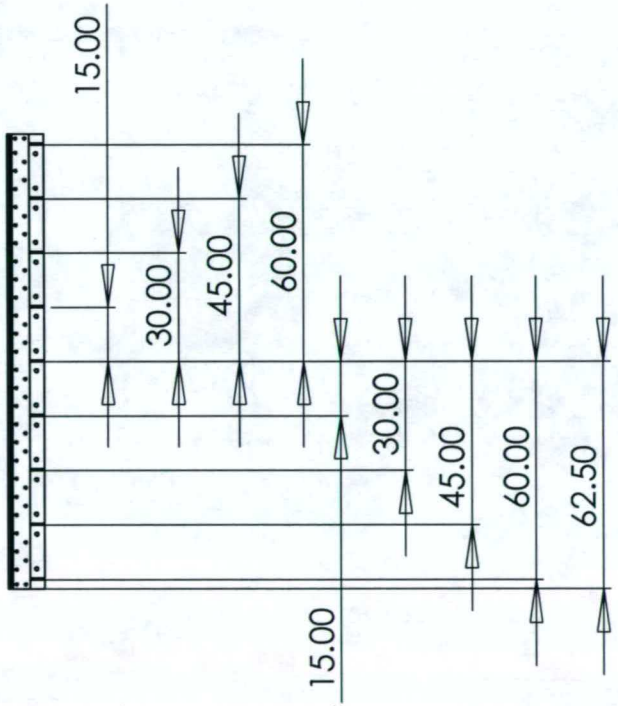

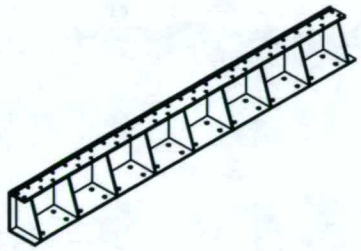

68

		DIMENSIONS ARE IN INCHES TOLERANCES: FRACTIONAL ± ANGULAR: MACH ± BEND ± TWO PLACE DECIMAL ± THREE PLACE DECIMAL ±		NAME	DATE
			DRAWN	J.W.	11/24/03
			CHECKED		
			ENG APPR.		
			MFG APPR.		
		MATERIAL —	Q.A.		
NEXT ASSY	USED ON	FINISH —	COMMENTS:		
APPLICATION		DO NOT SCALE DRAWING			

Applied Thermal Sciences, Inc

SIZE	DWG. NO.	REV.
A	North Channel	2
SCALE:1:50	WEIGHT:	SHEET 2 OF 7

REVISIONS				
ZONE	REV.	DESCRIPTION	DATE	APPROVED

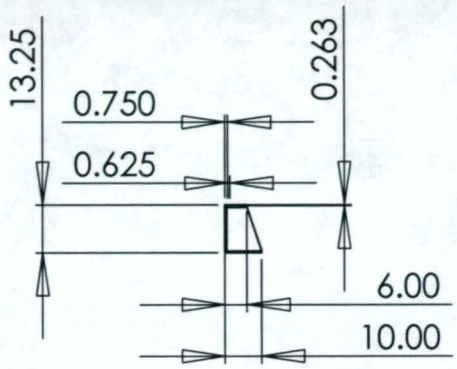

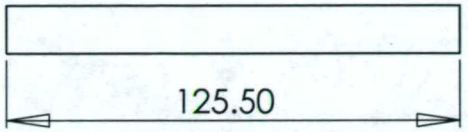

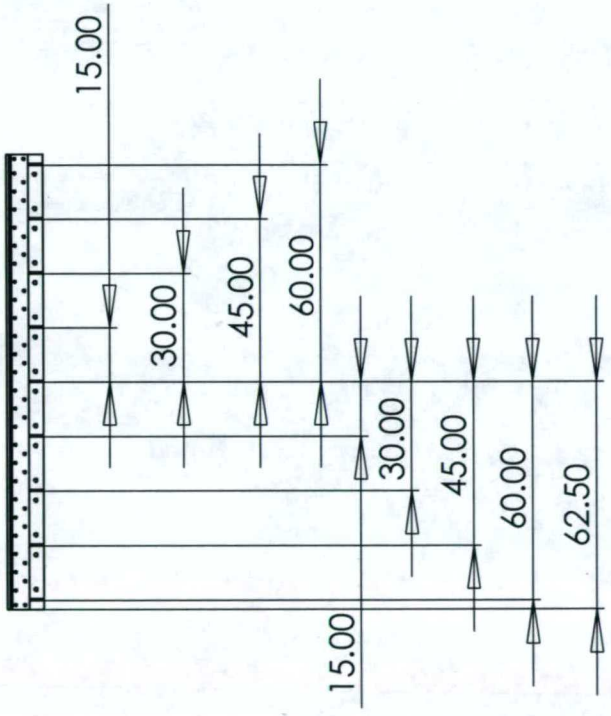

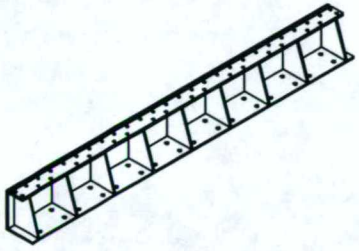

06

		DIMENSIONS ARE IN INCHES TOLERANCES: FRACTIONAL ± ANGULAR: MACH ± BEND ± TWO PLACE DECIMAL ± 0.1 THREE PLACE DECIMAL ± 0.010		NAME / DATE
		MATERIAL --	DRAWN	J.W. 11/24/03
		FINISH --	CHECKED	
			ENG APPR.	
			MFG APPR.	
			Q.A.	
NEXT ASSY	USED ON		COMMENTS:	
APPLICATION		DO NOT SCALE DRAWING		

Applied Thermal Sciences, Inc

SIZE	DWG. NO.	REV.
A	South Channel	2
SCALE:1:50	WEIGHT:	SHEET 3 OF 7

REVISIONS				
ZONE	REV.	DESCRIPTION	DATE	APPROVED

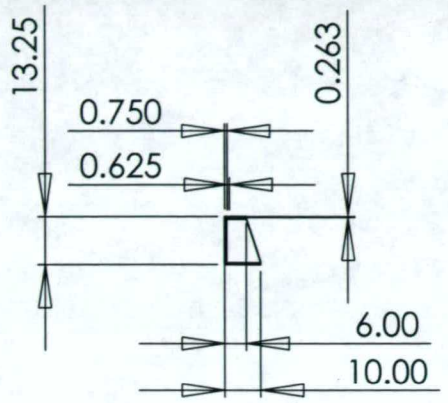

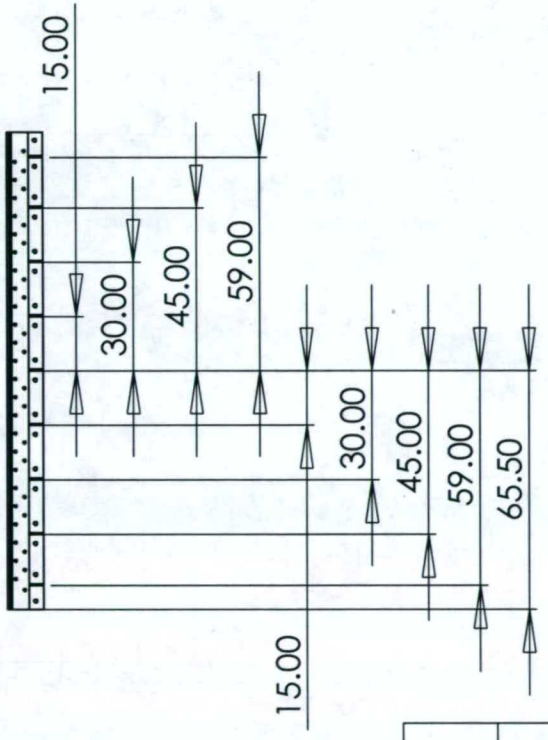

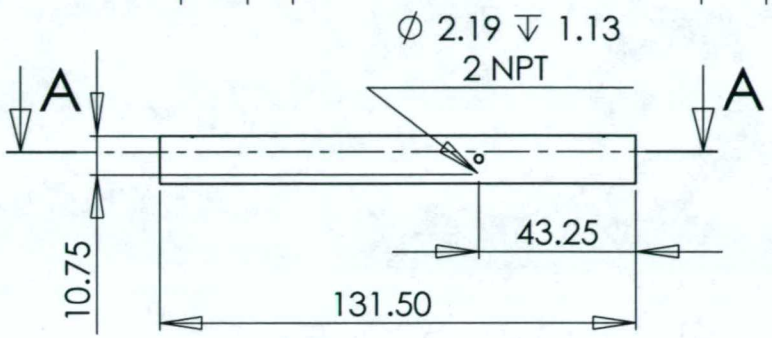

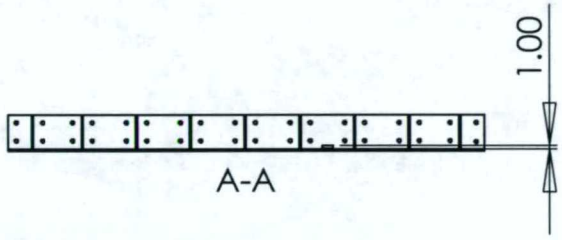

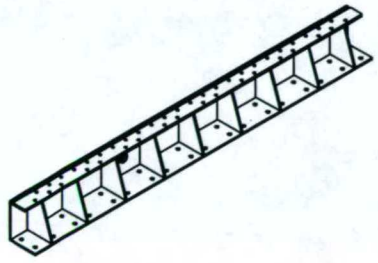

16

PROPRIETARY AND CONFIDENTIAL
THE INFORMATION CONTAINED IN THIS DRAWING IS THE SOLE PROPERTY OF APPLIED THERMAL SCIENCES, INC. ANY REPRODUCTION IN PART OR AS A WHOLE WITHOUT THE WRITTEN PERMISSION OF APPLIED THERMAL SCIENCES, INC. IS PROHIBITED.

NEXT ASSY	USED ON
APPLICATION	

DIMENSIONS ARE IN INCHES
TOLERANCES:
FRACTIONAL ±
ANGULAR: MACH ± BEND ±
TWO PLACE DECIMAL ±
THREE PLACE DECIMAL ±

MATERIAL --

FINISH --

DO NOT SCALE DRAWING

	NAME	DATE
DRAWN	J.W.	11/24/03
CHECKED		
ENG APPR.		
MFG APPR.		
Q.A.		

COMMENTS:

Applied Thermal Sciences, Inc

SIZE	DWG. NO.	REV.
A	East Channel	2
SCALE:1:50	WEIGHT:	SHEET 4 OF 7

REVISIONS				
ZONE	REV.	DESCRIPTION	DATE	APPROVED

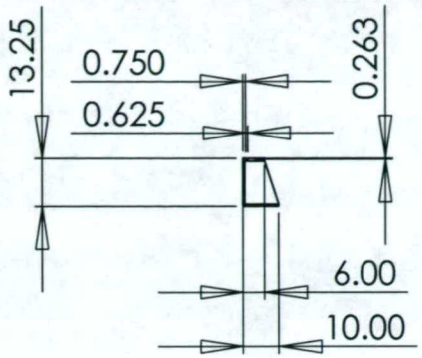

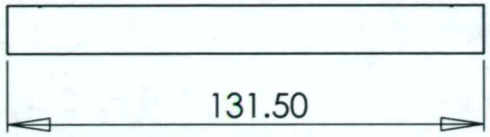

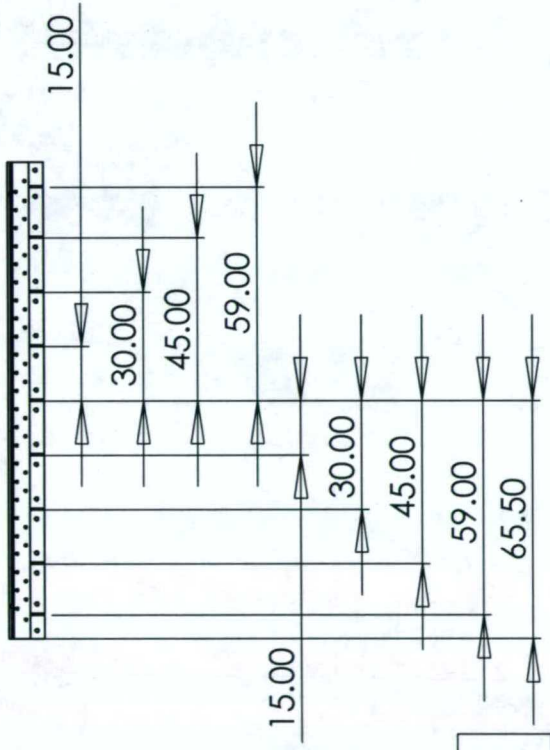

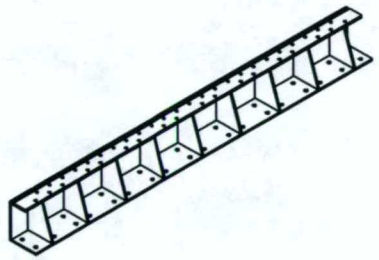

92

PROPRIETARY AND CONFIDENTIAL
THE INFORMATION CONTAINED IN THIS DRAWING IS THE SOLE PROPERTY OF APPLIED THERMAL SCIENCES, INC. ANY REPRODUCTION IN PART OR AS A WHOLE WITHOUT THE WRITTEN PERMISSION OF APPLIED THERMAL SCIENCES, INC. IS PROHIBITED.

NEXT ASSY	USED ON
APPLICATION	

DIMENSIONS ARE IN INCHES
TOLERANCES:
FRACTIONAL ±
ANGULAR: MACH ± BEND ±
TWO PLACE DECIMAL ± 0.1
THREE PLACE DECIMAL ± 0.010

MATERIAL —

FINISH —

DO NOT SCALE DRAWING

	NAME	DATE
DRAWN	J.W.	11/24/03
CHECKED		
ENG APPR.		
MFG APPR.		
Q.A.		

COMMENTS:

Applied Thermal Sciences, Inc

SIZE	DWG. NO.	REV.
A	West Channel	2
SCALE:1:50	WEIGHT:	SHEET 5 OF 7

REVISIONS				
ZONE	REV.	DESCRIPTION	DATE	APPROVED

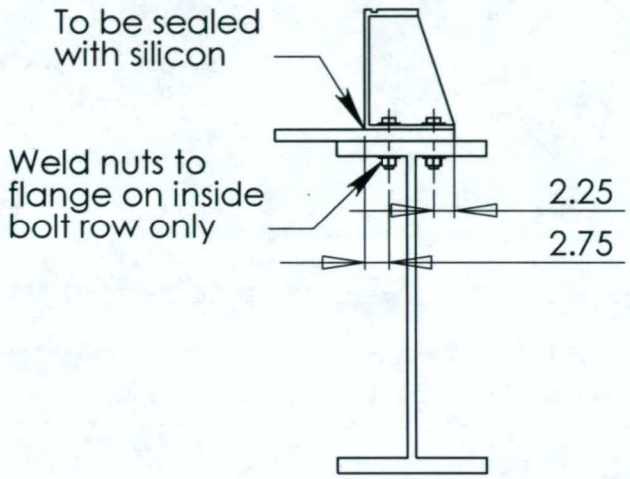

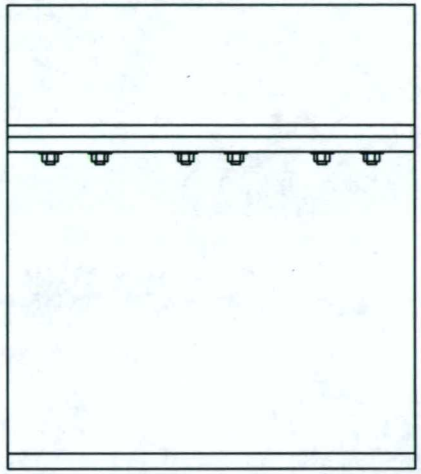

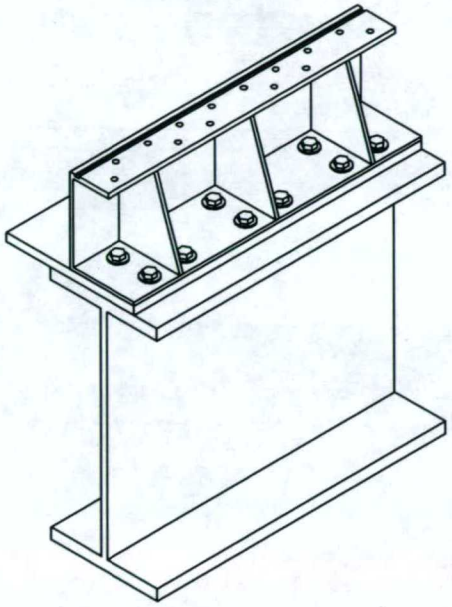

93

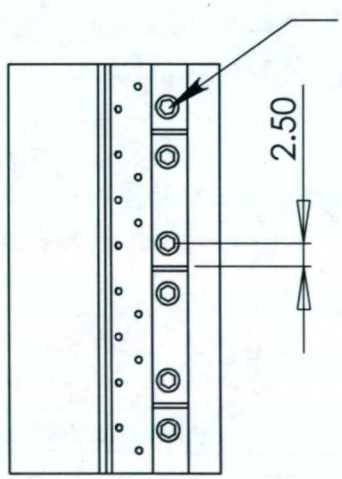

NEXT ASSY	USED ON	
APPLICATION		

DIMENSIONS ARE IN INCHES
TOLERANCES:
FRACTIONAL ±
ANGULAR: MACH ± BEND ±
TWO PLACE DECIMAL ±
THREE PLACE DECIMAL ±

MATERIAL --

FINISH --

DO NOT SCALE DRAWING

	NAME	DATE
DRAWN	J.W.	11/24/03
CHECKED		
ENG APPR.		
MFG APPR.		
Q.A.		

COMMENTS:

Applied Thermal Sciences, Inc

SIZE	DWG. NO.	REV.
A	Base Connection Detail	2
SCALE:1:20	WEIGHT:	SHEET 6 OF 7

REVISIONS				
ZONE	REV.	DESCRIPTION	DATE	APPROVED

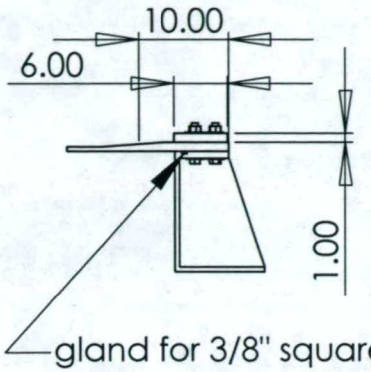

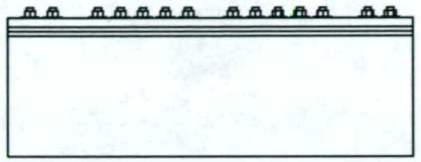

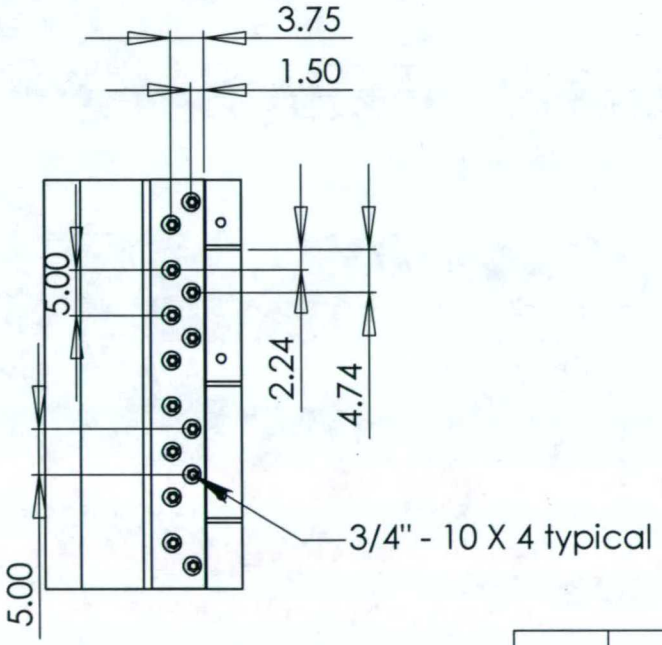

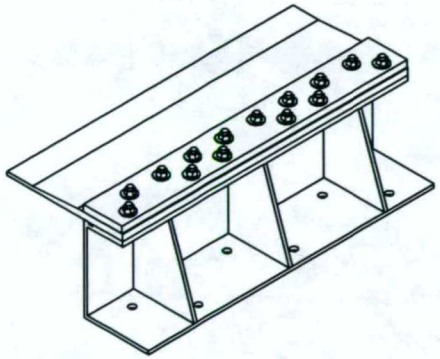

94

				NAME	DATE
		DIMENSIONS ARE IN INCHES	DRAWN	J.W.	8/22/03
		TOLERANCES:	CHECKED		
		FRACTIONAL ±	ENG APPR.		
		ANGULAR: MACH ± BEND ±	MFG APPR.		
		TWO PLACE DECIMAL ±	Q.A.		
		THREE PLACE DECIMAL ±	COMMENTS:		
		MATERIAL —			
NEXT ASSY	USED ON	FINISH —			
APPLICATION		DO NOT SCALE DRAWING			

Applied Thermal Sciences, Inc

SIZE	DWG. NO.	REV.
A	Top Connection Detail	1
SCALE:1:20	WEIGHT:	SHEET 7 OF 7

REVISIONS				
ZONE	REV.	DESCRIPTION	DATE	APPROVED

North

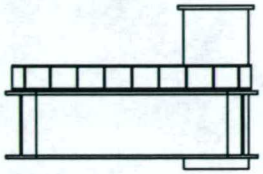

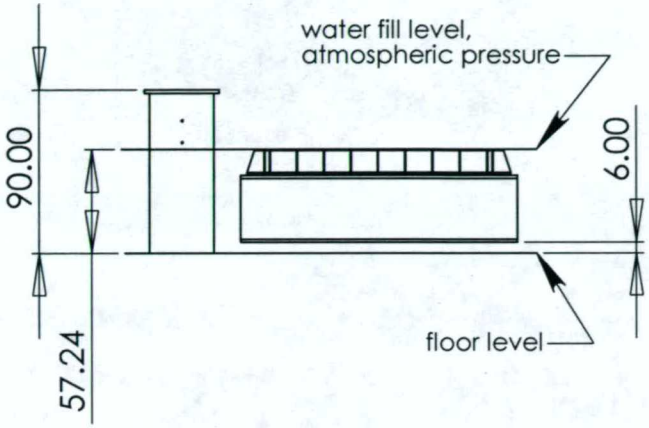

95

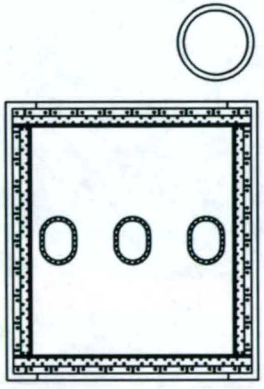

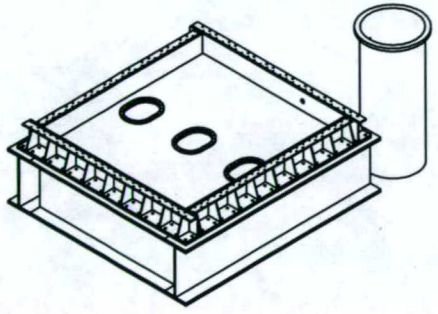

		DIMENSIONS ARE IN INCHES TOLERANCES: FRACTIONAL ± ANGULAR: MACH ± BEND ± TWO PLACE DECIMAL ± 0.1 THREE PLACE DECIMAL ± 0.010		NAME	DATE
			DRAWN	J.W.	9/11/03
			CHECKED		
			ENG APPR.		
			MFG APPR.		
			Q.A.		
		MATERIAL —	COMMENTS:		
NEXT ASSY	USED ON	FINISH —			
APPLICATION		DO NOT SCALE DRAWING			

Applied Thermal Sciences, Inc

Tank-Pressure Vessel Elevation

SIZE	DWG. NO.	REV.
A		1
SCALE:1:100	WEIGHT:	SHEET 1 OF 1

REPORT DOCUMENTATION PAGE

Form Approved
OMB No. 0704-0188

1. REPORT DATE *(DD-MM-YYYY)*	2. REPORT TYPE	3. DATES COVERED *(From - To)*
30-Jun-2005	Project Report	1-April-2002 to 30-Jun-2005

4. TITLE AND SUBTITLE

Design and Analysis of a Hybrid Composite/ Metal Structural System For Underwater Lifting Bodies

5a. CONTRACT NUMBER

5b. GRANT NUMBER
N00014-01-1-0916

5c. PROGRAM ELEMENT NUMBER

6. AUTHOR(S)

Thompson, Larry
Wall, Josh
Caccese, Vincent

5d. PROJECT NUMBER

5e. TASK NUMBER

5f. WORK UNIT NUMBER

7. PERFORMING ORGANIZATION NAME(S) AND ADDRESS(ES)

University of Maine
Office of Research and Sponsored Programs
5717 Corbett Hall
Orono, ME 04469-5717

8. PERFORMING ORGANIZATION REPORT NUMBER
UM-MACH-RPT-01-08

9. SPONSORING/MONITORING AGENCY NAME(S) AND ADDRESS(ES)

Office of Naval Research
Ballston Center Tower One
800 North Quincy St.
Arlington, VA 22217-5660

10. SPONSOR/MONITOR'S ACRONYM(S)
ONR

11. SPONSORING/MONITORING AGENCY REPORT NUMBER

12. DISTRIBUTION AVAILABILITY STATEMENT

Approved for Public Release, Distribution is Unlimited

13. SUPPLEMENTARY NOTES

14. ABSTRACT

This report summarizes the analysis and design of a hybrid underwater lifting body structure. It is part of an effort to investigate the response of hybrid composite/metal construction techniques and hybrid connection connections in U.S. Navy vessels. This effort includes structural analysis of a lifting body structure designed by Navatek, Ltd of Honolulu HI that was constructed of aluminum for the SES 200. Analysis of this structural system as an e-glass/vinylester – aluminum hybrid was undertaken. Additionally, a hydrostatic test system was developed used for a proof-of-concept study for a hybrid structural system, based upon the lifting body design.

15. SUBJECT TERMS

Hybrid Structures; Connection Design; Composites; Finite Element Analysis

16. SECURITY CLASSIFICATION OF:			17. LIMITATION OF ABSTRACT	18. NUMBER OF PAGES	19a. NAME OF RESPONSIBLE PERSON
a. REPORT	b. ABSTRACT	c. THIS PAGE			Vincent Caccese
U	U	U	UU	95	19b. TELEPONE NUMBER *(Include area code)* (207) 581-2131